



Narragansett Bay from Space:



A Perspective for the 21st Century



523

Commercial Data for Environmental Applications



Operational Satellites for Environmental Monitoring

A NASA, University Small Business, and State Partnership



Basic Research on Advanced Application



Advanced Experimental Data for New Applications



Applied Science Associates



RI Dept. Environmental Management

**Final Report for Project:
Narragansett Bay from Space: A Perspective for the 21st
Century.**

NAG-13-39

Principal Investigator

John F. Mustard
Department of Geological Sciences
Box 1846
Brown University
Providence, RI 02912
401-863-1264
John_Mustard@brown.edu

Co-Investigators

Craig Swanson
Applied Science Associates
70 Dean Knauss Drive
Narragansett, Rhode Island 02882-1143 USA
(401)789-6224
cswanson@appsci.com

Dr. Chris Deacutis
RIDEM Narragansett Bay Estuary Program / NB
NERR
235 Promenade Street
Providence, RI 02908
Tel. (401) 222-3961 x 7270
email: deacutis@etal.uri.edu

Final Report for Project: Narragansett Bay from Space: A Perspective for the 21st century.

EXECUTIVE SUMMARY	2
AREAS OF NEED AND CONCERN: THE ROLE OF REMOTE SENSING.....	3
OVERALL PROJECT GOALS	5
PARTNERSHIPS	5
SPECIFIC PROJECT OBJECTIVES.....	5
THERMAL REMOTE SENSING: ASSESSMENT OF ENVIRONMENTAL IMPACT AND INTEGRATION WITH HYDRODYNAMIC MODELING	7
REGIONAL CHARACTERIZATION OF THERMAL PROPERTIES OF NARRAGANSETT BAY:	9
<i>Methods</i>	9
<i>Results</i>	13
<i>Discussion</i>	16
EFFECTS OF TIDES ON THE DISTRIBUTION OF TEMPERATURE IN MOUNT HOPE BAY:	17
<i>Methods</i>	17
<i>Summer Observations</i>	18
<i>Spring Observations</i>	20
HYDRODYNAMIC MODELING:.....	22
<i>Numerical Simulation of Mt. Hope Bay</i>	22
<i>WQMAP Modeling System</i>	23
<i>Application of Hydro-Thermal Modeling to Mt. Hope Bay</i>	24
<i>Assimilation of In-Situ Data</i>	25
INTEGRATION OF REMOTELY SENSED DATA.....	27
<i>Processing of Remotely Sensed Data</i>	27
<i>Assimilation of Remotely Sensed Data</i>	28
<i>Remotely Sensed Data Assimilation Results</i>	28
MODELING RESULTS SUMMARY	29
SUGGESTED FUTURE ACTIVITIES.....	30
EVALUATION OF HYPERSPECTRAL DATA FOR ESTUARINE WATER CHARACTERIZATION	30
AVIRIS DATA CALIBRATION.....	31
ASSESSMENT OF CALIBRATION.....	32
INVERSE MODEL AND ANALYSIS.....	32
SUMMARY FOR HYPERSPECTRAL ANALYSIS.....	34
COMMERCIAL PRODUCT INTEGRATION	34
INTRODUCTION.....	34
MARKET NEEDS FOR THERMAL RELATED OVERFLIGHT INFORMATION	35
SPECIFIC USES BY THE COMMERCIAL PARTNER (ASA).....	36
LETTER FROM RHODE ISLAND DEPARTMENT OF ENVIRONMENTAL MANAGEMENT	38
PUBLICATIONS AND PRESENTATIONS RESULTING FROM THIS WORK	39
PROJECT WEB SITE:	39
PEER REVIEWED PUBLICATIONS.....	39
ABSTRACTS FOR PROFESSIONAL MEETINGS	39
PRESENTATIONS	40
STUDENT THESES:	40
LETTER FROM RI DEPARTMENT OF ENVIRONMENTAL MANAGEMENT	41
REFERENCES	42
TABLES.....	45
FIGURES.....	50

Executive Summary

In 1996, the NASA Administrator Dan Goldin and Rhode Island Congressman Patrick Kennedy challenged researchers in the Department of Geological Sciences at Brown University to develop a series of projects to apply remotely sensed data to problems of immediate concern to the State of Rhode Island. The result of that challenge was the project **Narragansett Bay from Space: A Perspective for the 21st Century**. The goals of the effort were to a) identify problems in coordination with state and local agencies, b) apply NASA technology to the problems and c) to involve small business that would benefit from incorporating remotely sensed data into their business operations. The overall effort was to serve two functions: help provide high quality science results based on remotely sensed data and increase the capacity of environmental managers and companies to use remotely sensed data. The effort has succeeded on both these fronts by providing new, quantitative information on the extent of environmental problems and developing a greater awareness and acceptance of remotely sensed data as a tool for monitoring and research.

The Rhode Island company that partnered in this effort is Applied Science Associates (ASA), an internationally recognized as a leader in the development and application of computer tools to investigate marine and freshwater environments. Using computer models to simulate physical, chemical, and biological processes, ASA solves problems about our aquatic environment and human interaction with that environment. The Rhode Island Department of Environmental Management, Division of Water Resources was the main state partner and provided leadership in the identification of important problems. This was coordinated through Dr. Chris Deacutis and was fully supported by this state agency (see attached letter). The effort was also augmented by the environmental advocacy group Save the Bay who also contributed resources to the project in terms of people and facilities coordinated through John Torgan. During the project, we also worked closely with various members of the Environmental Protection Agency including Darryl Keith of the Atlantic Ecology Division and Nick Prodan of EPA Region 1. Lastly, this project including the participation and support of the environmental staff at the Brayton Point Power Plant.

The principal findings of these work are as follows:

- The temperature of Mt. Hope Bay, an arm of Narragansett Bay that receives effluent from the Brayton Point Power Plant, is on average 0.8°C warmer during the summer and fall time frame. This higher temperature is due to the effluent from the power plant and impacts an area of 35 km².
- The effluent from the power plant is systematically distributed throughout the bay during the tidal cycle. On the falling tide the plume is detected as a temperature anomaly up to 3 km from the discharge point, and on the rising tide a pool of warmer water is created near the discharge point. Residual heating of the waters can be detected and suggest a memory from the previous tidal cycle.
- The tidal dynamics, and thus the effluent mixing, are a strong function of season with more stratified conditions during the summer and fall leading to a more expressed thermal plume on the surface than the winter and summer.
- Three dimensional hydrodynamic modeling of the system using independent calibration and validation methods provides results that are generally consistent with the remotely sensed data. This work shows that there is a residual heating of the bay of up to 1°C

during certain times of the year, the plume dynamics observed are reproduced in the model, and that there is a strong seasonal component.

- Remotely sensed data can be incorporated into hydrodynamic model for data assimilation. The procedures established in this project demonstrate the feasibility of this approach, and that it significantly improves the model performance. However, the increase in performance is short lived.
- Remotely sensed data provide a perspective that allows characterization and quantification of environmental impacts. The results are easily communicated to environmental managers and can be incorporated into monitoring efforts. The data also provide details of water's thermal properties not readily evidenced from field and modeling studies.
- Remotely sensed data have less direct application presently in modeling studies. Compared to assimilation of in situ data, remotely sensed data lack the time sensitivity, carry much larger processing costs and do not maintain a high enough accuracy to be readily integrated into modeling.
- The value of hyperspectral data for determining water optical properties and its constituents (e.g. chlorophyll, dissolved organic matter, and suspended sediment concentrations) was explored. It was found that this approach has significant promise in monitoring the water properties of the Bay and opens up new monitoring capabilities. We were able to determine the spatial distribution and abundance of phytoplankton, dissolved organic matter, suspended sediment, and the activity of phytoplankton.
- This project has led to continuing efforts on the part of the State of Rhode Island to incorporate remotely sensed data into monitoring efforts and ASA to use remotely sensed data in modeling.

This project has made a significant contribution to the understanding of thermal effluent and its impact on the environment. A significant component of community outreach has helped to promote these results as well as a web site devoted to the project and the results have been viewed by many groups and individuals. While the exact environmental problems that we encounter in the future will vary considerably, the new perspective that has been generated by this project will continue. We have also identified an number of basic research areas that are required to move environmental monitoring and modeling forward to better meet the needs of environmental managers.

Areas of Need and Concern: The Role of Remote Sensing

Narragansett Bay is the premier natural resource of Rhode Island. It directly affects important economic activities such as tourism and shellfishing, indirectly it is important for industries such as boat building and those associated with the Newport Naval facility, and it is a source of pride for all who live in Rhode Island. Furthermore, the influences of Narragansett Bay extend beyond its immediate borders as it is an important breeding ground and nursery for fin fish that form a key element of the Rhode Island and New England fishing industries. As is typical of heavily used resources, however, the health and functioning capacity of the Bay has been stressed over the years.

Through the efforts of environmental groups such as Save the Bay, state agencies such as the Rhode Island Department of Environmental Management, governing bodies, and cooperation with industry, the health of the Bay has improved dramatically over the last several decades.

These efforts have succeeded by tackling the most obvious problems, readily identified through ground-based surveys, such as large point sources of pollution, sewage treatment, and the dumping of heavy metals. However, the health of Narragansett Bay and its ability to sustain important commercial activities is not guaranteed. For example, algal blooms and increased turbidity in the Bay are thought to be responsible for the continuing decline in eel-grass beds, which are critical nurseries and habitats for many commercial species in the Bay. Solutions to this and other areas of concern could benefit greatly from a cost effective program that provides a better understanding of Narragansett Bay and a monitoring capability to track the health and functioning of the Bay through time. Not only would there be a direct benefit to the \$1.6 billion in commercial activities currently centered around Narragansett Bay, but such a program could provide support for the development of new endeavors which is an area of interest for the Rhode Island Economic Development Corporation. For example, aquaculture is an emerging activity in Rhode Island and locations for the aquatic infrastructure depends on knowledge of many aspects of the Bay.

Currently, the largest impediment to forward on these issues is cost. Measuring and monitoring water quality and dynamics in an area as large as Narragansett Bay requires large surveys and extensive laboratory analyses which are not possible in the current fiscal environment. Yet the complexity of the Bay and how it functions demands that we understand in greater detail what the spatial dynamics of seasonal productivity are, how this is related to circulation and river inputs, the affects on the life cycle of important species, and what the effects of land use and land use change in space and time are.

Remotely sensed data offer an excellent opportunity to address these issues and help Rhode Island preserve and enhance the future of this most important resource into the next millennium. Technological and analytical capabilities developed through basic research over the last decade make possible entirely new, and cost effective ways for assessing and monitoring Narragansett Bay. The specific strengths of remote sensing are:

- synoptic view (instantaneous coverage of large areas)
- multitemporal data acquisition (for analysis of historical patterns through archives covering 30 years and analysis of ongoing processes with current and future sensors)
- digital format (allows the use of quantitative algorithms to extract information on the physical properties of the bay and its contents).
- new technologies that allow greater spectral and spatial coverages
- correlation with other information (products of remote sensing studies are readily incorporated into Geographical Information System (GIS) data bases)

Thus, by using remote sensing, we can address some of the fundamental issues regarding the water quality of Narragansett Bay in a cost effective manner. These results are then meaningful information that, when integrated with other data sources and expertise, will be used to affect policy that will guide the future of the Bay, and assist in the economic activities around the Bay. The goals of this cooperative agreement were to investigate the uses of remote sensing for monitoring and analyzing coastal waters with specific focus towards the needs of the state of Rhode Island and the management of Narragansett Bay. A larger goal of this project was to transfer results and knowledge to state managers and small business to foster a greater use of remotely sensed data. The participation of small business in cooperation with Brown, the state, and NASA was implemented to enhanced business capabilities and opportunities for Rhode Island to provide a mechanism for the continuation of these efforts after the project has been completed.

Overall Project Goals

The goals of the project are:

- 1) To capitalize on the strengths of NASA remote sensing and Mission to Planet Earth to develop a better understanding of the near shore and estuarine environments of Narragansett Bay.
- 2) To work with small business to develop and make these tools and techniques available to other users in the nation and the world.
- 3) To work with state and city agencies to integrate this fundamental information into the ongoing planning and decision-making process.
- 4) To directly benefit existing and future commercial activities that have ties to Narragansett Bay.
- 5) To establish a sustainable commercial future for this activity beyond the commitment of NASA in this project

Partnerships

For this project to be successful, we needed to have full involvement of relevant state agencies and to pursue in cooperation specific research and applications activities that ultimately benefited the state natural resource agencies. Through discussions with Dr. Christopher Deacutis of the Rhode Island Department of Environmental Management (RIDEM), Water Resource Division, and others in the RIDEM, an understanding of the general capabilities of remote sensing in general and NASA's systems in particular was developed. This was coupled with a thorough overview of the general health of Narragansett Bay as seen by RIDEM where some of the critical areas of concern were articulated. These activities were followed by additional discussions with the RI Economic Development Council as well as Save the Bay, a local grassroots environmental advocacy and education organization, to engage a broader segment of interested parties and to build a greater perspective on how remotely sensed data could be usefully applied.

Through these discussions we developed a specific set of research and applications objectives, described below. A critical element of the partnerships was the full involvement of the RIDEM Department of Water Resources and Save the Bay throughout the project. They participated fully in field work in support of the project. All results derived from these efforts were conveyed in a timely manner to RIDEM where the results were used in their ongoing monitoring and regulatory efforts.

An important outgrowth of the partnerships with RIDEM and Save the Bay were additional collaborations with more regional groups such as the Brayton Point Technical Advisory Committee, the Environmental Protection Agency (EPA), and the University of Rhode Island (URI). The results of this project have been widely discussed among many arms of the EPA that operate in the northeast of the U.S. A continued partnership among EPA, Brown, URI, Save the Bay and the RIDEM is one of the fundamental outgrowths of this project.

Specific Project Objectives

On the basis of detailed discussion of general science problems in Narragansett Bay and specific regulatory and environmental problems, two principle project areas were defined. In the

area of general science problems, the understanding of water circulation, biology, and environmental change are overarching critical concerns for the State of Rhode Island. For an environmental system as dynamic and complex as Narragansett Bay, resources for measurement of bay systems and monitoring of its health are limited. Thus one clear objective was to explore the utility of NASA's most advanced remote sensing technology to derive cost-effective measures of the basic properties of this estuarine system. Particular areas of interest for application of information derived from remotely sensed data include:

- Spatial and temporal patterns of productivity and temperature
- Timing and determinants of harmful algal blooms
- Nutrient and energy exchanges between the estuary and the coastal ocean
- Effects of circulation and weather patterns
- Effects of land use and land-use change
- Impact of human activity on bay processes: temperature, turbidity, chlorophyll

The project sought to develop new measurements capabilities that could be incorporated into monitoring systems. This component of the project evaluated hyperspectral data that have shown great promise for the development of quantitative estimates of water properties, but have not been fully developed for estuarine environments.

The most pressing environmental problem facing Rhode Island at the time that this project was initiated was thermal pollution. In 1994 a preliminary report prepared by Mark Gibson documented a close link in time between a dramatic decline in fish abundance and diversity with a 50% increase in thermal effluent from the Brayton Point Power plant located on Mount Hope Bay, an arm of Narragansett Bay. The preliminary report raised significant concerns about the impact of thermal effluent from this power plant, yet there were also concerns raised as to the causality. Did the association in time also translate to a specific environmental impact on the fish populations and diversity of Narragansett Bay? While a number of detailed studies were being developed to address aspects of this complex problem, RIDEM felt that a temperature study that could encompass the entire bay and across all seasons would be of great benefit. In addition, there was only a very rudimentary knowledge of the specific temperature properties of the bay over the tidal cycle. Thus a specific applications project was developed to address three fundamental questions:

How does the temperature of Narragansett Bay vary as a function of season and what are the main exchanges among the major water bodies?

How does the temperature of Narragansett Bay vary as a function of tide and what are the main exchanges among the major water bodies?

Does the thermal effluent from the Brayton Point Power station have a measurable impact on the temperatures of any part of Narragansett Bay?

This applied research project employed three major components. The first was a time-series analysis of the surface temperature of Narragansett Bay measured remotely by the Landsat series of satellites covering the time period 1984-present. The second was a series of high temporal resolution time series to capture the dynamics of water temperatures over a tidal cycle. This component included extensive field campaigns to verify and validate the remotely acquired data. And the third was detailed 3-D hydrodynamic modeling of water movements in Narragansett

Bay led by Applied Science Associates (ASA). This effort required extensive inputs from the field campaigns and from other ancillary data sources. An outgrowth of this project was to incorporate remotely sensed data into the modeling as both a validation component as well as to tune and operate the model through time (data assimilation). While ASA commonly uses in situ data for model validation and verification, such data is generally limited to point measurements of temperature, salinity, and dissolved oxygen. The incorporation of spatially explicit temperature fields was a novel direction that required new thinking on data assimilation.

Thermal Remote Sensing: Assessment of Environmental Impact and Integration with Hydrodynamic Modeling

The Narragansett Bay estuary runs northward from the coast of Rhode Island (Figure 1), and has a drainage area of 4660 km² (Kremer and Nixon, 1978). Its 2.6 X 10⁹ m³ of water are spread over an area of almost 350 km², with a mean depth of 7.8 m (Chinman and Nixon, 1985). The mean tidal prism is much greater than the mean volume of river flow into the bay during an equivalent period of time, so that the estuary is generally well mixed, although occasionally stratified (measured by salinity gradients) in the upper bay (Kremer and Nixon, 1978). The semi-diurnal tide ranges from 0.8 to 1.6 m (Chinman and Nixon, 1985), but the prevailing winds, northwest during the winter and southwest during the summer, frequently dominate short-term circulation patterns (Kremer and Nixon, 1978). Water temperatures throughout the year range from below freezing up to the mid-20s (°C), and the annual water temperature cycle tends to lag solar radiation by about 40 days (Kremer and Nixon, 1978).

Mount Hope Bay, a central focus for our thermal studies, is a shallow estuary located on the state boundary between Rhode Island and Massachusetts. It is the northeast component of the Narragansett Bay system, connecting to the East Passage through Bristol Ferry (at the Mt. Hope Bridge) and to the Sakonnet River at Sakonnet (Figure 1). It has an area of ≈35 km² and an average depth of 5.5 m. A dredged channel system 120 m wide and 10.5 m deep begins approximately 3 km northeast of the Mt. Hope Bridge and continues up past Fall River and the Taunton River. A second channel extends easterly and then northerly toward Fall River and a third smaller channel extends from the main channel in Fall River northwesterly to the Brayton Point Station. Three subembayments line the northern boundary of Mt. Hope Bay to the west of the Taunton River mouth: the Lee, Cole and Kickamuit Rivers.

Tidal fluctuations in Mt. Hope Bay range from 1.0 m at neap to 1.68 m at spring with a mean range of 1.34 m. Tidal currents are typically 10-25 cm/s in the bay but can exceed 2 m/s in the narrows at Sakonnet. There is little amplitude or phase difference throughout the bay for the important tidal constituents M₂, S₂, N₂, O₁, K₁, and M₄ (Spaulding and White, 1990).

The major freshwater source is the Taunton River, averaging 30 m³/s (Ries, 1990). The Cole River is the only other significant freshwater source at 1.25 m³/s. The Lee and Kickamuit Rivers do not contribute measurable flows.

The water column is generally well mixed throughout the year although stratified conditions do occur near the mouth of the Taunton River at Fall River. Previous studies (Dallaire, 1990; Turner et al, 1990) have shown intermittent stratification from both salinity and temperature elsewhere in the bay with stronger thermal stratification in the northern reaches.

Spaulding and White (1990) showed that mean density induced flow is small, at a few centimeters per second, relative to the tidal driven flow. They also reported that wind driven flows are not important to net circulation. A dye study conducted to assess the travel time from the Fall River Wastewater Treatment Plant, located on the eastern side of Mt. Hope Bay (NETSU, 1989), provided some evidence of fast (~50 cm/s) flows in the near surface waters (less than 1 m deep). The cause of this flow was not examined, however.

The Narragansett Bay ecosystem is phytoplankton based, and usually experiences a bay-wide winter-early spring bloom, several localized short term blooms throughout the summer, and a late summer bay-wide bloom (Kremer and Nixon, 1978). The bay is inhabited by many commercially important fish species, is an important breeding and nursery area for fish, and the benthos is dominated by clams which are harvested in limited areas. The land surrounding the estuary is heavily populated and the estuary receives significant volumes of industrial and municipal effluents. Although the overall quality of the water in the estuary has improved dramatically over the last several decades, Gibson (1996) identified a strong, temporal correlation between fish abundance and changes in the operation of a power plant located on the upper reaches of Narragansett Bay. Specifically, the onset of a major decline in aggregate fin fish stocks and species diversity over the last decade was significantly correlated with a 50% increase in the volume of effluent discharged from the Brayton Point Power Station (BPPS) in 1985.

The BPPS is the largest fossil fuel power plant in the northeast United States. This coal-fired electric generating facility is located on Mount Hope Bay in the Narragansett Bay estuary (Figure 1) and releases approximately 1.4 billion gallons/day of thermal effluent ($\approx 60 \text{ m}^3/\text{sec}$), or about twice the flow of the major freshwater source to Mount Hope Bay, the Taunton River. The cooling water is extracted from the estuary at a depth of 20 ft returned with a typical temperature rise of 7-10°C over the ambient temperature of the input water. Concerns have been raised about the long term impacts of the thermal effluent on the Mount Hope Bay ecosystem such as the effects on dissolved oxygen and reproductive success of organisms (Jeffries, 1994; Lin and Regier, 1995) as well as the possibility that it may be a factor in the decline of fish stocks in this bay over the past 15 years (Gibson, 1996). However, detailed information on the fate of the thermal effluent and its spatial and temporal properties over short and long time periods are lacking. This essential information is required in order to objectively assess the overall impact of the thermal effluent on diurnal and seasonal time scales and to integrate this into a more detailed understanding of the local ecology.

Temperature affects organisms through direct physiological mechanisms. All organisms have a certain tolerable temperature range, above which prolonged exposure is lethal. Within this acceptable temperature range, metabolism, growth rates, reproduction, and recruitment success vary widely. In cold-blooded marine organisms, warmer ambient temperatures increase metabolic rates and related processes, such as feeding efficiency (Sanford et al., 1994). Growth and development rates usually increase with temperature, up to a threshold, beyond which excess energy is required for survival, and rates decline precipitously. Temperature variations are used as reproductive cues for many populations, including several Narragansett Bay fish species (Dixon, 1991). Increases in bacterial abundance with temperature (Valiela, 1995), further compound the community effects of reduced dissolved oxygen and nutrient concentrations in warm water (Paine, 1993).

All of these temperature-related responses affect different species, and the repercussions for ecosystem dynamics depend upon food web interactions. Despite lack of a clear understanding of the mechanisms at work, significant warming of coastal marine systems has been documented to have substantial and sometimes unpredictable impacts upon community composition and structure (Tissot et al., 1991). Thus, a detailed understanding of estuarine thermal processes and anthropogenic impacts upon them are vital to the successful management of coastal ecosystems and fisheries.

In this analysis we seek to establish the magnitude and scope of the impact of thermal effluent from the BPPS in the Narragansett Bay estuary, and Mount Hope Bay in particular. This study is composed of three major components: regional characterization of thermal properties of Narragansett Bay and the relationship to Mount Hope Bay using Landsat Thematic Mapper data,

high spatial and temporal resolution characterization of the thermal effluent as a function of tidal cycle during spring and summer conditions, and hydrodynamic modeling. Many aspects of these studies have been published (e.g. Mustard et al., 1999; ASA publications) or constitute senior and masters thesis at Brown University (e.g. Sen, 1996; 1997; Carney, 1997, Dave, 1998). In addition, the interim and summary results have been presented at numerous meetings, forums, and workshops (e.g. Mustard et al., 1997ab; Carney and Mustard, 1997; Swanson et al., 1997).

Regional Characterization of Thermal Properties of Narragansett Bay:

Methods

Landsat Thematic Mapper Data

Since 1981, the Landsat Thematic Mapper (TM) series instruments have acquired multispectral images of the surface of the Earth from an orbit of 700 km. Of importance to this investigation, the TM sensor includes one thermal infrared channel that covers the wavelength region 10.4-12.5 μm from which an estimate of surface temperature can be derived (see below). The spatial resolution of each picture element (pixel) on the surface in the thermal channel is 120 m x 120 m, or slightly more than 1.4 hectares. From its sun synchronous orbit, this sensor has the opportunity to re-visit a specific target every 16 days. However, the frequency of actual data collects is far less than this due to obscuration by clouds and scheduling of spacecraft data handling resources. Although other sensors have more frequent observations (e.g. the Advanced Very High Resolution Radiometer acquires thermal data twice a day and these sensors have been in operation since 1979), they lack the requisite spatial resolution to resolve the thermal properties of specific regions within Narragansett Bay.

Narragansett Bay is within Landsat TM Path 13, Row 31. For this investigation, we searched the Landsat TM archives at the United States Geological Survey's Earth Resources Observations Systems (EROS) data center for any acquisitions of Path 13, Row 31 that met an initial requirement of <20% cloud cover. This resulted in 35 listed acquisitions from 1981 to 1996. Unfortunately, many of the scenes had more cloud cover than estimated in the data base, or were no longer in the archive. A remarkable series of 8 scenes, well distributed across the year 1988 was acquired. However, there were no useable data acquired in the thermal channel for any of these scenes. Eliminating scenes with no useful data due to obscuration by clouds and other factors, a final total of 14 scenes reasonably well distributed across the calendar year was obtained (Table 1, Figure 2).

Temperature Derivation

Radiance measurements from band six of the Landsat Thematic Mapper (wavelength=10.4-12.5 μm) were used to derive surface temperatures by applying a form of Plank's Black Body Equation, which defines the relationship between the radiance emitted from an object at a certain wavelength and its absolute temperature. First, the image digital number (DN) values were converted to at sensor radiance by applying the gain and bias of the detectors where:

$$R_u = \alpha (\text{DN}) + \beta$$

where:

$$\begin{aligned}
R_u &= \text{uncorrected spectral radiance in } \text{mW cm}^{-2} \text{ Sr}^{-1} \mu\text{m}^{-1} \\
\alpha &= 0.005632 \text{ mW cm}^{-2} \text{ Sr}^{-1} \mu\text{m}^{-1} \text{ DN}^{-1} \\
\beta &= 0.1238 \text{ mW cm}^{-2} \text{ Sr}^{-1} \mu\text{m}^{-1}
\end{aligned}$$

Radiance was then converted to a black body temperature (Gibbons et al., 1989):

$$T_u = \frac{K_2}{\ln \left[\frac{K_1}{R_u} + 1 \right]}$$

where:

$$\begin{aligned}
T_u &= \text{black body temperature in K} \\
K_2 &= 1260.56 \text{ K} \\
K_1 &= 60.776 \text{ mW cm}^{-2} \text{ Sr}^{-1} \mu\text{m}^{-1}
\end{aligned}$$

Because water is not a perfect black body (or a perfect emitter), a correction was made using the emissivity of water (the ratio between the radiance of a particular "gray body" and that of a black body at the same temperature) (Avery & Berlin, 1992):

$$T_k = T_u / E^{1/4}$$

where:

$$\begin{aligned}
E &= \text{emissivity of water} = 0.986 \text{ (Gibbons et al., 1989)} \\
T_k &= \text{kinetic temperature in K}
\end{aligned}$$

Low atmospheric transmissivity can introduce some error into deriving surface temperature from satellites, as atmospheric constituents (especially water vapor) absorb radiation emitted from the surface, thus reducing the amount of radiation which actually reaches the sensor. The atmosphere also emits some radiation due to its own internal heat, in turn increasing at-satellite radiance. The net effect will typically reduce the magnitude of the at-sensor radiance compared to the surface radiance, as well as the contrast or dynamic range.

The accuracy and precision of deriving surface temperatures from Landsat TM band six data have been assessed by Schneider and Mauser (1996), who employed a full atmospheric model to convert at-satellite radiance to an accurate measure of water leaving radiance (and thus water temperature) of a lake in Germany for which extensive *in situ* water temperature data were available. On average (in 31 images), atmospheric correction increased satellite derived temperatures by 1.33 K. Thus, we may expect to slightly underestimate temperatures when corrections are not made, although the exact error is dependent upon specific atmospheric conditions. Atmospheric corrections also increased spacing, or the temperature step associated with one DN step, from 0.47 K/DN to 0.63 K/DN. Therefore, temperature *differences* may also be slightly underestimated. For their data, Schneider and Mauser (1996) estimated the average change in temperature difference was +0.16 K/DN.

A critical factor to consider is the relationship between the remotely sensed surface layer and the bulk water properties. Here we define the bulk water temperatures to include the water above the thermocline, which in a well mixed estuary may extend to the bottom. All of the energy exchanges between water and air take place within a very thin surface skin layer, the

layer that is sensed remotely. Due to evaporative cooling in the surface layer, this temperature is typically cooler than the bulk water temperature, though sea state, wind speed, and diurnal energy fluxes all affect the relationship. The exact nature of this relationship is complicated and has been studied by numerous investigators. Yokoyama et al. (1995) showed that under typical coastal ocean conditions, thermal gradients from the surface to 2 meters were weak to absent and they concluded that the skin temperature was a reasonable estimate of the bulk temperature. They did note that under extremely calm conditions, strong thermal gradients developed in the near surface, sometimes exceeding several °C. However, the time of maximum divergence was typically between 12:00 and 4:00 PM local time. Schneider and Mauser (1996) investigated the relationship between radiometric measurements of surface temperatures and bulk water temperature over many diurnal cycles. On average, the temperature difference was found to be at a minimum (0.1 K) between 9 and 11 am, the standard crossing time of the Landsat satellites. On the basis of these and other studies it is concluded that remotely measured skin temperatures are representative of bulk water temperature below the surface.

As a test of this relationship, temperatures derived from the fourteen satellite images were compared to *in situ* measurements to assess the level of accuracy of the calculated temperatures for this study (Figure 3). In cases where an *in situ* measurement was available for the day of the overflight, a direct comparison could be made. Because these situations were rare, any *in situ* data available within one day of the overflight were used as estimates. When measurements were not available within one day, temperatures were linearly interpolated from measurements within 3 days before and after the scene date.

Satellite-derived temperatures were all within 3°C, and many within 1°C of *in situ* measurements. All of the other differences greater than 1°C were satellite underestimates probably resulted from atmospheric interference. The derived temperatures were used to compare the general seasonal water temperature trend in the satellite images to actual trends observed through years of *in situ* monitoring. The seasonal composite created from fourteen satellite images which actually span over twelve years (Figure 2) was found to be an appropriate representation of the general seasonal trends observed over the long term (Figure 4).

While the level of accuracy of the remotely acquired data is important, the goal of this investigation is to determine if the thermal effluent has a measurable impact on water temperatures beyond the immediate area of the effluent discharge point. For this purpose we can take advantage of the high precision of the remote measurements (0.5°C) and image format of the data and analyze the temperature of each area relative to a baseline, thus eliminating the uncertainty involved in deriving exact temperatures. For a baseline we chose the mean temperature of the entire Narragansett Bay estuary. Deviations of specific areas from the estuary mean were generally within the range of ± 5 DN or $\pm 2.5^\circ\text{C}$. Given the fact that atmospheric effects tend to increase the temperature/DN relationship, this range in temperatures may be an underestimate of the order of 0.8°C, for the largest deviations. A fundamental assumption of this approach is that the atmosphere does not vary significantly across the scene ($\approx 60 \times 90$ km). This assumption will be valid under clear sky conditions. However the presence of clouds or fog may introduce non-uniform variations and thus scenes with significant clouds or fog were removed from the study.

Regional Classification of Narragansett Bay

To facilitate studies of the physical characteristics of Narragansett Bay, Chinman and Nixon (1985) divided the estuary into a series of distinct segments related to basin bathymetry and

circulation patterns, and defined the depth, area, and volume of each of these segments (Table 2). Based upon this breakdown as well as observations of overall temperature patterns in the estuary, we defined twelve study areas within Narragansett Bay (Figure 5), in order to investigate spatial variations in seasonal temperature trends. The "regional classification" consisted of categorizing the behavior of these pre-defined regions relative to the system as a whole. Four areas were defined in the upper estuary (Greenwich Bay, Providence River, Upper Narragansett Bay, Mount Hope Bay), and the West Passage, East Passage, and Sakonnet Rivers were each divided into two or three sections so that estuary-to-ocean gradients could be detected where present. The known physical characteristics for each area (Table 2) provide a context for comparison of their seasonal temperature patterns. Temperature data were also extracted from two inland water bodies and the coastal ocean (Figure 5) for comparison to estuarine characteristics. The temperature of the estuary as a whole was defined as the mean of the combination of all of the Narragansett Bay study areas.

Surface temperature signals were produced by extracting the mean temperature from each study area and calculating its temperature difference from the Narragansett Bay mean for each scene ((regional mean) - (Narr. Bay mean)). Correlation coefficients among each of the normalized seasonal temperature signals were used as a means for classifying the estuary in terms of its thermal properties (Table 3). Three natural groups are defined from the correlations in Table 3, where each group exhibits a positive correlation among its members and a negative correlation with the other groups.

Unsupervised Classification of Narragansett Bay

The regional approach discussed above incorporated knowledge of the estuary's morphology and circulation patterns to define study areas such that thermal properties could be related to known physical characteristics, i.e. depth, area, and volume relationships, and tidal and fresh water flushing. This breakdown was well-suited for gaining an understanding of the seasonal thermal behavior of different areas of the bay, and comparing them to one another in the context of their physical characteristics. However, in treating the estuary as twelve large areas, each with a mean temperature, we fail to maximize the advantages provided by the spatial extent and resolution of remotely sensed data. The large number of data points does give us great confidence that the mean temperature is an accurate representation of the study area, but the process of assigning one value to each pre-defined area may prevent us from observing some important patterns within the data. By pre-defining the study areas, we assume that each of these areas behaves as one fairly cohesive system, and that this set of study areas is somewhat representative of temperature variations within the estuary. Though these assumptions are valid in the context of a comparison of the properties of different areas, another technique was employed to obtain a more complete view of the estuary's temperature dynamics.

Unsupervised classification is a commonly used technique in the analysis of remotely sensed data (e.g. Jahne, 1991; Foody et al., 1990; Jensen, 1996). It is typically applied to multispectral data of a single date to derive land cover units, but can be readily applied to any multivariate data set. In contrast to the directed, regional classification, unsupervised classification is a completely objective method where statistical relationships among data determine which areas could be treated as cohesive systems. Instead of comparing the averaged seasonal temperature signals of the selected bay regions, the signals (or vectors) of each pixel are analyzed and grouped into statistically categorized classes, thereby dividing the estuary into natural groupings based upon seasonal temperature patterns.

The approach to unsupervised classification that we employ here is a clustering algorithm referred to as the Iterative Self Organizing Data Analysis Technique (ISODATA, Tou and Conzales, 1977; Sabins, 1987; Jain, 1989). As an iterative technique, many passes are made through the data set, successively refining the clustering of the data to achieve the specific constraints imposed on the algorithm or until no further improvement in the clustering is made. The initial characteristics of each class (expressed as a vector, which describes the values of a pixel in all bands, or times, in n-dimensional space) are chosen randomly, and then redefined as the classes are formed. Each pixel is placed into the class to which its vector is most similar, and once all of the pixels are classified, a new class vector is defined as the mean vector of all of the pixels in the class. The image is then reclassified, mean vectors recalculated, and the process continues until no significant change occurs between classifications.

Unsupervised classification provides the distinct advantage of objectivity, while allowing some control over the character of the results. The optimum, minimum, and maximum number of classes desired (8, 5, and 14 respectively), the maximum allowable variance within a class (± 10 DN), and the minimum size for a class (999) were all input to shape the analysis. By defining these constraints and a set of computational parameters, the splitting and merging of classes was controlled without making any assumptions about the specific character of each class.

Eight scenes were selected from the fourteen scenes used in this study to perform an unsupervised classification of temperature data. All scenes with any indication of atmospheric interference were removed from the initial set of fourteen as well as one scene where ice was present in the bay, and a seasonal spread was selected from those remaining. This was to minimize a bias in the results from the large number of September scenes in the full data set. The water area defined for classification included all of Narragansett Bay and surrounding fresh water bodies, as well as a small part of the coastal ocean.

To test if the specific selection of the 8 scenes had a direct effect on the resulting classes, we performed several tests of the approach using different combinations of 8 scenes from among the 14 available, while maintaining a seasonal spread in the dates, as well as using all scenes that were free of atmospheric interference or ice. As expected, there were minor differences among these solutions. However, the gross characteristics of the most important 6 classes did not change in these tests.

Results

The general patterns observed in the seasonal temperature signals of the classes identified by both the regional and unsupervised classification analyses are intuitive, controlled primarily by surface to volume ratios of the respective regions (Table 2), and modified to some extent by tidal exchange among the regions. Estuarine regions lose more heat proportionately than the ocean during the winter, and gain more heat during the summer. Lakes exhibit an extreme of this behavior, as they are generally the warmest bodies during the summer and coldest during the winter. The ocean temperature is obviously much more moderate, due to the relatively vast volume of these regions.

Although these general results are not at all surprising, they provide the critical context for assessing the spatial extent, thermal magnitude, and temporal character of the effects of thermal effluent from the BPPS. In order to apply a Space for Time Substitution, it is critical to establish that the physical properties of the region selected to be the control are indeed functionally comparable to the impacted site. As presented in Table 2, Upper Narragansett Bay is the region

that most closely matches the physical and functional properties of Mount Hope Bay. Employing both deductive (regional classification) and inductive (unsupervised classification) methods to the satellite data, the same basic conclusion is reached; the thermal properties of Mount Hope Bay are unique, with relatively greater temperatures in the summer and fall than the control sites. These results are discussed in detail below.

Regional Classification

The seasonal surface temperature signals of the twelve Narragansett Bay areas relative to the Narragansett Bay mean exhibited three different patterns (Figure 6). The upper estuarine regions were generally warmer than the bay average during the summer, and cooler during the winter, whereas the lower estuarine regions had the opposite behavior, and intermediate regions had damped temperature signals relative to the estuary mean. Correlation coefficients among the 12 seasonal temperature signals provide a statistical basis for the breakdown of the estuary into these three groups (Table 3). Significant correlations ($R > 0.6$) existed among the members of each group (although each area was not necessarily correlated with every other area within its group) and only negative or insignificant correlations existed between areas of different groups.

The seasonal temperature signals of the twelve pre-defined study areas provide the opportunity to relate thermal properties to the known physical characteristics of each area. In the lower estuary, the Lower East Passage and Lower West Passage exhibited the most extreme thermal behavior relative to the Narragansett Bay mean, as they are most influenced by advective exchange between the estuary and oceanic waters. The strength of oceanic influence in the East Passage is reflected by the facts that the entire East Passage was classified as lower estuarine and that the lower East Passage exhibited the strongest "oceanic" signal (Figure 6c). It is known that on a rising tide, most of the oceanic water enters the estuary through the East Passage, which is the deepest part of the system (Kremmer and Nixon, 1978). The Upper West Passage and Upper Sakonnet River formed a transitional group, characterized as a zone of mixing between waters which are more influenced by shallow water processes and those which are more tidally influenced (Figure 6b).

The character of the regions within the upper estuarine group were more strongly dependent upon the varying physical characteristics among the areas (Figure 6a). For example, Greenwich Bay is shallow with a theoretically high tidal flushing rate and low fresh water input; its seasonal temperature signal was fairly extreme in comparison to the other upper estuarine areas. Greenwich Bay's high surface area to volume relationship is the most important factor determining its thermal behavior. Though the high predicted tidal flushing (the highest among all areas, Table 2) would tend to counter the effect of the surface to volume ratio and thus the seasonal temperature fluctuations, studies have shown that there is much less tidal exchange than expected due to the specific geographic characteristics. The other three upper estuarine areas all have smaller surface area to volume ratios and weaker seasonal temperature signals. In comparison, the fresh water lakes, which are shallow and isolated, have even stronger signals than Greenwich Bay. These relationships suggest that regional surface to volume ratio is the most important factor in determining thermal characteristics in the upper estuary.

Of all the regions of Narragansett Bay characterized by Kremmer and Nixon (1978), Upper Narragansett Bay and Mount Hope Bay are the most similar on the basis of physical properties and location relative to important tidal exchanges with the coastal ocean (Table 2). The two areas are about the same size and their surface area to volume ratios are nearly identical. Upper Narragansett Bay flushing times are slightly faster, but are in the same general range as those for

Mount Hope Bay. In a natural system, we would expect that regions with similar physical characteristics would have comparable seasonal temperature characteristics. Thus, based upon its similar size, shape, and physical forcing, Upper Narragansett Bay serves as an appropriate area for comparison to Mount Hope Bay and its thermal characteristics in a Space for Time Substitution impact assessment.

The seasonal temperature characteristics of Mount Hope Bay and Upper Narragansett Bay were somewhat correlated during the winter months, but Mount Hope Bay failed to cool down at the rate of Upper Narragansett Bay through the fall (Figure 6a). T-tests between Upper Narragansett Bay and Mount Hope Bay proved their mean temperatures to be significantly different during the summer-fall period, during which time Mount Hope Bay had a mean temperature 0.8°C warmer than Upper Narragansett Bay. Greenwich Bay, the Providence River, and Upper Narragansett Bay all became cooler than the Narragansett Bay mean by early October, yet Mount Hope Bay was only colder than the bay mean in one January scene.

Unsupervised Classification

The selected water area was successfully divided into six different classes, based upon seasonal surface temperature signals (Figure 7). The classes consisted of fresh water lakes, the ocean, the upper estuary, the lower estuary, Greenwich Bay, and Mount Hope Bay, and the total area covered by each class is given in Table 4. Four additional classes were generated, mainly consisting of pixels at the boundaries between land and water (not shown). These classes were all small and their behavior was probably affected by the presence of land in some of the pixels, so they were not considered further in the analysis.

In general, the fresh water lakes exhibited the strongest seasonal temperature signal relative to the estuary mean: they were very warm during the summer months and very cold during the winter. Greenwich Bay behaved similarly, only to a lesser degree. The upper estuary was the largest class (Table 4), and therefore provided the greatest contribution toward the mean value for each scene. Thus, the upper estuary temperature signal relative to the mean was fairly weak. The ocean was significantly warmer than the study area mean during the winter and colder during the summer, as would be expected, and the lower estuary exhibited temperatures transitional between the ocean and the upper estuary.

Mount Hope Bay exhibited a unique temperature behavior, as it was on average 0.8°C warmer than the rest of the upper estuary over the range of scenes analyzed (Figure 8). Unlike Greenwich Bay, which was relatively warm during the summer and cold during the winter, or the lower estuary which behaved in an opposite manner, Mount Hope Bay was consistently warm, only dropping below the estuary-wide average in November, at which point it was still warmer than the rest of the upper estuary.

One of the strengths of the unsupervised classification is that patterns of seasonal thermal behavior are objectively mapped. Almost without exception, a consistent sequence of seasonal thermal behaviors are observed moving from the buffered signals of the coastal ocean, through the transitional and dominant estuary regions to the shallow estuary and lakes. This can be observed in Figure 7 through to the highest reaches of Narragansett Bay as well as smaller inlets along the coast. This general pattern, however, is interrupted in Mount Hope Bay, with a small cluster of similar seasonal properties on the west side of the Providence River. Significantly, this correlates with the location of the Manchester Street Power Plant which discharges a relatively small volume of thermal effluent.

Discussion

The most striking behavior among the four upper estuarine signals in the regional classification is that Mount Hope Bay fails to cool from mid-summer through autumn in comparison to the Narragansett Bay mean (Figure 6). These anomalously warm temperatures cannot be explained by simple physical characteristics. If anything, Mount Hope Bay's slightly slower tidal flushing rate in comparison to the other upper estuarine areas (Table 2) would theoretically cause a stronger cooling affect during the fall. The unique behavior of Mount Hope Bay is highlighted by the fact that the bay comprises it's own class in the unsupervised classification. Mount Hope Bay is not distinctively shallow or isolated from tidal waters, in fact it has very similar physical characteristics to the rest of upper Narragansett Bay. In addition, there are no natural physical parameters which would cause a water body to remain anomalously warm year-round

Seasonal temperature patterns in the estuary are a direct result of radiant heat exchange at the surface and advective exchange with oceanic waters. Both processes are seasonal in nature, such that heat is gained through the surface during the summer (lost during the winter), and gained from relatively warm tidal waters during the winter (lost during the summer). The seasonal temperature signal of a particular area is a direct reflection of the balance between these processes, which in this region is a function of surface area to volume ratio first and advective exchange second. The upper estuary reflects a fairly level balance of these processes measured relative to the study area mean.

Mount Hope Bay, however, exhibits temperatures that are anomalous for the patterns of seasonal temperatures determined through this analysis. This is illustrated most succinctly in Figure 9. The seasonal temperature signatures derived from the unsupervised classification were summed over the 8 scenes to produce a single number. When plotted against the surface to volume ratio, there is a clear trend from low values for high ratios and high values for low ratios. Mount Hope Bay, however, departs significantly from this trend

Excess summer warming relative to Upper Narragansett Bay could result from the shallow average depth of Mount Hope Bay. However, this hypothesis predicts that the bay should also lose proportionately more heat during the winter, which is not evidence in these data. Alternatively, we could explain relatively warm temperatures during the winter with a potentially large tidal influence, but this would similarly lead to cooler temperatures during the summer. Again, there is no evidence to support this hypothesis through either our understanding of the physical character of the bay or the analysis of the satellite data.

On average, Mount Hope Bay was typically 1°C warmer than the upper estuarine class. Major alterations to the system's heat budget are required to create an anomaly with the spatial extent and temporal consistency of this feature. The simplest and most likely explanation for the relatively warm year-round temperatures in Mount Hope Bay is the constant discharge of thermal effluent into the bay by the Brayton Point Power Station. The excess heat load is the only plausible explanation for the consistently warm temperatures in the bay. The extent of the Mount Hope Bay class (Figure 7), is an indication of the boundaries of the area which was consistently affected by constant warming. This thermally anomalous area covers an area of approximately 35 km² (Table 4).

Unsupervised classification also facilitated the recognition of smaller scale patterns which were averaged out by the regional approach. For example, there was an identifiable trace of the "Mount Hope Bay" class in the upper Providence River, near the location of the Manchester Street Power Plant (figure 7). Although the thermal affects of this plant were not as visible in the

satellite images as the plume from the larger Brayton Point Station in Mount Hope Bay, the fact that water in the upper Providence River exhibited similar seasonal behavior to that of Mount Hope Bay (the temperature of which is known to be driven by the influence of thermal effluent) suggests that the Manchester St. Plant may after all have an identifiable effect on the thermal properties of adjacent waters. This potential effect does however occur on a much smaller scale than the apparent influence of BPPS on Mount Hope Bay.

The almost year-round persistence of a decreasing temperature gradient with distance from the Brayton Point Power Station in Mount Hope Bay suggests that the plant's thermal effluent constantly drives the distribution of heat within the bay. The persistent temperature gradient and the extent of the Mount Hope Bay class in the unsupervised classification both suggest that the influence of the plant's thermal effluent is widespread throughout the bay, and is not an isolated feature.

Effects of Tides on the Distribution of Temperature in Mount Hope Bay:

Methods

Resolution of the effects of tides on the distribution of temperature requires a temporal sampling that allows the movements of water bodies to be resolved. In the Landsat analyses described above, each image was acquired on different dates and years, as well as different times within the tidal cycle. When organized according to tidal cycle, we can identify certain key characteristics (e.g. maximum extent of the plume is correlated with acquisition during maximum ebb tides) and hypothesize the movements of water bodies as a function of tide. However, tidal movement is affected by season (i.e. salinity and temperature stratification) and more importantly winds and these must be understood if such data can be evaluated for use in data assimilation. Thus, it is imperative to assess water movements with carefully controlled data acquisitions where essential driving parameters (winds, salinity, etc.) can be measured simultaneously with remotely sensed water temperatures.

Over the course of this project we implemented four measurement campaigns with sufficient temporal resolution to identify the movements of water bodies and the temperature distribution in Mount Hope Bay. These are listed in Table 5 with the timing and range of the tides on the days of the overflights given in Table 6. Three were specifically supported by in situ measurement campaigns while one occurred as a target of opportunity during a period when a suite of in situ sensors was deployed. The measurement campaigns included moored instruments as well as profiles of water properties on the day of the overflights. The moored instruments consisted of thermistors located at 0.2, 0.5, 1.0, 2.0, and 4.0 meters below the surface placed at 30 locations in Mount Hope Bay (Figure 10). These instruments acquired data at 15 minute intervals and were placed in the water 14 days before the expected day of the overflight and left in the water at least two weeks following the overflight. The thermistor data were used to validate the calibration of radiance to temperature from the remotely acquired data. They were also used for model validation and to generate interpolated temperature fields to compare the 3-dimensional temperature fields derived from the in situ sensors with the surface temperature field derived from the remotely sensed data.

Due to the seasonal variations in salinity and temperature in the Narragansett Bay estuary, the overflight campaigns fall into two seasonal classes: summer and spring. Three of the measurement campaigns occurred in the summer and only one in the spring. However, the expressions of the water dynamics were sufficiently different to warrant analysis of the water

dynamics separately. The focus of our analysis is primarily a description of the expression of the thermal effluent and the patterns of movement in response to tidal variations.

The data were coregistered to a common image base map formed by a SPOT Image scene of the area. This was geocoded to a UTM coordinate system with a 10 meter pixel spacing. The May 28, 1997 and August 19, 1997 data were calibrated to at sensor radiance using the instrument parameters. For the May 28 data collect, the data were further processed to correct for atmospheric attenuation and upwelling radiance by the data providers using the ELAS Trade atmospheric model driven by actual atmospheric profiles of temperature and humidity acquired on the day of the overflights. Using the calibrated radiance values, the kinetic temperature of the water was derived by inverting the blackbody equation. The calculated temperatures were validated against in situ temperatures at 20 cm below the surface for up to 30 different locations on Mount Hope Bay. The August 30 and September 11 data collects were calibrated to temperature using an empirical line method. We had a minimum of two temperature observations for each remotely sensed observation and regressed the remotely sensed radiance against the in situ temperature.

Summer Observations

All three summer measurement suites show the same distribution patterns of the thermal effluent in response to the tidal variation. Figure 11 corresponds to August 30, 1996, Figure 12 to August 19, 1997, and Figure 13 to September 11, 1998. On the maximum flood tide (9:44 am August 30, 1996 and 12:48 pm September 11, 1998) there are strong currents moving water up the Taunton River from Mt. Hope Bay. This confines the thermal effluent to a highly localized region near the effluent discharge point and wrapping around the shore to the east. Depending on the time of the observations and the specific tide range this may extend out into the main channel and reach across to the eastern shore of the Taunton River. The effluent plume has a smooth edge to the south and the orientation relative to the currents indicated this confinement and concentration of the thermal effluent was largely a function of the effect of the rising tide. With the falling tide the region of concentrated effluent expands relatively rapidly (11:12 am August 30, 1996; 14:11 to 15:34 September 11, 1998; 10:58 am August 19, 1997). The movement of the water at this stage is driven primarily by the flux of tidal water out of Taunton River. The expansion of this region of water with elevated temperatures occurs through approximately 180° of arc, down the bay as well as to the west across the relatively shallow shelf than comprises the majority of Mt. Hope Bay. The leading edge of the warm water pool is relatively smooth, suggesting that this water is more buoyant than the surrounding water and that it is over-riding. The trailing edge of the warm water pool is typically ill defined and grades irregularly into the ambient waters of the Taunton River.

By the midpoint of the falling tide (15:34 to 16:57 September 11, 1998; 12:45 pm August 30, 1996) the pool of warm water has expanded more and now consists of two distinct parts. There is the region of warm water that was pooled during high tide that has expanded across the bay and is 1-2°C warmer than the ambient background temperature. Connected to this is a warmer region of water that is relatively narrow and linear that connects back to the discharge point. In the August 1996 data, the warm pool has moved very rapidly down the bay, while in the other two data sets the pool is still largely within the upper regions of Mount Hope Bay. The linear region of warm water is 2-3°C warmer than the ambient background and has been deflected towards the western side of the bay by the tidal currents spreading across the shallow shelf of Mount Hope Bay. At low tide (2:11 to 3:28 pm, August 30 1996; 16:57-18:20 September 11,

1998) the warm pool has been dissipated and has poorly defined borders but is still visible as a distinct entity. Importantly, this diffuse region of warm water covers much of Mount Hope Bay and is approximately 0.5°C above the ambient temperature. The region of strongly warmed water near the discharge point is now deflected towards the center and eastern regions of the bay. At this point the plume exhibits a smooth leading edge its eastern side and a diffuse and irregular edge on its western side.

On the rising tide (6:00, 7:42, 9:24, 11:26 am, September 11, 1998) we observe the main element of the plume is dominated by the direct discharge from the power plant. The plume is narrow and well confined. It is observed to be deflected towards the east, into the main tidal channel of the Taunton River. The warm pool that was created during the previous tidal cycle and the distributed across Mount Hope Bay on the falling tide can still be observed as a diffuse region of water that is 0.25-0.5°C above the ambient temperatures of Mount Hope Bay (e.g. 9:24 am on September 11, 1998).

In two of the summer observations (August 19, 1997 and September 11, 1998) distinct thermal fronts can be observed between multiple time observations. The specific shapes of the fronts are preserved between time observations and permit the velocity of the surface currents to be estimated. Using the co-registered and geolocated remotely sensed data, we estimated two surface velocities for the August 19, 1997 observations of 35 and 45 m/sec. For the September 11 observations we estimated maximum velocities of 26, 23, and 34 m/sec for a front observed to move coherently between the 12:48, 14:11, 15:34, and 16:57 observations. While these are in general agreement with the 10-25 cm/sec velocities expected (Spaulding and White, 1990), they are all at the high end of the scale while the August 19 observations are considerably higher. The thermister data also allows the timing of thermal fronts to be identified and linked to water transport. Tracking the same fronts as seen in the thermal images with the thermisters indicates transport speeds of between 20 and 25 cm/sec. A dye study conducted to assess the travel time from the Fall River Wastewater Treatment Plant, located on the eastern side of Mt. Hope Bay (NETSU, 1989), provided some evidence of fast (≈ 50 cm/s) flows in the near surface waters (less than 1 m deep). The consistency of the remote observations demonstrating fast currents in the upper layers of the estuary with the observations from the dye study suggest that surface currents may be faster than previously thought.

The most important aspects of the distribution of thermal effluent over the course of a tidal cycle is that the effluent is distributed throughout Mount Hope Bay by the end of a complete cycle. The pool of warm water collected near the discharge point on the flood tide is observed to spread down and across the bay on the ebb tide and can almost be traced to the outlet to the main body of Narragansett Bay at the Mount Hope Bay bridge. Currents on the flood and ebb tides cause the plume to oscillate back and forth across the upper reaches of Mount Hope Bay. The net effect is that effluent from the previous tidal cycle can still be recognized at the beginning of the next tidal cycle. Thus a residual heating of the entire Mount Hope Bay is implied, consistent with the satellite observations that 36 km² of Mount Hope Bay shows an anomalous temperature of 0.8°C above the ambient.

To summarize these main observations:

- At the height of the flood tide, the thermal effluent from the power plant is concentrated in a small region immediately to the south and east of the effluent discharge point.

- On the ebb tide, the pool of warmer water moves southward in the bay with the tidal currents, and expands in size.
- At the mid-point of the ebb tide, the leading edge of the warmer water has been transported to a point approximately parallel to Spar Island or 3 km from the discharge point. Here the thermal front is on the order of 1-2°C. Velocities of this near surface layer of 20-35 cm/sec are implied.
- At the mid-point of the ebb tide, the pool of warmer water is effectively detached from the plume at the effluent discharge point. This plume has now been deflected to the west.
- By the end of the ebb tide, the leading edge of the warm water pool has reached the Mt Hope Bay Bridge, and the plume has begun to be deflected back to the east.
- At the beginning of a tidal cycle, waters warmed by the distribution of effluent from the previous cycle are evident. This indicates that effluent is efficiently redistributed over the course of a tidal cycle and that a net heating of Mount Hope Bay results.

Spring Observations

The distribution of thermal effluent due to tidal dynamics in the spring is considerably different than the summer (Figure 14). While there was only one measurement campaign on May 28, 1997, we have noted that the satellite observations in the winter and spring are notable in the apparent lack of thermal effects from the Brayton Point station. The explanation for this is evident from the May 28 overflight.

The weather conditions on the day of this acquisition were highly variable. The sky was essentially cloudless the entire day. During the morning, the winds were light and variable out of the northwest. By midmorning, the winds had dropped and it was dead calm. Then, around 12:00 pm, a strong southwest wind began to move up the bay from southwest to northeast. By 2:00 pm this had reached the location of the Brayton Point station. These weather conditions have a significant effect on our observations.

The first two observations are largely unaffected by the weather due to the early morning time and the light and variable winds. Here we see regions of relatively warm water in the shallow embayments of the Lee, Kickamuit and Cole rivers. A thermal front characterized by cooler water can be observed moving out of the Taunton River and across Mount Hope Bay towards the southwest. This is particularly evident in the 8:24 am data where the warmer water from the Cole River embayment are truncated by the overriding cooler water from the Taunton River. The actual plume associated with the thermal effluent from the power plant is virtually undetectable against this broad backdrop. While the temperatures near the outfall are among the warmest in the scene, the plume itself is very small and confined. This characteristic is maintained throughout the observations until the late afternoon.

The 10:13 am observation marks the period of extremely calm winds. Here we can see linear features across Mount Hope Bay which are in fact the wakes of boats which have disturbed the near surface thermal structure. With such calm conditions, a strong thermal gradient is established in the near surface waters which under ideal conditions may exceed 3-4°C across a vertical distance of less than 20 cm (Yokoyama et al., 1995). This is indeed what occurred at the time of the 10:13 am overpass. Detailed comparisons of the remotely measured skin temperature

and the in situ temperature at 20 cm showed a difference of 2°C. Thus these data are not particularly useful for identifying thermal fronts and their movements over time. A compound situation is observed in the 12:06 pm scene. The disorganized patterns of temperature in Mount Hope Bay reflect the changing conditions from dead calm to a developing southwest wind. At the extreme southwest corner of the scene, the winds have picked up mixing the strongly heated surface water with the cooler water below the surface. By the 2:09 pm scene, the winds have mostly mixed the surface waters, though a boat wake can be observed among the warm waters on the western boundary of Mount Hope Bay. By 3:20 pm, the strong thermal gradients have been removed and a reasonable measurement of the bulk surface temperature is possible. Thus the last four scenes provide the best view of the movements of water during this spring observation, with the caveat that there was a very strong southwest wind blowing throughout the afternoon.

The principal characteristics that define the thermal effluent at this time are that it is small, confined, and rapidly mixed into the ambient waters of Mount Hope Bay. The plume temperatures are comparable to warm waters in the shallow embayments of the Cole and Lee rivers. The confinement of the plume is particularly interesting, as there is virtually no mixing zone or gradation in temperature from the plume to the surrounding waters. Field data collected of the temperature and salinity of the water seem to offer an explanation. The effluent is higher in salinity than the receiving waters. This is because the cooling waters are taken from the bottom of the estuary (20 ft depth) and at this time of year the estuary is stratified due to the high flux of fresh water from the Taunton River. The temperatures are also quite low (average of 15°C). At these temperatures, salinity strongly controls the density of water. Thus despite the warmer temperatures, the effluent is denser than the surface water and sinks beneath the surface. It is not known how deeply the water sinks and whether it impinges upon the bottom. However, examination of the thermister data sets as well as hydrodynamic modeling suggests that the plume sinks to a level between the surface and the bottom and does not significantly impinge upon the bottom.

The wind conditions during this campaign significantly affected the observations. This included the anomalous heating of the near-surface during the calm morning period described above, as well as strong south west winds that occurred during the afternoon. These winds effectively pushed the surface water up Mount Hope Bay and limited any movement of the surface water. This observation is supported by measurements made of current drogues. These were deposited at the thermal front of the effluent at the time of high tide. Over the course of the afternoon, the positions of these drogues was tracked and mapped with a GPS. Despite the falling tide, these drogues maintained a position very close to their drop points, and some even moved up the bay into the Cole River embayment.

Another important environmental effect observed during this campaign was the heating of the estuary waters by solar radiation. Over the course of the day, the surface temperatures measured both remotely and by the thermisters placed at 20, 50, and 100 cm depth showed an increase in temperature of on the order of 3°C (Figure 15). While there was stratification developed during the calm period between 9:00 am and 12:00 pm, the volume of water heated (at least the upper 1 m) indicated the thermal input from solar radiation was substantial. In fact in all the remotely acquired measurements, the shallow embayments were consistently as warm or warmer than the water immediately adjacent to the discharge point for the thermal effluent. At the time these data were acquired (late May) the sun is very strong and high in the sky yet the water has not yet warmed to an equilibrium point with the thermal input from the solar radiation.

Thus it appear that solar radiation has a much greater impact than the effluent from the power plant on the diurnal and secular change in water temperature at this time of the year.

To summarize the main observations from the spring measurements:

- At slack low tide (6:47 am) plume is very short in length, narrow, and apparently has little effect on the surface temperatures: This pattern is maintained over the course of the flooding tide
- During the falling tide, the surface expression of the plume is more extensive and exhibits the same generally patterns as observed in the summer scenes, and satellite data:
 - Deflection to the west during the max ebb flow
 - Deflection back to the east towards the end of ebb flowHowever extent is less that summer observations
- Winds were calm in the morning, picked up from southwest in early afternoon and became strong: Typical water temperatures increased from $\approx 13^{\circ}\text{C}$ to $\approx 16^{\circ}\text{C}$ due to solar heating. Insitu and remotely sensed data agree.
- Surface tow data indicates that the plume is much denser ($4-5 \sigma^T$ units) than surface
- Best explanation: the plume water sinks below the surface during the flooding tide, less so during the ebbing tide, due to stratified water column in the upper reaches of Mt. Hope Bay
- Overall, the thermal effluent appears to have a minimal impact on the temperatures of Mount Hope Bay in the winter/spring months. This is supported by satellite imaging where the plume is rarely visible during this time of year.

Hydrodynamic Modeling:

Numerical Simulation of Mt. Hope Bay

Applied Science Associates (ASA) conducted hydrodynamic/thermal simulations of Mt. Hope Bay (MHB) to study the BPPS thermal effluent plume and to investigate the uses of remotely sensed and in-situ data for monitoring and modeling coastal waters using the WQMAP (Water Quality Mapping and Analysis Program) system developed by ASA. The application of numerical models and the collection of remotely sensed and in-situ data in the coastal environment has dramatically increased over the past few decades. The current state of data model coupling in the coastal environment is to calibrate the model to local conditions through both qualitative and quantitative comparisons between data observations and model predictions. This study provided a unique opportunity to develop and investigate coastal hydrodynamic data assimilation techniques. The application of data assimilation techniques has the potential to improve model accuracy and provide guidance on the efficiency on the monitoring effort in terms of instrument placement and sampling frequency. The synoptic collection of remotely sensed and in-situ field measurements will allow for not only individual but combined and comparative data set skill assessment.

WQMAP Modeling System

WQMAP is an integrated system for modeling the circulation and water quality of estuarine and coastal waters in a geographic information system (GIS) framework. The embedded GIS architecture allows WQMAP to be globally re-locatable and allows the user to input, store, manipulate, analyze, and display geographically referenced information. Figure 16 presents an example view of MHB within the WQMAP interface. The system also allows the user to generate boundary conforming grids to represent the computational domain, to perform simulations with a suite of circulation and water quality models and to display the model predictions in the form of time series plots, vector and contour plots, and color animations.

The WQMAP hydrodynamic model, (BFHYDRO) is a state-of-the-art, general curvilinear coordinate, boundary-fitted hydrodynamic model (Muin and Spaulding, 1997; Huang and Spaulding, 1995b; Swanson et al., 1989). The model is used to generate tidal elevations, velocities, and salinity and temperature distributions. The boundary-fitting technique matches the model coordinates with the shoreline boundaries of the water body accurately representing the study area. This system also allows the user to adjust the model grid resolution as desired. Development of the boundary-fitted model approach has proceeded over the last 15 years in a joint effort involving the University of Rhode Island and Applied Science Associates, Inc. (Spaulding, 1984; Swanson et al., 1989; Muin, 1993; and, Huang and Spaulding, 1995a). The model may be applied in either two or three dimensions depending on the nature of the problem and the complexity of the study.

The boundary-fitted method uses a set of coupled quasi-linear elliptic transformation equations to map an arbitrary horizontal multi-connected region from physical space to a rectangular mesh structure in the transformed horizontal plane (Spaulding, 1984). The three-dimensional conservation of mass and momentum equations, with approximations suitable for lakes, rivers, and estuaries (Swanson, 1986; Muin, 1993) that form the basis of the model, are then solved in this transformed space. In addition, an algebraic transformation is used in the vertical to map the free surface and bottom onto coordinate surfaces. The resulting equations are solved using an efficient semi-implicit finite difference algorithm for the exterior mode (two-dimensional vertically averaged) and by an explicit finite difference leveled algorithm for the vertical structure of the interior mode (three-dimensional) (Swanson, 1986).

The basic equations are written in spherical coordinates to allow for accurate representation of large model areas. The conservation equations in three dimensions, for water mass, momentum, energy (temperature) and constituent mass (salinity) form the basis of the model. It is assumed that the flow is incompressible, that the fluid is in hydrostatic balance, the horizontal friction is not significant, and the Boussinesq approximation applies.

The boundary conditions are as follows:

- At land, the normal component of velocity is zero.
- There is no salt or temperature transfer through land boundaries.
- At open boundaries, the free surface elevation must be specified and salinity and temperature are specified on inflow. On outflow, salinity and temperature are advected out of the model domain.
- A bottom stress or a no-slip condition can be applied at the bottom.
- There is no salt or temperature transfer through the bottom boundary.

- A wind stress is applied at the surface.
- No salt passes through the water surface.
- An energy balance boundary condition is applied at the water surface. The terms included are:
 - > shortwave solar radiation
 - > longwave atmospheric radiation
 - > longwave radiation emitted from the water surface
 - > convection (sensible) heat transfer between water and air
 - > evaporation (latent) heat transfer between water and air

The set of governing equations with dependent and independent variables transformed from spherical to curvilinear coordinates, in concert with the boundary conditions, is solved by a semi-implicit, split-mode finite difference procedure (Swanson, 1986). The equations of motion are vertically integrated and, through simple algebraic manipulation, are recast in terms of a single Helmholtz equation in surface elevation. This equation is solved using a sparse matrix solution technique to predict the spatial distribution of surface elevation for each grid.

The vertically averaged velocity is then determined explicitly using the momentum equation. This step constitutes the external or vertically averaged mode. Deviations of the velocity field from this vertically averaged value are then calculated, using a tri-diagonal matrix technique. The deviations are added to the vertically averaged values to obtain the vertical profile of velocity at each grid cell, thereby generating the complete current patterns. This constitutes the internal mode. The methodology allows time steps based on the advective, rather than the gravity, wave speed as in conventional explicit finite difference methods and, therefore, results in a computationally efficient solution procedure (Swanson, 1986; Swanson et al., 1989; Muin, 1993).

The salinity and temperature transport equations are solved by a simple explicit technique in the horizontal. The vertical diffusion term is solved by a three time level, implicit scheme to ease the time step restriction due to the small vertical length scale. The advection terms are solved using either an upwind-differencing scheme which introduces minor numerical (artificial) diffusivities and is first order accurate or the second order accurate QUICKEST formulation. Horizontal gradients in temperature, (as well as in salinity, density and pressure) are evaluated along lines of constant depth to reduce the artificial numerical dispersion in the vertical associated with the sigma transform system.

Application of Hydro-Thermal Modeling to Mt. Hope Bay

In order to properly represent the circulation and thermal dynamics within Mt. Hope Bay it was necessary to calibrate and verify the model. Calibration is an important step in the process of applying a model to a specific problem, particularly those models that contain many degrees of freedom. In general the calibration process is an organized procedure to select model coefficients to best match experimental data. The verification process is a confirmation that the chosen model coefficients are applicable to one or more independent data sets. This process required seasonal thermal and physical monitoring to map the BPPS thermal effluent plume and the circulation characteristics of Mt. Hope Bay in three dimensions. In order to accomplish this task four monitoring studies were conducted during the periods May-June 1997, August-September 1997, September 1998 and February-March 1999. The thermal mapping studies

consisted of thermistor strings distributed radially around the BPPSs outfall (Figure 10) and selected sites in the Lee, Cole and Taunton Rivers. This distribution provided high resolution in the area surrounding the outfall and decreased in resolution toward the mouth of Mt. Hope Bay. Each study used approximately 30 buoy-mounted thermistor strings with four to six thermistors per string, located at depths of 0.25, 0.5, 1, 2, 4, and 6m, recording temperature at five minute intervals. The model was calibrated to the August-September 1997 data set and verified using the remaining data sets. Tables 7 and Table 8 present a summary of temperature calibration statistics computed at three locations within MT. Hope Bay (Borden Flats, Brayton Point, and Gardners Neck). The computational grid (Figure 17) consisted of 11 layers in the vertical and had a horizontal resolution of 200-300m in most of the bay and high resolution of 50-100m in the vicinity of the powerplant.

Assimilation of In-Situ Data

The data assimilation study was conducted for the May-June 1997 field survey, which provided the longest and most complete data set. A baseline simulation in which no data was assimilated was run in order to obtain baseline statistical performance parameters. A statistical comparison between the model predicted temperature and thermistor measurements resulted in a maximum relative mean error of 9%, a maximum error coefficient of variation of 5%, minimum and maximum correlation coefficients of 0.39 and 0.79, respectively, and an average root mean square error (RMS) of 1.4°C. Figure 18 shows the RMS error between the baseline simulation and thermistor data at the surface, areas where no bars are present indicate that the thermistor data was incomplete relative to the length of the simulation. The RMS error is greatest in the region directly surrounding the outfall (thermistor strings 8, 9, 10, 11 and 12) and decreases as approach the mouth of the bay. Figure 19a-b presents a plan view of contoured thermistor data and model predicted temperature at the surface. The reasons for this error distribution becomes clear by examining the time series of the model predicted temperature and thermistor data at the surface near the outfall (Figure 20) and near the mouth of the bay (Figure 21). The motion of the thermal plume is governed by the semi-diurnal tide and capturing the proper phasing and extent of the plume in the near field surrounding the powerplant significantly impacts the results. However, the temperature data collected from the thermal mapping program should prove useful in adjusting the model to capture the near-field dynamics and improving the predictions in the far-field.

In order to distribute the discrete temperature observations over the computational domain a spatial interpolation scheme was required. The technique chosen for this study is based upon the method of successive correction as presented by Moore, et. al. (1987). Using this scheme, the model forecast is combined with the temperature observations within a region of influence determined by a correlation length scale. The new temperature at any grid cell is that predicted by the model plus a weighted mean of observational errors within the correlation region. The data assimilation scheme is then expressed as

$$T_i^{AN} = T_i^f + \frac{\sum_{k=1}^N \alpha_k (T_k^o - T_k^f)}{\alpha_p + \sum_{k=1}^N \alpha_k}$$

where the weighting coefficient α_k is defined as

$$\alpha_k = \exp\left\{-\left[\left(\frac{x_i - x_k}{a_x}\right)^2 + \left(\frac{y_i - y_k}{a_y}\right)^2\right]\right\}$$

if $|x_i - x_k| < a_x$ and $|y_i - y_k| < a_y$ otherwise the value is zero, where a_x and a_y are the correlation length scales in the longitudinal and latitudinal directions, respectively, T_i^{AN} is the analyzed temperature within a grid cell, T_i^f is the model predicted temperature within a grid cell, T_k^o is the observed temperature at the thermistor locations, and T_k^f is the model predicted temperature at a grid cell coincident with the thermistor observations. The term α_p is the weight assigned to the model predictions and was assigned the value of one. This corresponds to the new temperature, when the grid cell corresponds to the thermistor location and no other thermistors are within the correlation radius, being the average of the observation and model prediction.

The correlation length scale was kept constant for this study versus applying the above equation a number of times with successively smaller correlation length scales as in previous applications of this technique in the analysis of meteorological data for numerical weather forecasting (Cressman, 1959; Barnes, 1964; Lorenc, 1986). The correlation length scale was determined by developing a zero phase correlation matrix for all of the thermistor data at each depth and plotting it versus the corresponding distance matrix. Most of the results with a correlation coefficient above 0.8 were clustered within a distance of 0.5 NM (0.93 km) (Figure 22). This distance was chosen as the correlation length scale in both the longitudinal and latitudinal direction.

In order to determine the effectiveness of the scheme, two types of tests were developed. The first directly addresses the question of improving the model predictions, in a hindcasting and/or nowcasting sense, and studying the efficiency of the monitoring program. This was accomplished by varying the spatial distribution of thermistor strings while continuously assimilating the data and included cases where all the thermistor strings were used, only the even numbered strings, only the odd numbered strings, only strings at the open boundary and outfall (11 and 29), and five strategically chosen strings (6, 11, 13, 23, and 29). Refer to Figure 10 for thermistor string locations. The second tested the scheme's predictive capability by assimilating the data from all the thermistor strings and from only the outfall and open boundary for one day then ceasing the assimilation.

Figure 23 shows the RMS error between the model predictions and thermistor data at the surface, for the baseline simulation and the case where all 30 thermistor strings were continuously assimilated. As in the baseline simulation, the error is greatest in the area surrounding the outfall. However, the maximum error was reduced to 0.68°C compared to 2.73°C for the baseline simulation. The effect of assimilating all the thermistor data reduced the mean RMS error by 81% from 1.71°C to 0.32°C . A time series plot of the temperature in the region of the outfall at the surface (Figure 24) demonstrates the ability of the data assimilation scheme to improve model predictions in capturing the appropriate plume dynamics.

The results for the cases where only data from the even and odd numbered thermistor strings were assimilated was similar to those for the case where all of the thermistor data was used (Figure 25). The reduction in RMS error relative to the baseline simulation was 69% and 71% for the even and odd numbered thermistor string cases, respectively. This is an important step in evaluating the efficiency of the monitoring program, since the result of using 15 thermistors is almost equivalent to using all 30, the long-term cost of such a program could be dramatically reduced.

The next step was to test model predictions by assimilating data from only two representative thermistor strings located near the outfall and open boundary. The improvement was primarily seen in the region directly in front of the outfall, while those on the periphery saw

little improvement (Figure 26). The resulting reduction in the mean RMS error at the surface for this case was 35% relative to the baseline assimilation.

We also investigated the impact of assimilating the data from five strategically located thermistor strings (6, 11, 13, and 29). The result was a fairly uniform RMS error distribution throughout the bay (Figure 27), a desirable result, with a mean RMS error of 0.84°C at the surface. So, even though reducing the number of thermistor strings by a factor of six, a 51% reduction in the mean RMS error relative to the baseline simulation was still achieved.

This series of tests was designed to examine the forecasting capability of the data assimilation scheme. Since no time dependent term was included in the data assimilation scheme nor any feedback included to modify the model coefficients, the predictive capability was expected to be limited. Figure 28 shows the mean RMS error as a function of time for four cases: 1) the continuous assimilation of all the thermistor data; 2) the intermittent assimilation of all the thermistor data; 3) only two thermistor strings, located near the outfall and the open boundary, for one day; and 4) the baseline simulation. The mean RMS error of the continuous assimilation of all the data and the baseline simulation provide lower and upper bounds of the predictive capability tests, respectively. For cases where data was assimilated for only one day, there was a two-stage response. The first was an initial rapid increase of the error occurring on the order of 12 hours, which is also the dominant tidal period for Mt. Hope Bay. The second was a longer-term decay towards the baseline simulation on the order of days. This can be attributed to the data assimilation scheme effectively raising the bulk temperature of the bay and is clearly a function of the number of thermistor data sets assimilated.

Integration of Remotely Sensed Data

Processing of Remotely Sensed Data

The remotely sensed data calibrated to surface temperature were supplied to Applied Science Associates by Brown University in the form of GEOTIFF images. These images, which for practical purposes can be considered continuous data, must be sub-sampled to the computational hydrodynamic grid. The process was accomplished through the development of an Overflight Visualization and Analysis Extension for the ArcView Geographic Information System (GIS). The analysis extension allows the user to display a GeoTiff image (e.g. Figures 11-14) in order to visually assess the quality and spatial extent of the data, sub-sample an image to the hydrodynamic grid, and develop a transfer function between image values and water temperature. This application development focused on the May 28, 1997 data acquisition (Figure 14) and used primarily the time periods from 2:09 pm, 3:20 pm, 4:25 pm, 5:46 pm, and 7:02 pm. This was to use data that were not affected by the low wind speeds and excess surface heating observed in the data acquisitions from earlier in the day.

When a remotely sensed image is accepted, an overlay of the computational hydrodynamic grid is applied (Figure 29) and the image is sub-sampled to fill the computational cells with a single unique DN value (Figure 30). The sub-sampling is accomplished by determining the average DN value of the remotely sensed image pixels that fall within the bounds of a computational cell.

Once a set of remotely sensed images are accepted, a transfer function is required to connect the remotely sensed DN values to the water surface temperature. This function is created using the *in-situ* thermistor data (Figure 10). Values of surface thermistor measured temperature at the time of each chosen overflight is plotted versus the average DN value within a 5-pixel radius

surrounding the thermistor. A least squares regression analysis is applied to the data to create the transfer function. The transfer function is then applied to sub-sampled remotely sensed images resulting in data sets ready for model assimilation.

Assimilation of Remotely Sensed Data

The remotely sensed data chosen for assimilation was a series of five images taken over an ebbing tide on May 28, 1997 (Figure 14). Figure 31 shows the time of each image to the actual tide. The first remotely sensed image was taken just shortly after the tide begins to ebb (1409 EDT) with successive images at approximately one- to two-hour intervals (1520, 1625, 1746) with the last image being captured shortly after the tide begins to flood.

The sub-sampled remotely sensed images were assimilated into the model surface layer using a direct insertion technique. Direct insertion is the simplest method of data assimilation in which the model data is simply replaced by the measured data. This was deemed appropriate due to the spatial density of the remotely sensed data. Techniques do exist to propagate remotely sensed temperature data into the lower layers of a numerical simulation (Bennett, 1992). However, these techniques were developed for ocean modeling in which the stratification of temperature is reasonably well defined. Estuarine simulations such as this application present unique challenges in that thermal stratification of the water column is highly dependent upon environmental conditions such as river flow, solar radiation and weather patterns. This particular simulation is further complicated by the presence of a powerplant, which discharges its thermal effluent into Mt. Hope Bay.

A series of assimilation experiments were conducted in order to determine the temporal impact of various combinations of images. A baseline simulation was conducted in which no data was assimilated in order to determine baseline performance parameters. The performance parameter used is the mean temperature difference between the sub-sampled remotely sensed image and the numerical simulation at the time of each overflight. Therefore, a decrease in the performance parameter marks improved model performance. The temporal impact of assimilating the remotely sensed data can then be tracked by observing how quickly this measure returns to its baseline value. Table 9 presents a matrix of the assimilation experiments an "X" refers to data assimilated, while "--" refers to no data assimilated.

Remotely Sensed Data Assimilation Results

The results of the remotely sensed data assimilation experiments are presented in Table 10. The baseline simulation, in which no remotely sensed data were assimilated, has performance parameters ranging from 0.18 at 1520 EDT to 0.79 at 1902 EDT. Simulation May97ovt1, in which remotely sensed data were assimilated only at 1409 EDT, show dramatic performance improvement relative to the baseline simulation at 1520 EDT from 0.18 to 0.06. However, the effect of assimilating the remotely sensed data can no longer be seen by 1625 EDT where the performance parameter is 0.51 relative to a value of 0.59 for the baseline simulation. The performance parameters for simulation May97ovt2, in which remotely sensed data were assimilated at 1409 EDT and 1520 EDT, show no significant improvement over the baseline simulation. The performance parameters for simulation May97ovt3, in which remotely sensed data were assimilated at 1409 EDT and 1625 EDT, show an improvement at 1520 EDT from 0.18 to 0.06 and at 1746 EDT from 0.47 to 0.20 while at 1902 EDT the change is from 0.79 to 0.65. The performance parameters of simulation May97ovt4, in which the remotely sensed data was assimilated at 1409 EDT and 1746 EDT, again show marked improvement at 1520 EDT

from 0.18 to 0.06. However the improvements seen at 1625 EDT and 1902 EDT show less improvement from 0.59 to 0.51 and 0.79 to 0.64, respectively. Simulation May97ovt5, in which remotely sensed data was assimilated at 1409 EDT, 1520 EDT and 1625 EDT, showed a significant decrease in the performance parameter at 1746 EDT from 0.47 to 0.20, while the decrease at 1902 EDT was only 0.79 to 0.66. Simulation May97ovt6 assimilated all of the remotely sensed data except at 1902 EDT which showed a reduction in the performance parameter from 0.79 to 0.61.

The results of the remotely sensed data assimilation experiments show that simulations are significantly improved for approximately one hour after assimilation takes at which time the simulation sharply begins to return to the state of the baseline simulation. A clear example of this being simulation May97ovt1, where after assimilation takes place the performance parameter decreases by 67% (from 0.18 to 0.06) while shortly thereafter the performance parameter has decreased by only 14% (from 0.59 to 0.51). Also, the time of the tide also seems to play an important role in the performance of the data assimilation. For example, simulation May97ovt4 assimilates data at 1746 EDT and the performance parameter at 1902 EDT has only decreased by 19% while for simulation May97ovt1, where data is assimilated at 1409 EDT, the decrease in the performance parameter at 1520 EDT is 67%.

Modeling Results Summary

This study investigated assimilating in-situ thermistor measurements and remotely sensed thermal images into a three-dimensional baroclinic circulation model of Mt. Hope Bay, located in the northwestern portion of Narragansett Bay. The in-situ thermistor measurements were collected, during May-June 1997, using 30 buoy-mounted thermistor strings with four to six thermistors per string, located at depths of 0.25, 0.5, 1, 2, 4 and 6 m, recording temperature at five minute intervals. The remotely sensed thermal data consisted of five GEOTIFF images, prepared by Brown University, collected over an ebbing tide on May 28, 1997 at 1409 EDT, 1520 EDT, 1625 EDT, 1746 EDT and 1902 EDT.

The in-situ thermistor data was assimilated into the hydrodynamic model using the method of successive correction. This technique combines the model forecast with temperature observations within an area of influence determined by the correlation length scale of the data. The new temperature at any grid cell is then defined by that predicted by the model plus a weighted mean of observational errors within the correlation region.

Two types of tests were developed to determine the impact of assimilating the thermistor data on model performance and to study the efficiency of the monitoring program. The first set of tests were conducted by varying the spatial distribution of the thermistor strings while continuously assimilating data and included cases where all the thermistor strings were used, only the even numbered strings, only the odd numbered strings, only the strings at the open boundary and the outfall (11 and 29), and five strategically chosen strings (6,11,13,23 and 29). For these test the data assimilation scheme proved successful in improving the model predictions by reducing the RMS error by as much as 80% in a hindcast/nowcast mode. This result is useful in situations when an environmental monitoring-modeling program is required for regulatory concerns or a better understanding of the environment. The data assimilation scheme also proved useful in studying the efficiency of the monitoring program. By reducing the number of thermistor strings from 30 to 5 a 51% reduction in the mean RMS error relative to the baseline simulation was achieved. Using this technique has the potential to dramatically reduce the long-term cost of future programs of this type and still provide the error reduction advantages of data

assimilation. The second set of tests evaluated the assimilation schemes predictive capability by assimilating the data from all the thermistor strings and from only the open boundary and outfall for one day then ceasing the assimilation. This resulted in a two-stage response. The first was an initial rapid increase of the RMS error on the order of 12 hours. The second is a longer term decay of the RMS error towards that of the case of no data assimilation on the order of days.

The remotely sensed thermal data were assimilated into the hydrodynamic model using a direct insertion technique. Direct insertion is the simplest method of data assimilation in which the model data is simply replaced by the measured data. The use of this technique is justified due to the remotely sensed data being spatially continuous relative to the model resolution.

A series of numerical experiments were conducted to determine the temporal impact on the model performance by assimilating various combinations of remotely sensed images. The performance parameter for these tests was chosen to be the mean temperature difference between the remotely sensed data and the numerical simulation at the time of each overflight. The temporal impact of assimilating the remotely sensed data was then tracked by observing how quickly the performance parameter returns to a baseline value. The baseline value was determined by conducting a numerical simulation in which no data was assimilated. These tests showed that the assimilation of remotely sensed data provides limited model improvement over time. The simulations are improved for approximately one hour after assimilation takes place after which time the performance parameter quickly returns to that of the baseline simulation.

Suggested Future Activities

Three issues need to be addressed in order to efficiently assimilate remotely sensed data into coastal and estuarine models. The first is higher temporal resolution. The numerical experiment presented above show the time required between remotely sensed images can be no longer than one hour if increased model performance is expected. This can possibly be accomplished through the use of a geostationary satellite with the capability to capture images with a resolution between 100 and 1000 m. The second is rapid transfer of remotely sensed images to the modeling system. At the present time a significant number of steps are involved: georeferencing of the image, transformation of the image to an accepted file type, visual acceptance of the image quality and geographic region, calibration of the remotely sensed DN values to temperature data and finally discretization of the remotely sensed image to the hydrodynamic model computational grid. It is recommended that a focus be put on developing an automated system to accomplish these task through the use of artificial intelligence and further developing the science required to determine the ocean surface temperature from remotely acquired image DN values under all environmental conditions. The third issue involves the development of nontraditional data assimilation techniques. Since in the near future it is unlikely that geostaionary satellite will be dedicated to collecting environmental data continuously for a single estuary and there is a certain amount of uncertainty involved in the calibration of the remotely sensed data to actual surface temperatures the data contained in the remotely sensed images could be used in a pattern adjust mode. This would involve capturing features in the remotely sensed image such as the thermal plume from the Brayton Point Power station evident in Figure 14 (or Figures 11-13) and adjusting the hydrodynamic model to conform to this pattern without actually ingesting any temperature data.

Evaluation of Hyperspectral Data for Estuarine Water Characterization

Visible-near infrared reflectance spectra of coastal and estuarine waters are a complex convolution of the optical properties of water, phytoplankton, gelbstoff, dissolved organic matter, and suspended sediment. Our long term goals are to develop quantitative methods for extraction of the physical abundances of these contributing constituents to the observed reflectance spectra. The work consists of observations with airborne sensors such as AVIRIS and insitu measurements using water samples, towed salinity, temperature, and fluorescence sensors, and field spectra obtained with portable spectrometers. In this paper, we report on results of calibration and reflectance modeling of AVIRIS data obtained on August 19, 1997. The data discussed here were obtained at 10:58 and 11:22 EDT on a flight path from the north to the south along the eastern and western borders of the bay (Figure 32). The solar zenith angle was 55.5° and the solar azimuth was 141° .

AVIRIS Data Calibration

The goal of calibration was to provide the best estimate of reflectance for all the AVIRIS data. Radiometrically corrected data were provided by the AVIRIS Data Facility. Data were acquired as 12-bit and converted to units of radiance in units of microwatts per square centimeter per nanometer per steradian, or $\mu\text{W} / (\text{cm}^2 * \text{nm} * \text{sr})$, using inflight and ground calibration files. AVIRIS radiometric calibration factors are calculated by measuring the response of AVIRIS to an integrating sphere (a known target illuminated by a known light source). This calibration is reported to be accurate to within 7%, absolute, over time while intra-flight accuracy is within 2%.

Accurate calibration of radiance to reflectance over water targets is challenging, since up to 90% of the measured radiance can be contributed by sources other than water. The AVIRIS radiance data over Narragansett Bay exhibited two such sources that varied spatially across the scene; one was a phase angle dependent variation in the path radiance (Figure 33) and the other a fresnel reflection off water surfaces optimally oriented with respect to the solar incidence angle and the viewing angle. Both these sources are additive to the total radiance and the spatially dependent properties need to be removed prior to the reflectance calibration. The spectral properties of these sources were characterized empirically using the fact that large regions of the scene were occupied by water with relatively homogeneous spectral properties. Thus any variations in radiance would be due to the phase angle dependent path radiance and fresnel reflections. Radiance spectra from regions that exhibited minimal effects from these sources were subtracted from radiance spectra from regions exhibiting maximum effect to derive the spectral signatures of phase-angle dependent path radiance and fresnel reflection off the water. These signatures were then used to derive magnitude coefficients on a pixel by pixel basis for the entire scene. The magnitude coefficients thus determine the amount of these sources to remove from each pixel. A representative result of this approach is shown in Figure 34.

A number of approaches were examined for reducing the AVIRIS calibrated radiance data to reflectance, including atmospheric modeling, empirical line calibration, and an empirical radiance calibration. Atmospheric modeling was performed using the ATREM model. However, due to a lack of adequate characterization of the atmosphere, the resulting spectral shapes were unsatisfactory, particularly at shorter wavelengths. Though typical land cover units exhibited realistic spectral shapes (e.g. vegetation, soils), the spectra for the estuary were unlike any field spectra that we had obtained to date. An empirical line calibration was attempted. However, this resulted in systematic features in the water spectra unrelated to the spectral properties of water. In essence, the gain and offset corrections were weighted towards the noise

statistics of the low albedo calibration target. Projection to the even lower albedo properties of water resulted in the unacceptable spectral features.

Fortuitously, several small low altitude cumulous clouds were present in the AVIRIS flight line. These cast shadows over both land and water. Radiance spectra were extracted from shadowed and unshadowed regions of approximately similar terrain cover and analyzed. Regardless of terrain cover, all the shadowed spectra exhibited a consistent spectral shape between 0.4-0.8 μm , and ratios of the various shadowed terrains to shadowed water produced a relatively flat ratio spectrum. Furthermore, ratios of the shadowed regions to unshadowed regions produced relative spectra that exhibited a $1/\lambda^4$ dependence. Shadowed regions are thus dominated by the global path radiance in the scenes and we propose that shadowed water can provide a first order estimate of path radiance.

Cumulous clouds scatter light very efficiently in the 0.4-0.8 μm region without any significant absorptions. They can therefore provide a first order estimate of solar radiance. To provide a first order estimate of reflectance we therefore subtract the spectrum of shadowed water, with a small reduction to account for reflected sky irradiance (basically attenuate the spectrum by a factor of 0.95) from every pixel in the scene, and divide by the spectrum of a homogeneous cloud, which also has had the estimate of path radiance removed. Carder et al. (1992) presented an approach based on the same concept but with a more thorough development of the radiance contributions for all sources. This was used to constrain a radiative transfer model for the calculation of reflectance and they showed the cloud-shadow approach has merit in the calibration of hyperspectral data in aquatic environments.

Assessment of Calibration

The simple approach to calibration provided remarkably clean spectra of the estuary that are highly consistent with reflectance spectra measured insitu. This is illustrated in Figure 35. The AVIRIS spectra are 3x3 pixel averages selected from regions representative of the typical estuarine waters. The field spectra were acquired with ASD portable spectrometers using a 20% reflective Spectralon target as a standard and corrected for the absolute reflectance of the standard. We see that the AVIRIS spectra reproduce the main important characteristics of the field spectra of the estuary: strong chlorophyll absorption between 0.4 and 0.55 μm , strong drop in reflectance after 0.58 μm due to increased water absorption, the presence of a small chlorophyll absorption near 0.67 μm , and chlorophyll fluorescence between 0.67 and 0.71 μm . These spectra are also comparable to estuarine spectra collected by other researchers (e.g. Roesler and Perry, 1995).

Inverse Model and Analysis

The high quality of the AVIRIS hyperspectral data shown here provide the opportunity to perform inverse modeling of reflectance to obtain constituent properties remotely. There have been a number of analytical algorithms developed for this purpose (e.g. Carder et al., 1991; Lee et al., 1994; Roesler and Perry, 1995; Hoge and Lyon, 1996). For this analysis we employ the approach of Roesler and Perry (1995), discussed briefly below.

Remote sensing reflectance (ratio of radiance measured in a particular solid angle to the downward irradiance) of coastal and estuarine waters is primarily governed by the optical properties of water, phytoplankton, organic matter (tripton, gelbstoff), and suspended sediment. The reflectance is defined by the ratio of the backscattering properties of these optical components to the absorbing properties. Roesler and Perry (1995) simplified the basic radiative transfer theory to arrive at the fundamental relationship:

$$R(\lambda) = G \frac{\sum_j M_j b_j(\lambda)}{\sum_i M_i a_i(\lambda)} \quad (1)$$

where λ is wavelength, R is the reflectance, G accounts for the angular dependence of the upward light field, b_j and a_i are the backscattering and absorption coefficients for the j th and i th components in the water, and M_j , M_i are the magnitudes of the contribution of those components to the measured reflectance. To perform inverse modeling of reflectance to obtain the relative contributions of the optically active components, this equation needs to be solved for the magnitude parameters. Furthermore, some knowledge of the optical properties of these components is required.

The absorption and backscattering properties of pure water are relatively well known and most researchers use the values published by Smith and Baker (1981). The magnitude of the water contributions of backscatter and absorption are fixed to be 1.0. The optical properties of phytoplankton, dissolved organic matter, and suspended sediment vary with location, season, and over the course of tides. Nevertheless, the backscattering and absorption properties of organic matter vary within a relatively narrow range over the visible to near-infrared wavelength range and can be reasonably approximated by simple functions of wavelength. For this application we ignore suspended sediment. This is a reasonable approximation for some regions of Narragansett Bay which is fed by mature rivers with virtually no bedload or suspended sediment. However, in regions of strong tidal currents, sediment may be re-suspended from the bottom.

Phytoplankton absorption is known to vary with pigment concentration, packing, and composition (Sathyendranath et al., 1987; Bricaud et al., 1988). In addition, solar-stimulated chlorophyll fluorescence contributes to the measured reflectance, but varies with phytoplankton production. One approach is to use known phytoplankton absorption coefficients to invert the optical model. However, this limits general application and requires a library of local phytoplankton absorption. In addition, phytoplankton species vary seasonally and spatially in estuaries, complicating the building of such libraries. The model of Roesler and Perry (1995) employs novel techniques to simultaneously account for fluorescence and variable phytoplankton absorption through a three-step model inversion.

Solutions to equation (1) are obtained by simultaneous inversion over the number of wavelengths to determine the values of M for the absorption and backscattering basis vectors. The basis vectors used are shown in Figure 36. Because this is a nonlinear equation, we employ the Levenberg-Marquardt method (Press et al., 1986), setting the values for water equal to 1. The first set of iterations to a solution provide a first-order estimate of the reflectance, using a prescribed value for the phytoplankton absorption spectrum. We use only the wavelengths up to 660 nm to avoid contributions from chlorophyll fluorescence affecting the solutions. In the second step, contributions from chlorophyll *a* fluorescence are determined as the difference between the measured and modeled reflectance over the wavelength region 660-730 nm. The solutions provide values of the concentration of optical constituents and the fluorescence activity. Example solutions are shown in Figure 37 for two different water types.

Roesler and Perry (1995) demonstrated that this method allowed them to consistently invert reflectance spectra to the relative magnitudes of the various optical components, as well as an estimate of the specific phytoplankton absorption coefficient spectrum for aquatic environments

ranging from open ocean to estuarine. We have successfully applied this model to AVIRIS data calibrated using the methods described in this paper. Example results for the concentration of phytoplankton and the activity of phytoplankton (fluorescence) are shown in Figure 38. While there is a general correspondence between high chlorophyll and high fluorescence, also note that there are regions where there is high fluorescence but moderate chlorophyll and vice versa. High fluorescence generally indicates very active photosynthesis and thus may be a good indicator of ecosystem health. Additional results of model applications to AVIRIS data over the Narragansett Bay will be presented at the meeting.

Summary for Hyperspectral Analysis

The very high fidelity of AVIRIS data afford the opportunity to apply deterministic models to remote acquired data over relatively large regions. AVIRIS data acquired over Narragansett Bay, RI in August, 1997 were calibrated to reflectance, taking into account spatially variable contributions from path radiance and fresnel reflectance. A simple cloud-shadow approach was used to derive estimates of global path radiance and downward irradiance. This provided an estimate of reflectance that was highly consistent with reflectance spectra acquired with a field spectrometer. The complications of deterministic models in Case II waters has long been recognized, due to the high concentrations of chlorophyll and organic matter, suspended sediment, and highly variable phytoplankton species and optical properties. The analytical mixing model of Roesler and Perry (1995) offers the promise of simultaneous determination of the concentrations of optically active components as well as the absorption spectrum of the most dynamically variable of these components, chlorophyll. Application of this model to the calibrated AVIRIS data is very promising, offering not only the concentrations of key optically active species, but also the activity of phytoplankton through the fluorescence parameter. Our future plans are to validate the modeling through field research and to apply this model to additional AVIRIS scenes over this estuary.

Commercial Product Integration

Introduction

The potential application of the thermal mapping and modeling research performed for this study continues to be monitoring thermal plumes, particularly from power generation plants. These facilities discharge large quantities of heated effluent and provide a strong thermal signal above ambient conditions. The thermal signature is easily acquired by one or more thermal bands and can be used to estimate the size of the zone of elevated temperatures. The problem with either satellite or aircraft based systems, however, is the temporal sampling frequency. This frequency is too low to provide a sufficient level of monitoring for the extent of a thermal plume. In coastal systems where tidal forces dominate, a sampling frequency of hours is necessary as opposed to days or weeks with satellite return periods.

This under sampling can be ameliorated by interpolating conditions between observations. Since the process (tidal) time scale is much shorter than the acquisition time scale it is necessary that the interpolation account for the process time frequency. One such approach is to use numerical hydrothermal models that simulate the distribution of temperature. Such a model deterministically solves the underlying equations governing fluid flow and the distribution of heat. This methodology can then interpolate between observed temperature distributions from

satellite observations to provide a time history of temperature at a reasonable resolution. Data assimilation of observations into models has been shown in this study to be an accurate technique to minimize differences between model predictions and satellite (or aircraft) observations.

The second problem that prevents widespread use of remotely sensed observations is the level of accuracy possible without ground truth information to calibrate the observations. The obvious solution is the use of in situ temperature observations. In fact the use of in situ observations is also critical in the successful calibration of numerical hydrothermal models. Thus a well-designed in situ observation program provides critical information to both the remotely sensed data and the model predictions.

The third problem is that the thermal signal acquired by satellite is a measure of the water surface temperature and thus does not necessarily provide subsurface temperature information. The use of in situ data and a three-dimensional hydrothermal model in this study has been successfully shown to provide accurate three-dimensional estimates.

It is with this three pronged approach of high spatial but low temporal resolution satellite data, low spatial but high temporal resolution of in situ data, along with the mid to high spatial and temporal resolution of hydrothermal model predictions that provide a solution to the monitoring of thermal plumes.

Market Needs for Thermal Related Overflight Information

The primary need for information on the extent of thermal plumes is related to the generator of such plumes, usually an electrical generating facility with once through cooling. The facility used for this study generates 1600 MW of electricity and discharges 925 mgd of heated effluent with a temperature rise of 10 to 15 °F. These types of facilities require permits to withdraw water discharge the heated effluent to adjacent water bodies. Historically the permits were written with restrictions on maximum flowrate, temperature rise and, often, total heat rejected over a specified time period. Additional requirements might define a mixing zone, the edge of which must not exceed a given temperature rise. An additional or alternative requirement might be for the permitting agencies to require monitoring of the thermal distribution by the permittee to assure that the plume stays in compliance with specified mixing zones.

Likewise the operators of the facility could use the thermal mapping and modeling system to evaluate and predict the amount of electricity they could generate by optimizing generation to predictions of the plume. For instance during neap tides the plume may not move far from the plant offering the potential for increased generation without exceeding the limits of their permitted mixing zone. Conversely during spring tides the plant operator may have to cut back to ensure compliance. For facilities located on river systems, the optimization would be controlled not by tides but by predictions of air temperature and solar radiation affecting the receiving water body. For facilities located on lakes, an additional factor may be the wind-induced circulation that will affect the plume extent.

Other potential users, besides permitting agencies and facilities with thermal discharges, of thermal mapping and modeling systems include the following:

- Recreational users of water bodies and / or weather forecasters that would supply such information in addition to their meteorological forecasts. As atmospheric forecasts are important so would be an aquatic forecast.
- Commercial users of water bodies that want to know the thermal structure. Fishermen want to optimize their harvest potential (some species are attracted or repelled by

different water temperatures). The aquaculture industry is concerned about the variability of temperatures to time their harvest, to determine whether their crops may be adversely affected by extremes, or to site new facilities.

- Environmental and educational groups that want to monitor a water body to educate the public on the temperature variability that occurs and perhaps seek changes (if the variability is related to anthropogenic causes).
- Environmental managers that have special requirements concerning the temporal and spatial temperature regime of a water body. Restoration efforts often require that temperatures be appropriate for the intended restoration, just as water quality or salinity is.

Specific Uses by the Commercial Partner (ASA)

Applied Science Associates (ASA) has been involved in the development of analysis techniques and computer models to simulate physical, chemical and biological processes in aquatic environments since its inception in 1979. With the simultaneous advent of low cost computing platforms (personal computers) and improved techniques (boundary fitted grids, etc.) to model environmental processes, ASA has been successful in building a market for both products and services related to use of its modeling tools. ASA presently focuses on three major areas: hydrodynamic and water quality modeling (including thermal), oil spill modeling, and biological impacts modeling.

Remotely sensed thermal data offers another tool to evaluate the effects of temperature in aquatic environments. ASA has performed a number of studies that involved the estimation of thermal plume extent. Specifically ASA has been retained to predict the resulting thermal plume under different loading scenarios. This has most often involved either the re-permitting of existing facilities or the seeking of permits for expanded facilities. The first step in these analyses is to determine present conditions so that a predictive hydrothermal model can be calibrated. A field program is performed using a series of thermistors measuring temperature at selected locations and depths for a period of time. This data lacks the synoptic view that remotely sensed data can provide. Such remotely sensed data, taken during the deployment period of the thermistors, provides an additional and important means of model calibration. A more complete characterization of present thermal conditions is possible thus allowing a better understanding of the physical processes controlling the distribution of heat in the water body.

For larger projects that require a more accurate estimate of the thermal distribution under proposed new loading scenarios, the level of analysis requires that additional model validation be undertaken. This approach uses an independent data set preferably acquired under different environmental conditions than existed for the calibration data set. A set of remotely sensed data, preferably sampling the important process frequencies (usually tidal in coastal environments) would provide a more complete synoptic characterization.

As noted in the earlier sections the use of observations, whether in situ or remote, assimilated into predictive models is well tested. Various techniques are available and some have been used in this study. These techniques can be used in a semi automatic mode (i.e., some can be implemented automatically without expert human intervention, while others cannot). That being the case, a two-pronged approach for commercialization is possible. The first is the development and marketing of a set of tools that will ingest the remotely sensed data, quality assure and process it, and assimilate it into a predictive model. It is expected that such a software system will not be ready until some years in the future. The other approach is to market the processing

service and provide end product nowcasts or forecasts. This approach allows for a phased development of tools and appears preferable until the software becomes more mature.

The clear strength of using remotely sensed data to estimate the extent of thermal plumes is its ability to provide a synoptic view over a large surface area. This allows the analyst to better understand the physical processes affecting the plume by showing in detail the spatial thermal patterns. Under certain environmental conditions, the residual plume from earlier times can also be discerned, giving some indication of the temporal changes.

The clear weaknesses of using remotely sensed data to estimate the extent of thermal plumes are its inability to provide information of the vertical structure and temporal variation. The sensors measure the bulk surface temperature, which varies in thickness depending on the mixing energy in the surface layer. No information can be deduced about subsurface temperature distributions. It is only with in situ data and a hydrothermal model that the full three dimensional structure of the thermal plume can be determined.

The inability of present sensor platforms to remain stationary over the area of interest and provide temporal variation consistent with the environmentally important time scales is also a limiting factor. For instance this study has shown that the forecast of the thermal plume location begins to degrade after only an hour in a tidal environment. Multiple overflights with aircraft based sensors would solve this problem but it requires that the aircraft spend enough time on site to provide information on plume location throughout the tide cycle. Since spacecraft orbits allow a return to the same site on the order of a week or more, such repetition is not useful at tidal time scales.

The present study of the use of remotely-acquired thermal data as a data source for thermal plume prediction has proved valuable for ASA. This data, when combined with in situ data, provides a synoptic three-dimensional view of the plume, and is useful both in understanding the physical processes that affect the plume as well as assimilating the data into a prediction hydrothermal model. The ability to use this information has allowed ASA to become more competitive in providing understanding and, ultimately, solutions to the problem of prediction thermal plume extent. We expect to propose this technology in similar projects as it adds another perspective on the problem. For larger projects, particularly, the potential costs of this approach are within the range of resources usually expended.

STATE OF RHODE ISLAND AND PROVIDENCE PLANTATIONS

**Department of Environmental Management
OFFICE OF WATER RESOURCES
235 Promenade Street
Providence, Rhode Island 02908-5767
(401) 222-3961
(401) 521-4230 (FAX)
(401) 831-5508 (TDD)**

September 21, 2000

To Whom It May Concern

I am pleased to provide a brief discussion of the State's response to the results of the NASA-Brown-ASA-RI collaborative study using modern remote sensing for environmental issues related to Narragansett Bay.

Through the efforts of Dr. John Mustard and ASA , RIDEM gained a much clearer understanding of the extent of temperature-linked impacts to Mount Hope Bay waters in RI from a large power plant at Brayton Point in Somerset, MA.

The work completed under this cooperative project was invaluable to the state of Rhode Island, and in particular to the RI Department of Environmental Management in recent discussions with USEPA, MA, and the power company concerning permit renewal issues and the impact of the facility on RI waters.

Results of the infra-red remote sensing analyses of upper Narragansett Bay and Mount Hope Bay helped guide the state in recommendations for permit renewal requirements , including objective ground-truth monitoring of remote sensing results and modeling studies.

The more recent hyperspectral work will likely play a role in the state's efforts to understand impacts of excess nutrients to Narragansett Bay. From the remote sensing analyses, it is clear that the urbanized areas of the Bay show geographically distinct signals of high primary productivity. Such areas are significant organic loads, and cause significant decreases in dissolved oxygen levels during summer temperatures. This work will complement RIDEM's ongoing efforts to develop a nutrient model and load reduction plan.

RIDEM sees great benefits in these technological tools, and expects to incorporate more such analyses into complex regulatory environmental impact analyses and management issues.

Sincerely,



Angelo Liberti
Chief
Surface Water Protection

Publications and Presentations Resulting from This Work

Project Web Site:

(www.planetary.brown.edu/~mustard/apurva/index.html)

Peer Reviewed Publications

- Mustard, J. F., M. Staid, and W. Fripp, A semi-analytical approach to the calibration of AVIRIS data to reflectance over water: Application to a temperate estuary, *Remote Sensing of Environment (in press)*, 2000.
- Mustard, J. F., M. Carney, and A. Sen, The use of satellite data to quantify thermal effluent impacts, *Estuarine, Coastal, and Shelf Science*, 49, 509-524, 1999.
- Mustard, J. F., A. Sen, C. Swanson, D. Mendelsohn, and C. Deacutis, Integration of remotely sensed data and hydrodynamic modeling into a GIS to assess the impacts of thermal effluent in an estuary, in *Proc. 4th International Conference on Remote Sensing for Marine and Coastal Environments*, II-34-II-43, 1997.
- Swanson, J. C. and Ward, M. C., Improving coastal model predictions through data assimilation, in *Proc. 6th International Conference on Estuarine and Coastal Modeling (ECM6)*, November 3-5, 1999, New Orleans, LA.

Abstracts for Professional Meetings

- Mustard, J. F., M. Staid, and W. Fripp, Atmospheric Correction and Inverse Modeling of AVIRIS Data to Obtain Water Constituent Abundances International Symposium on the Digital Earth,, Beijing, China 1999
- Mustard, J. F., M. L. Staid, and W. Fripp, Atmospheric correction and inverse modeling of AVIRIS data to obtain water constituent abundances, The AVIRIS Earth Science and Applications Workshop, http://makalu.jpl.nasa.gov/docs/workshops/99_docs/44.pdf, 1999.
- Mustard, J. F. and W. L. Prell, Diverse spectral properties in a temperate estuary: First results from Narragansett Bay, Rhode Island, Summaries of the 7th JPL Airborne Earth Science Workshop, (R.O. Green ed), JPL Publication 97-21, Vol. 1, 1998.
- Mustard, J. F., W. L. Prell, C. Swanson, and H. Rines, Seasonal Dependence on the Buoyancy and Dissipation of a Thermal Plume in a Confined Estuary, *EOS, Trans. Amer. Geophys. Union*, v 78, 1997.
- Swanson J. C., D. Mendelsohn, H. Rines, J. Mustard, and R. DeHart, Effects of an electric power generating facility on the circulation in a shallow estuary, *Estuarine Research Foundation 14th International Conference*, p. 179, 1997.
- Carney, M., and J. F. Mustard, Surface temperatures in Narragansett Bay: Seasonal dynamics and anthropogenic effects, *Estuarine Research Foundation 14th International Conference*, p. 31, 1997.
- Mustard, J. F., W. L. Prell, A. Sen, M. Carney, and C. Swanson, The impact of thermal effluent in a confined estuary: Remote sensing observations and models, *Estuarine Research Foundation 14th International Conference*, p. 130, 1997.

Presentations

- *The Dynamics of Thermal Effluent from the Brayton Point Power Plant*, Mt. Hope Bay Research Forum, Mass. Coastal Zone Management, Executive Office of Environmental Affairs, 6/24/97
- *Seasonal and Tidal Dynamics of Thermal Effluent in the Mt. Hope Bay Estuary*, Environmental Protection Agency, Atlantic Ecology Division, Narragansett RI, 8/97
- *Application of Remotely Sensed Data to Environmental Problems in Narragansett Bay*, Dept. Ecology and Evolutionary Biology, Brown University, 9/97.
- *Impact of Brayton Point thermal effluent on the Mt. Hope Bay estuary*, Environmental Protection Agency, Boston MA, December, 1998.
- *Impact of Brayton Point thermal effluent on the Mt. Hope Bay estuary*, Rhode Island Department of Environmental Management, December, 1998.
- *Quantifying Thermal Impacts of Effluent with Remotely Sensed Data*, Environmental Protection Agency, Research Division, Lexington MA, January, 1999.
- *Remote Sensing of the Narragansett Bay Waters: Progress and Promise*, invited talk to the symposium "Integrating science in the decision making process: Managing estuarine habitats in Narragansett Bay, Northeast Regional GSA Meeting, March, 1999
- *Hyperspectral Remote Sensing of Estuarine Waters*, University of Rhode Island, Graduate School of Oceanography Biological Oceanography colloquium, April, 1999.
- *Water Quality Information from Remotely Sensed Data*, invited speaker for the 1999 Environmental Expo special session on advances in hydrodynamic analyses, May, 1999.
- *Remote Sensing for Monitoring Estuarine Dynamics*, EMAP Symposium 2001, 4/2001.

Student Theses:

Masters

- A. Sen, MSc, Environmental Studies 1997, (Joint with S. Hamburg)

Undergraduate Senior Theses

- A. Sen, '96, Senior Thesis in Environmental Science (with S. Hamburg)
- G. Proctor, Senior Thesis, Geological Sciences, '97 (Prell)
- M. Carney, Senior Thesis Environmental Science, '97 (Hamburg, Prell)
- E. Wolf, Senior Thesis, Geological Sciences, '98.5 (Prell)

REFERENCES

- Adams, J. B., M. O. Smith, and A. R. Gillespie. 1993. "Imaging Spectroscopy: Interpretations Based on Spectral Mixture Analysis." *Remote Geochemical Analysis: Elemental and Mineralogical Composition* (C. M. Pieters and P. A. Englert, Eds.), 145-166.
- Avery, T. E. & G.L. Berlin. 1992. *Fundamentals of Remote Sensing and Airphoto Interpretation*, 5th Ed. Prentice Hall: Upper Saddle River, NJ.
- Barnes, S.L., 1964. A technique for maximizing details in numerical weather map analysis, *Journal of Applied Meteorology*, Vol. 3, pp. 369-409.
- Bricaud A., A. Bedhomme, and A. Morel, "Optical properties of diverse phytoplankton species: Experimental results and theoretical interpretation," *J. Plankton Res.*, Vol. 10, pp. 851-873, 1988.
- Carder K. L., S. K. Hawes, K A. Baker, R. C. Smith, R. G. Steward, and B. G. Mitchell, "Reflectance model for quantifying chlorophyll a in the presence of productivity degradation products," *J. Geophys. Res.*, Vol. 96, pp. 7457-7466, 1994.
- Carder K. L., P. Reinersman, and A. R. F. Chen, "AVIRIS calibration using the cloud-shadow method," *Summaries of the Fourth Annual JPL Airborne Geoscience Workshop*, (R. O. Green, ed.) JPL Publication 92-14, vol. 1, pp. 26-28, 1992
- Chinman R.A. and S. W. Nixon. "Depth-Area-Volume Relationships in Narragansett Bay. Graduate School of Oceanography, the University of Rhode Island". *NOAA/Sea Grant Marine Technical Report 87*, 1985.
- Cressman, G.P., 1959. An operational objective analysis system, *Monthly Weather Review*, Vol. 87, pp. 367-374.
- Dallaire T., Letter to Craig Swanson dated 4 Oct. 91 containing description of field data, Massachusetts Department of Environmental Protection, Worcester, MA, 1991.
- Dixon, A. M., C. Karp, & C. Penniman. 1991. Mount Hope Bay Briefing Paper and Proceedings from Narragansett Bay Project Management Committee. Narragansett Bay Project Report 91-65.
- Footy, G. M, Campbell, N. A., Trood, N. M. & Wood, T. F., 1992 Derivation and applicatins of probabilistic measures of class membership from the maximum-likelihood classification, *Photogrammetric Engineering and Remote Sensing*, **58**, 1335-1341.
- Gibbons, D. E., G.E. Wukelic, J.P. Leighton, & M.J. Doyle. 1989. Application of Landsat Thematic Mapper Data for Coastal Thermal Plume Analysis at Diablo Canyon. *Photogrammetric Engineering and Remote Sensing*, 55(3): 903-909.
- Gibson M. R., Comparisons of trends in the finfish assemblage of Mt. Hope Bay and Narragansett Bay in relation to the operation at the New England Power Brayton Point station, *RI Division Fish and Wildlife Research Reference Document 95/1*, 39 pp, 1996.
- Hamburg, S. P. 1984 Organic matter and nitrogen accumulation during 70 years of old-field succession in central New Hampshire., Ph.D. Tehsis, Yale University, 278pp.
- Hargrove, W. W. & J. Pickering 1992. Psuedoreplication: A sine Qua Non for regional ecology, *Landscape Ecology*, 6, 251-258.
- Huang, W. and M. Spaulding, A three dimensional numerical model of estuarine circulation and water quality induced by surface discharges, *ASCE Journal of Hydraulic Engineering*, 121: (4) April 1995, p. 300-311, 1995a.
- Huang, W. and M. Spaulding, Modeling of CSO-induced pollutant transport in Mt. Hope Bay, *ASCE J. of Environmental Engineering*, Vol. 121, No. 7, July, 1995, 492-498, 1995b.
- Hode and R. P. Lyon, "Satellite retrieval of inherent optical properties by linear matrix inversion of oceanic radiance models: An analysis of model and radiance measurement errors," *J. Geophys. Res.*, Vol. 101, pp. 16631-16648, 1996.
- Hurlbuert, S. H. 1984. Psuedoreplication and the design of ecological field experiments, *Ecological Monographs*, 54, 187-211.
- Jahne, B., 1991. *Digital Image Processing*. Springer-Verlag, New York, 250 pp.

- Jain, A. K. 1989. *Fundamentals of Digital Image Processing*, Prentice Hall, New Jersey, 500 pp.
- Jeffries H. P., The impacts of warming climate on fish populations, *Maritimes*, Vol. 37, No. 1, pp. 12-15, 1994.
- Jensen, J. R. 1996 *Introductory Digital Image Processing: A Remote Sensing Perspective*, Simon and Schuster, New Jersey, 316 pp.
- Kremer, J.N. and S.W. Nixon, *A Coastal Marine Ecosystem*, New York: Springer-Verlag Berlin Heidelberg, 1978.
- Lin, P. and H. A. Regier, "Use of Arrhenius models to describe temperature dependence of organismal rates in fish", In *Climate Change in Northern Fish Populations*, ed. R. J. Beamish, Can. Spec. Pub. Fish. Aquat. Sci., p. 121, 1995.
- Lee Z., K. L. Carder, S. K. Hawes, R. G. Steward, T. G. Peacock, and C. O. Davis, "Model for the interpretation of hyperspectral remote-sensing reflectance," *Appl. Opt.*, Vol. 33, pp. 5721-5732.
- Lorenc, A.C., 1986. Analysis methods for numerical weather prediction, *Quarterly Journal of the Royal Meteorological Society*, Vol. 112, pp. 1177-1194.
- Madala, R.V., and S.A. Piacsek, 1977. A semi-implicit numerical model for baroclinic oceans, *Journal of Computational Physics*, 23, pp. 167-178.
- Mendelsohn, D.L., 1998. Development of an estuarine thermal environmental model in a boundary-fitted, curvilinear coordinate system, *Applied Science Associates Internal Document*.
- Mendelsohn D., E. Howlett, and J.C. Swanson, WQMAP for Windows, *Estuarine and Coastal Modeling IV*, Proceedings of the 4th International Conference, sponsored by the Waterway, Port, Coastal and Ocean Division of the ASCE, San Diego, CA, October 26-28, 1995.
- Moore, A.M., N.S. Cooper, and D.L.T. Anderson, 1987. Initialization and data assimilation in models of the Indian Ocean, *Journal of Physical Oceanography*, Vol. 17, pp. 1965-1977.
- Muin, M., and M. Spaulding, 1996. Two-dimensional boundary fitted circulation model in spherical coordinates, *Journal of Hydraulic Engineering*, Vol. 122, No. 9, pp. 512-521.
- Muin, M., and Spaulding, 1997. Three-dimensional boundary-fitted circulation model, *Journal of Hydraulic Engineering*, Vol. 123, No. 1, pp. 2-12.
- Mustard J. F., A. Sen, C. Swanson, D. Mendelsohn, and C. Deacutis, "Integration of remotely sensed data and hydrodynamic modeling into a GIS to assess the impacts of thermal effluent in an estuary", in *Proc. 4th International Conference on Remote Sensing for Marine and Coastal Environments*, Environmental Research Institute of Michigan, Ann Arbor, MI, II 34-II 43, 1997.
- Mustard, J. F., W. L. Prell, C. Swanson, & H. Rines, 1997 Seasonal Dependence on the Buoyancy and Dissipation of a Thermal Plume in a Confined Estuary, *EOS, Trans. Amer. Geophys. Union*, 78, 555.
- NETSU, Hydrographic Study of Mt. Hope Bay, Rhode Island, Northeast Technical Services Unit, Food and Drug Administration, North Kingstown, RI, 1990.
- Paine, R.T. 1993. A Salty and Salutary Perspective on Global Change. In: *Biotic Interactions and Global Change*. P.M. Kareiva, J.G. Kingsolver, & R.B. Huey, eds. Sinauer Assoc.: Sunderland, MA.
- Pilson, M.E.Q. 1985. On the Residence Time of Water in Narragansett Bay. *Estuaries* V8 #1:2-14.
- Press W. H., B. P. Flannery, S. A. Teukolsky, and W. T. Vetterling, *Numerical Recipes, The Art of Scientific Computing*, Cambridge University Press, New York, 1986.
- Ries K. G., Estimating surface-water runoff to Narragansett Bay, Rhode Island and Massachusetts, U. S. Geological Survey Water Resources Investigations Report 89-4164, Providence, RI, 1990.
- Rines, H. and H. Schuttenberg, 1998. Data report New England Power Company, Brayton Point Station, Mount Hope Bay field studies for 1997. Report to New England Power company. Applied Science Associates, Inc., Narragansett, RI.
- Rines, H., 1999. Mapping temperature distributions in Mount Hope Bay, Fall 1998 deployment. Report submitted to PG&E Generating Company, ASA project 96-076. 44pp.
- Roesler, C. S. and M. J. Perry, "In situ phytoplankton absorption, fluorescence emission, and particulate backscatter determined from reflectance", *J. Geophys. Res.* v. 100, 13,279-13,294, 1995.

- Sabins, M. J. Convergence and consistency of fuzzy c-Means/ISODATA algorithms, *IEEE Transactions Pattern and Machine Intelligence*, **9**, 661-688, 1987.
- Sanford, E., D. Bermudez, M. D. Mertness, and S. D. Gaines, Flow, food supply and acorn barnacle population dynamics, *Marine Ecology Progress Series*, 104, 49-62, 1994.
- Sathyendranath S., L. Lazarra, and L. Prieur, "Variations in the spectral values of specific absorption of phytoplankton," *Limnol. Oceanogr.*, Vol. 32., pp. 403-415, 1987.
- Schneider, K & W. Mauser. 1996. Processing and Accuracy of Landsat Thematic Mapper Data for Lake Surface Temperature Measurement. *Int. J. Remote Sensing*, 17(7): 2027-2041.
- Smith, R. C. and K. S. Baker, "Optical properties of the clearest natural waters (200-800 nm)," *Appl. Opt.* Vol. 20, pp. 177-183, 1981.
- Spaulding M.L., E. Howlett, E. Anderson and K. Jayko, OILMAP: A global approach to spill modeling, 15th Annual Arctic and Marine Oil Spill Program, Technical Seminar, Edmonton, Alberta, Canada, June 9-11, 1992.
- Spaulding M.L., and F.M. White, Circulation dynamics in Mt. Hope Bay and the lower Taunton River, *Coastal and Estuarine Studies*, Vol. 38, R.T. Cheng (Ed.), Residual Currents and Long-Term Transport, Springer-Verlag, New York, Inc., 1990.
- Spaulding M.L., A vertically averaged circulation model using boundary fitted coordinates, *Journal of Physical Oceanography*, May, pp. 973-982, 1984.
- Swanson J.C., M. Spaulding, J-P. Mathisen and O. O. Jenssen, A three dimensional boundary fitted coordinate hydrodynamic model, Part I: development and testing, *Dt. hydrog, Z.42*, 1989, p. 169-186, 1989.
- Swanson, J.C., D. Mendelsohn, H. Rines, H. Schuttenberg, 1998. Mt. Hope Bay hydrodynamic model calibration and confirmation. Applied Science Associates report to New England Power Company.
- Stewart-Oaten, W., W. W. Murdoch & K. R. Parker 1986 Environmental impact assessment: "Pseudoreplication" in time? *Ecology*, **67**, 929-940.
- Tissot, B.N., J. Lubchenco, & S. Navarrette. 1991. Effects of global Warming on Coastal Marine Ecosystems: Implications of thermal discharge studies. *Bull. Ecol. Soc. Am.* 72:268.
- Tou, J. T. & Gonzalez, R. C. 1977 *Pattern Recognition Principles*, Addison-Wesley, Massachusetts, 377 pp.
- Turner C., S. Asselin, and S. Feng, City of Fall River combined sewer overflow facilities plan: receiving water impacts field measurement program, Report by Applied Science Associates, Inc., Narragansett, RI to The Maguire Group, Foxborough, MA, 1990.
- Underwood, A. J 1993 The mechanics of spatially replicated sampling programmes to detect environmental impacts in a variable world, *Australian Journal of Ecology*, **18**, 99-116.
- Valiela, I. 1995. *Marine Ecological Processes*. Springer: New York.

Tables

Table 1: Landsat Scene Acquisition Dates

Date	Tidal Stage
1992/01/01	72% Ebb
1987/02/20	60% Flood
1984/05/02	23% Ebb
1989/07/03	40% Ebb
1985/08/09	44% Flood
1993/08/15	82% Ebb
1995/09/06	82% Ebb
1984/09/07	70% Ebb
1986/09/13	17% Flood
1987/09/16	33% Flood
1991/09/27	98% Flood
1985/10/28	44% Ebb
1986/10/31	67% Ebb
1984/11/26	96% Flood

Table 2. Physical Characteristics of Regions within Narragansett Bay (Chinman and Nixon, 1985).

Segment	PRR	UNB	MHB	GRB	UWP	LWP	UEP	MEP	LEP	SR
Area (km ²)	21.28	43.29	35.2	11.64	77.92	17.94	23.81	34.34	25.34	50.97
Mean depth (m)	5.21	5.57	5.73	2.11	6.09	8.93	7.33	13.96	18.72	6.5
Mean Low Water volume (m ³ x10 ⁶)	110.9	241.3	201.7	24.6	474.5	160.2	174.6	479.4	474.3	331.5
Mean High Water volume	137.5	294.1	239.4	38.8	564.9	179.4	202.9	518.2	501.5	386.1
Tidal prism	26.6	52.8	37.7	14.2	90.4	19.2	28.3	38.8	27.2	54.6
Tidal flushing (# cycles)	4.17	4.57	5.35	1.73	5.25	8.34	6.17	12.36	17.44	6.07
Tidal flushing (days)	2.17	2.38	2.79	0.90	2.73	4.35	3.21	6.44	9.08	3.16
Annual average Fresh Water Flux (m ³ /s)	43.22	46.86	30.56	4.01						
Fresh Water Flushing (days)	29.7	59.6	76.4	71.0						
Surface Area/Volume	0.192	0.179	0.175	0.473	0.164	0.112	0.136	0.072	0.053	0.154

PRR Providence River; UNB, Upper Narragansett Bay; MHB, Mount Hope Bay, GRB, Greenwich Bay; UWP, Upper West Passage; LWP, Lower West Passage; UEP, Upper East Passage; MEP, Middle East Passage; LEP, Lower East Passage; SR, Sakonnet River; MLW, Mean Low Water; MHW, Mean High Water; FW, Fresh Water

Table 3. Correlations of relative seasonal temperature signals among Narragansett Bay regions

	GRB	MHB	PRR	UNB	USR	UWP	MWP	LWP	UEP	MEP	LEP	LSR
GRB	1	0.86	0.88	0.78	0.26	0.10	-0.55	-0.92	-0.96	-0.99	-0.94	-0.71
MHB		1	0.80	0.48	-0.02	-0.18	-0.47	-0.73	-0.85	-0.83	-0.75	-0.61
PRR			1	0.75	0.02	-0.09	-0.68	-0.81	-0.89	-0.90	-0.81	-0.51
UNB				1	0.40	0.38	-0.81	-0.89	-0.73	-0.84	-0.83	-0.67
USR					1	0.91	-0.19	-0.51	-0.14	-0.32	-0.53	-0.55
UWP						1	-0.18	-0.40	0.00	-0.19	-0.41	-0.56
MWP							1	0.71	0.47	0.62	0.60	0.42
LWP								1	0.85	0.96	0.98	0.83
UEP									1	0.95	0.88	0.63
MEP										1	0.96	0.74
LEP											1	0.85
LSR												1

Table 4. Area covered by specific classes from the Unsupervised Classification

	Lakes	Greenwich Bay	Upper Estuary	Mount Hope Bay	Lower Estuary	Oceanic
Number of Pixels	4,625	6,635	36,227	10,127	18,290	115,520
Area (km ²)	16.6	23.8	130.4	36.5	65.8	415.9

Table 5: Measurement Campaigns to Resolve Tidal Properties

Date	Sensor	NeΔT (°C)	Times (Eastern Daylight Time)
August 30, 1996	Geophysical Environmental Research (GER) 37-channel scanner, 1 thermal channel	0.2 (reported)	9:44 am
			11:12 am
			12:45 pm
			2:11 pm
			3:30 pm
May 28, 1997	Locheed ATLAS 15-channel scanner with 6 thermal channels	0.2°(reported)	6:47 am
			8:24 am
			10:13 am
			12:06 pm
			2:09 pm
			3:20 pm
			4:25 pm
August 19, 1997	NASA MODIS Airborne Simulator	0.2 °(reported)	10:58 am
			11:24 am
September 11, 1998	Geophysical Environmental Research 37-channel scanner, 1 thermal channel	0.2° (reported)	6:00 am
			7:42 am
			9:24 am
			11:26 am
			12:48 pm
			2:11 pm
			3:34 pm
			4:57 pm
6:20 pm			

Table 6. Tides on the Days of the Overflights (Eastern Daylight Time)

Date	High		Low		High		Low		High	
	Time	M	Time	M	Time	M	Time	M	Time	M
8/30/1996			2:58	-0.14	09:31	1.22	15:26	-0.11	21:55	1.16
5/28/1997	00:56	0.98	06:32	-0.03	13:34	0.92	18:56	0.05		
8/19/1997			02:22	-0.16	08:59	1.19	14:41	-0.15	21:23	1.23
9/11/1998	00:05	1.01	05:40	-0.03	12:36	1.14	18:32	0.03		

Table 7. Statistics of temperature observations and model predictions for model calibrated to August-September 1997 data set.

Location	Observations			Model Predictions		
	Mean (°C)	Standard Deviation (°C)	Coefficient of Variation (%)	Mean (°C)	Standard Deviation (°C)	Coefficient of Variation (%)
Borden Flats - Surface	23.9 6	0.86	4	23.2 5	0.82	4
Borden Flats - Bottom	23.0 5	0.75	3	23.2 7	0.60	3
Brayton Point - Surface	24.5 4	0.89	4	25.8 7	1.95	8
Brayton Point - Bottom	23.5 6	0.79	3	23.9 9	0.90	4
Gardners Neck - Surface	23.9 7	0.74	3	25.5 0	1.10	4
Gardners Neck - Bottom	23.3 2	0.72	3	25.5 0	1.10	4

Table 8. Statistical comparison of temperature observations and model predictions for model calibrated to August-September 1997 data set.

Location	Relative Mean Error (%)	Root Mean Square Error (°C)	Correlation Coefficient t	Error Coefficient of Variation (%)
Borden Flats - Surface	3	0.90	0.79	4
Borden Flats - Bottom	1	0.56	0.73	2
Brayton Point - Surface	5	2.08	0.58	8
Brayton Point - Bottom	2	0.75	0.74	3
Gardners Neck - Surface	6	1.73	0.66	7
Gardners Neck - Bottom	9	2.42	0.39	10

Table 9. Remotely sensed Data Assimilation Numerical Experiment Matrix
Time of Overflight on May 28, 1997

Simulation	1409 EDT	1520 EDT	1625 EDT	1746 EDT	1902 EDT
Baseline	--	--	--	--	--
May97ovt1	X	--	--	--	--
May97ovt2	X	X	--	--	--
May97ovt3	X	--	X	--	--
May97ovt4	X	--	--	X	--
May97ovt5	X	X	X	--	--
May97ovt6	X	X	X	X	--

Table 10. Remotely sensed Data Assimilation Performance Parameters.
Time of Overflight on May 28, 1997

Simulation	1409 EDT	1520 EDT	1625 EDT	1746 EDT	1902 EDT
Baseline	0.63	0.18	0.59	0.47	0.79
May97ovt1	0	0.06	0.51	0.41	0.75
May97ovt2	0	0	0.53	0.42	0.76
May97ovt3	0	0.06	0	0.20	0.65
May97ovt4	0	0.06	0.51	0	0.64
May97ovt5	0	0	0	0.20	0.66
May97ovt6	0	0	0	0	0.61

Figures

(Note: Captions for Figures 1-9 are on this page, captions for the other figures are with the figures)

- Figure 1 Location of the study area. Narragansett Bay is largely within the state of Rhode Island, although Mount Hope Bay, and the Brayton Point Power Station are within the state of Massachusetts.
- Figure 2. Distribution of the 14 Landsat TM scenes used in this analysis as a function of year (horizontal axis) and month (vertical axis)
- Figure 3. Satellite derived surface temperatures compared to in situ water temperatures. The solid line represents the 1:1 relationship.
- Figure 4. Seasonal composite of satellite derived temperatures, covering the period 1984-1996 and a 20-year record of temperatures from one station in Mount Hope Bay. The satellite temperatures track well within the range of the insitu records.
- Figure 5. Areas from which seasonal temperature signatures were derived for the Regional Classification analysis. Three letter codes are explained in Table 3.
- Figure 6. Seasonal temperature signals for the twelve study areas used in the Regional Classification, separated into the three main groups defined in Table 3. All temperatures are the difference in temperature from the mean of all twelve regions. Negative values are colder than the mean and positive are greater than the mean.
- Figure 7. Results of the Unsupervised Classification. Each of the 6 major classes represents areas with common seasonal temperature signatures. Note that the Mount Hope Bay class is unique spatially, largely confined to Mount Hope Bay, with a minor grouping in the upper Providence River.
- Figure 8. Magnitude of the Mount Hope Bay temperature anomaly from both the Regional and Unsupervised classifications. These are the anomalies between the Mount Hope Bay class and the class containing Upper Narragansett Bay.
- Figure 9. Relationship between the surface to volume ratio for each region and the integrated temperature across the scenes used in the regional classification. All the regions follow a monotonic relationship except for Mount Hope Bay.

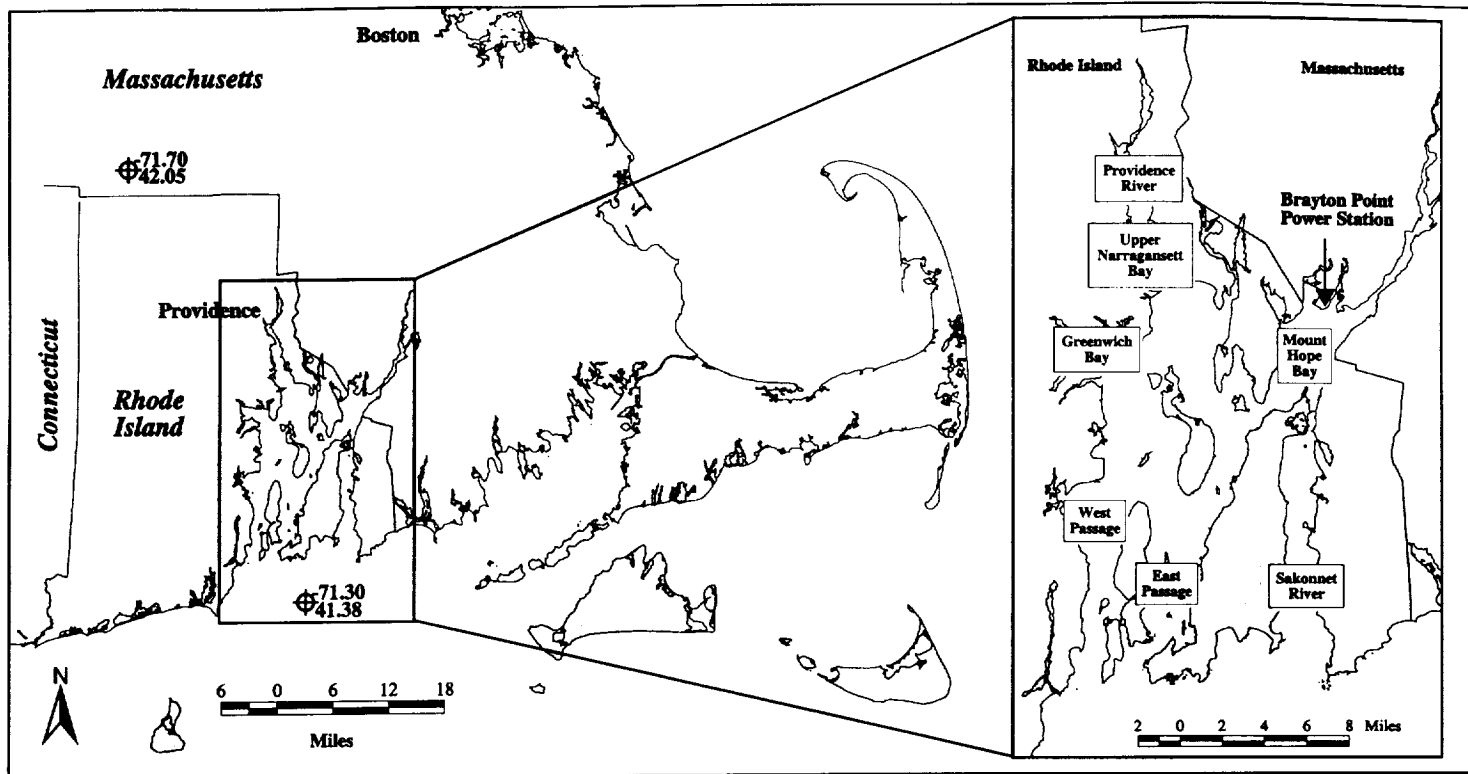


Figure 1

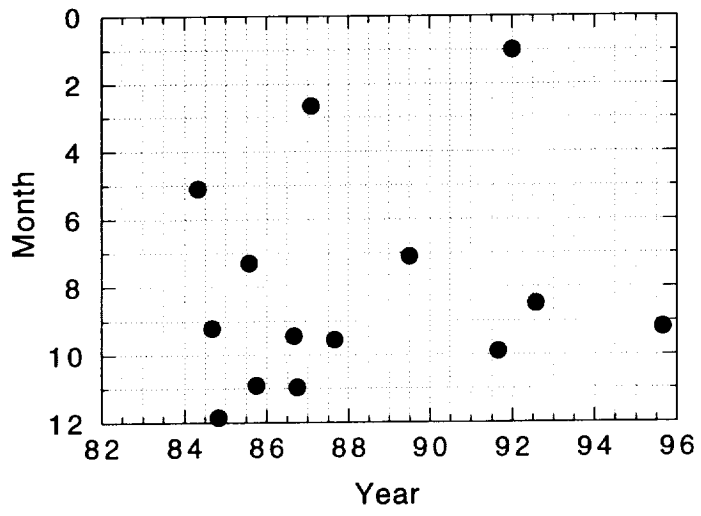


Figure 2

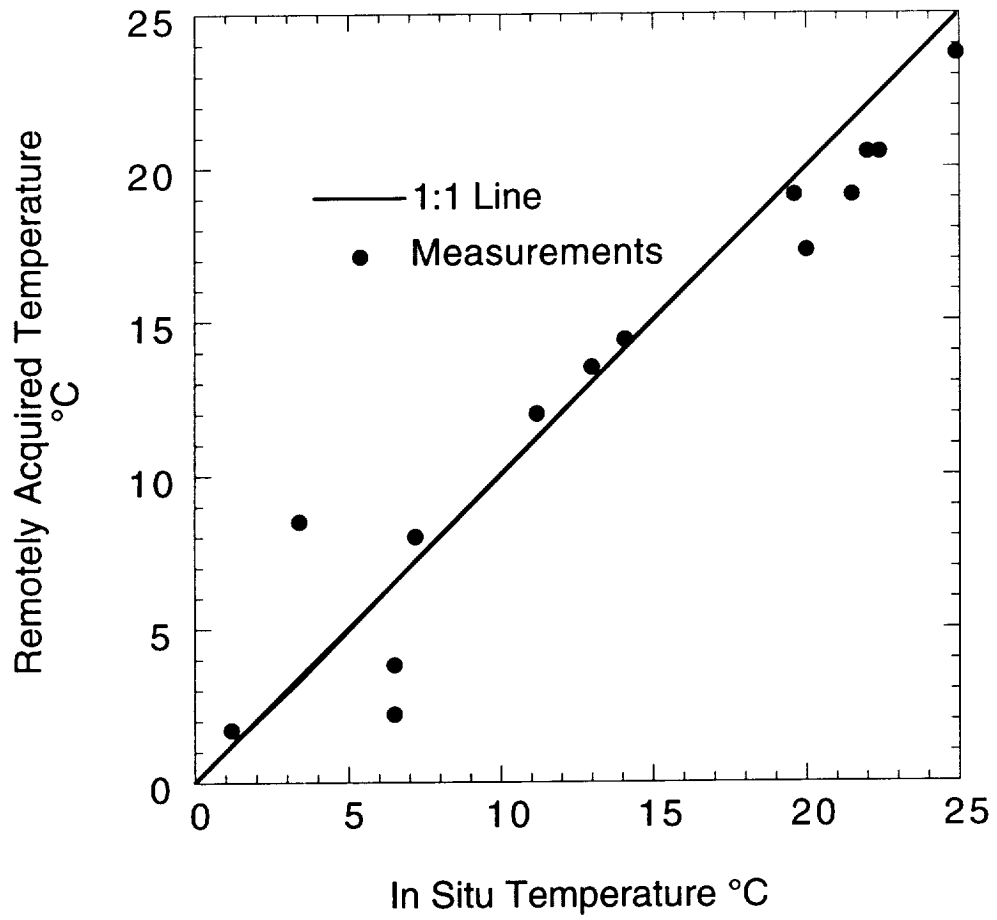


Figure 3

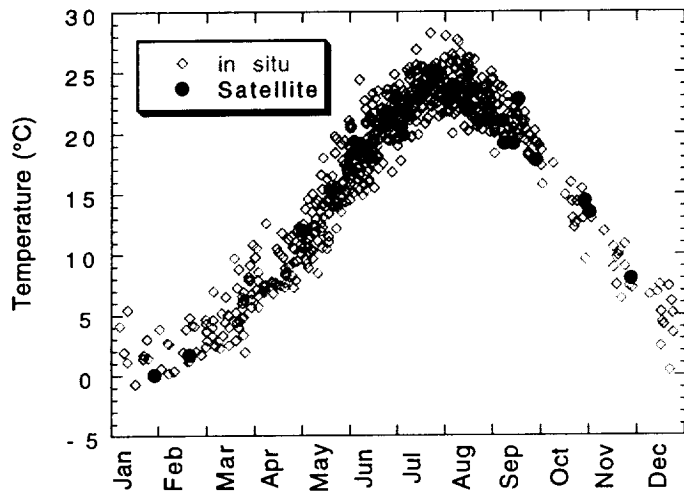


Figure 4

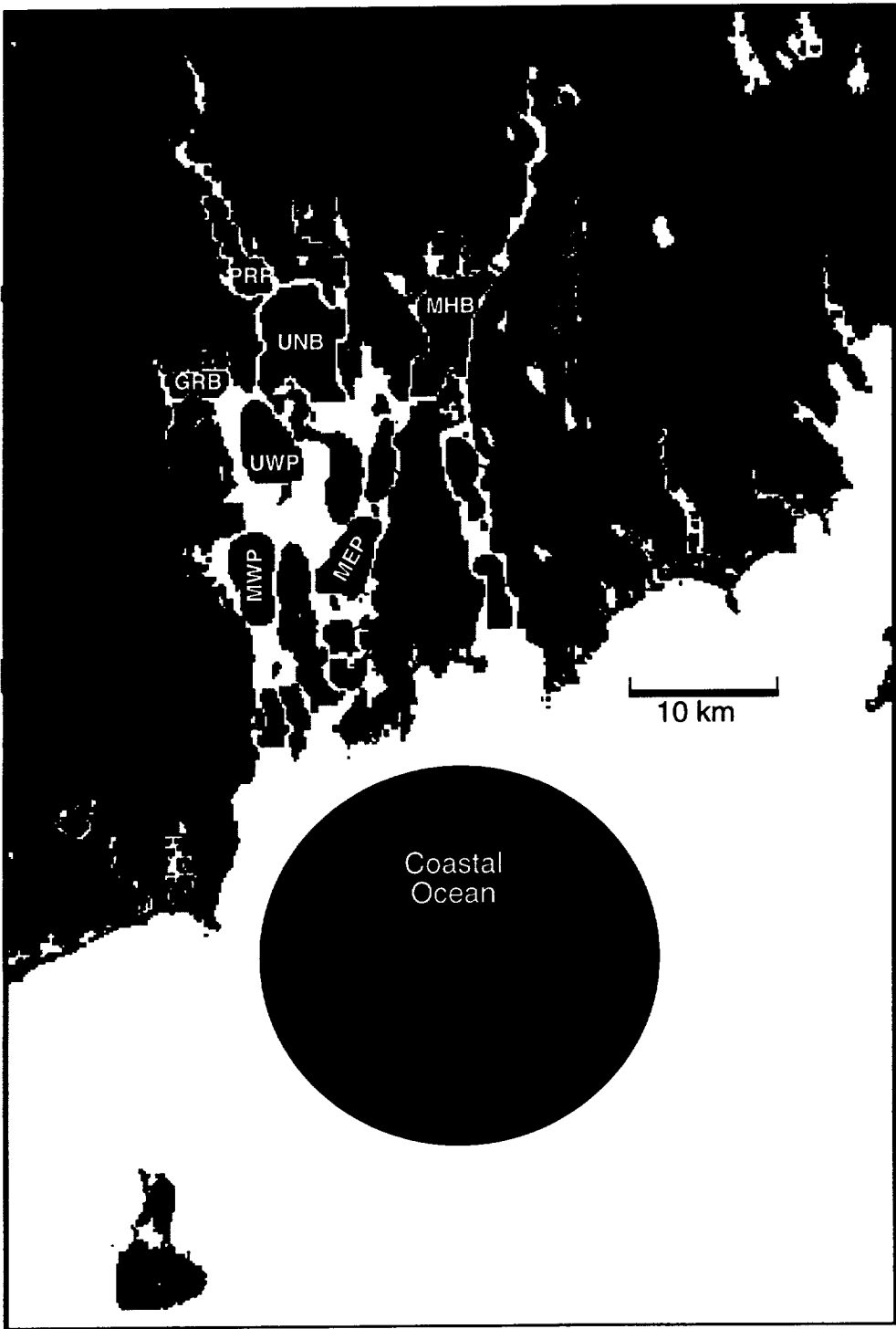


Figure 5

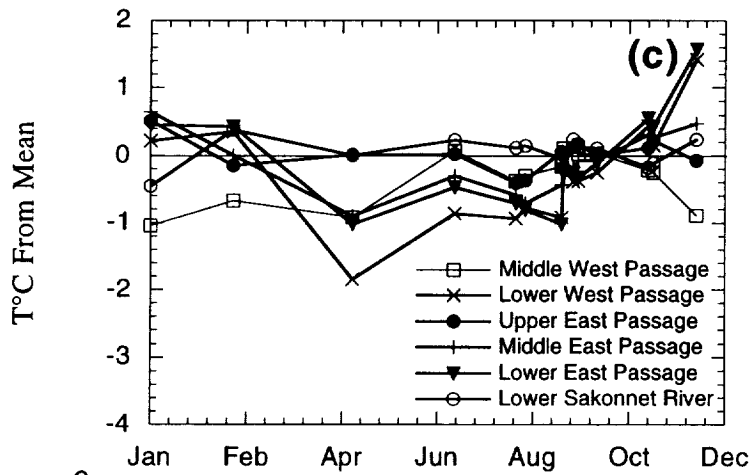
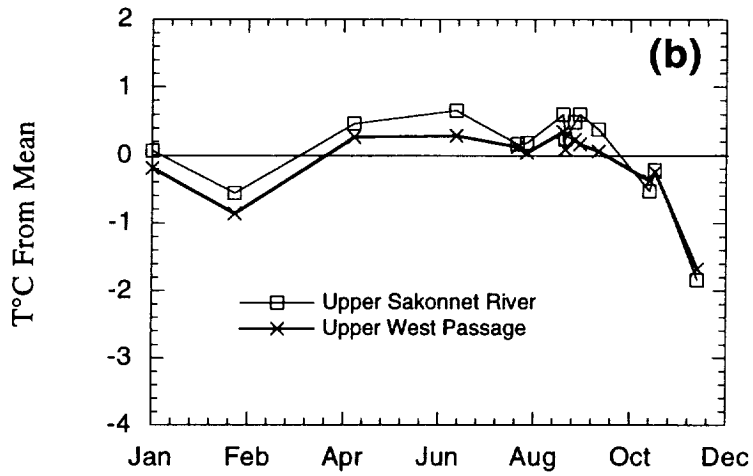
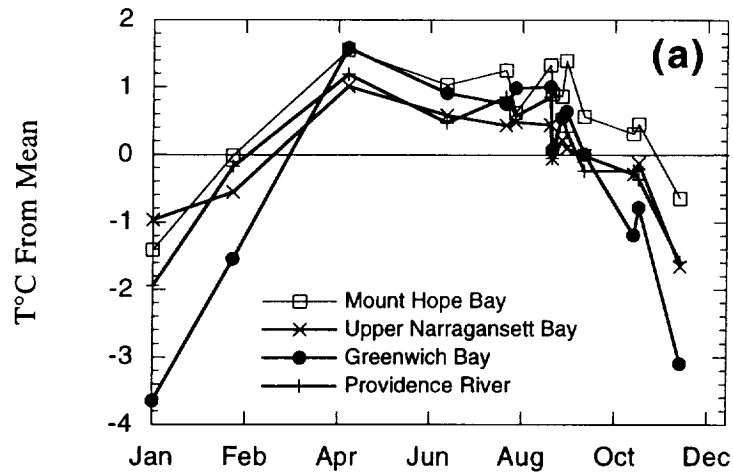
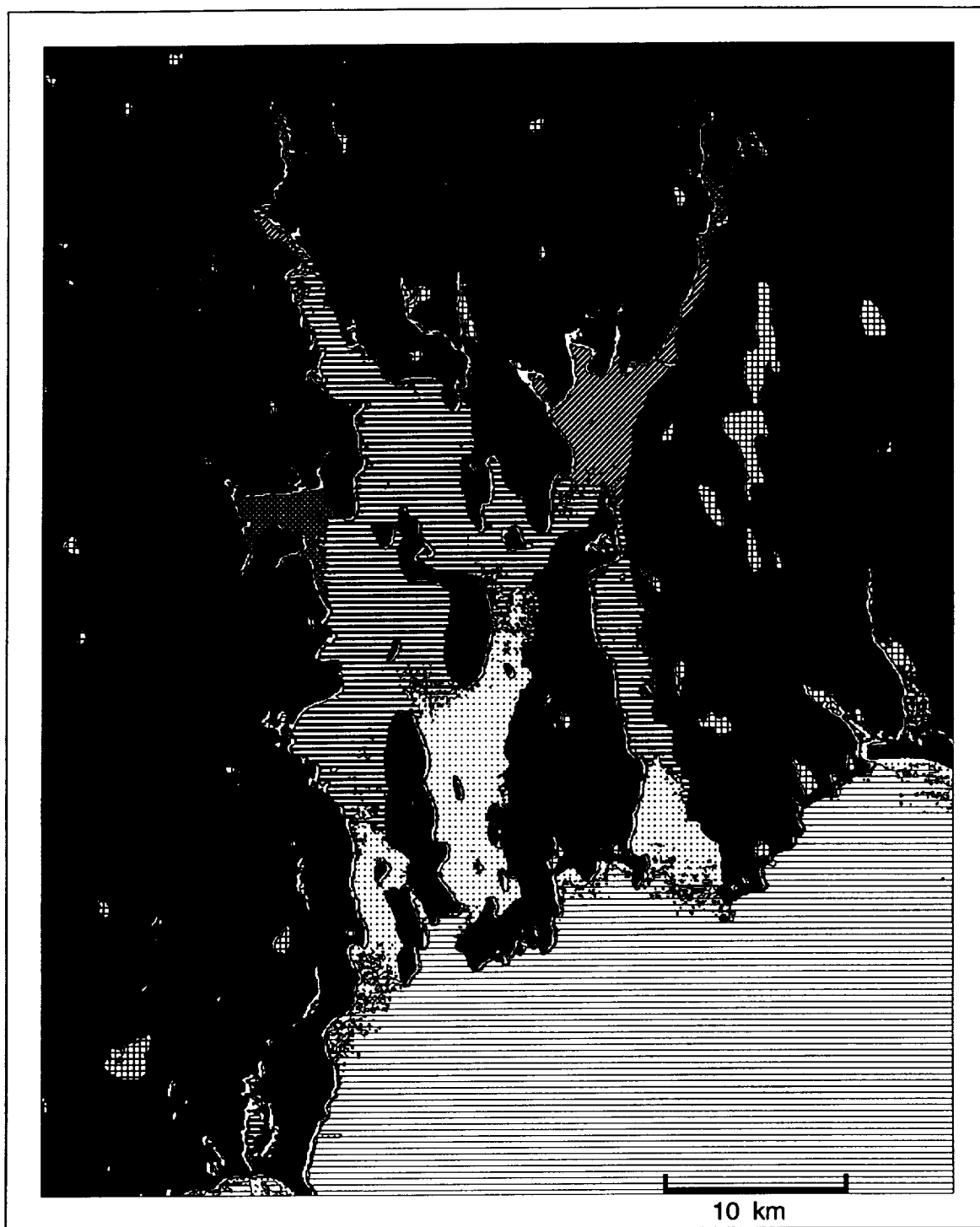


Figure 6



- | | | | | | |
|---|---------------|---|----------------|---|--------------|
|  | Oceanic |  | Greenwich Bay |  | Unclassified |
|  | Lower Estuary |  | Lakes | | |
|  | Upper Estuary |  | Mount Hope Bay | | |

Figure 7

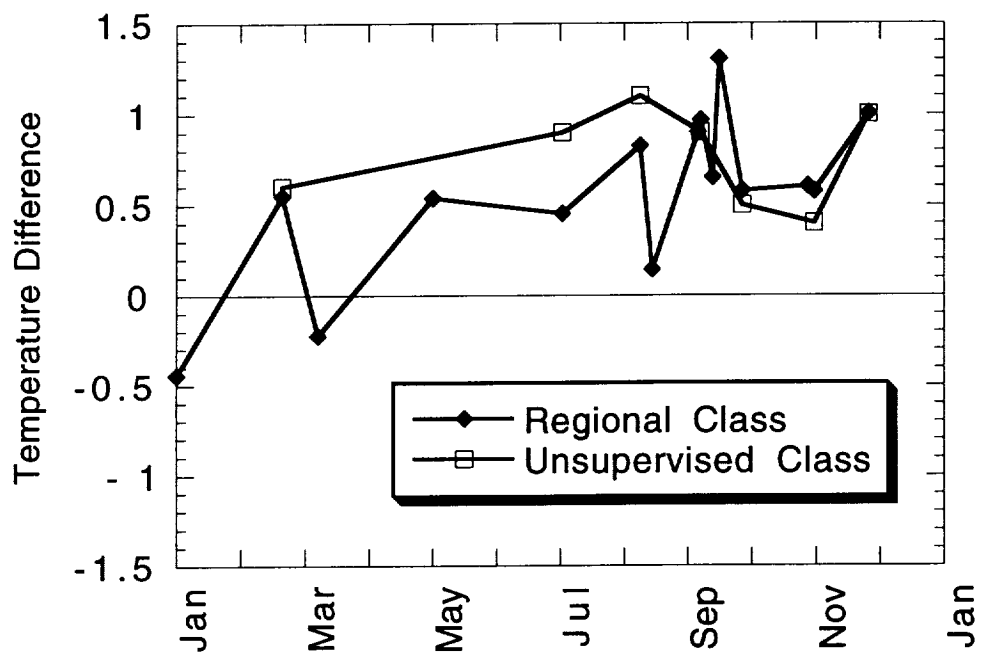


Figure 8

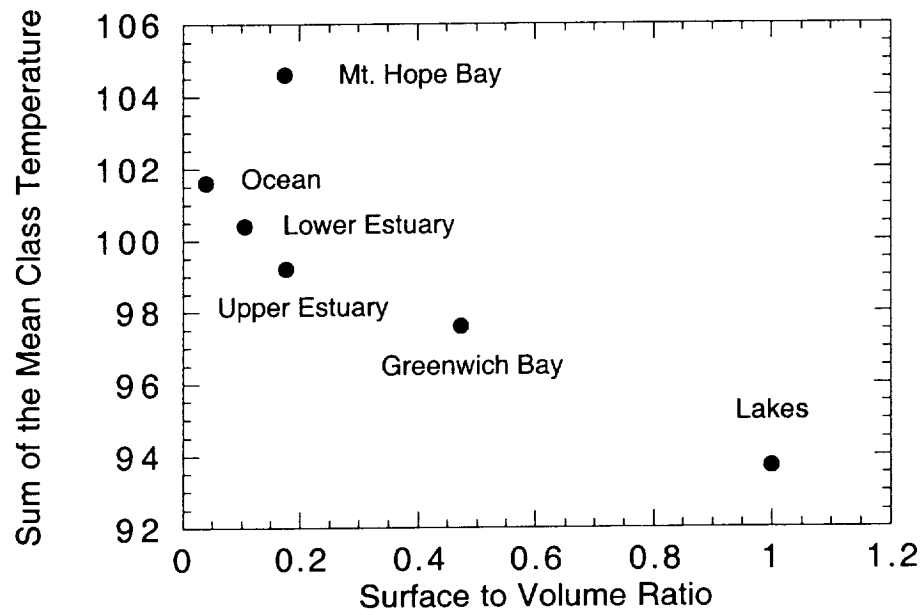


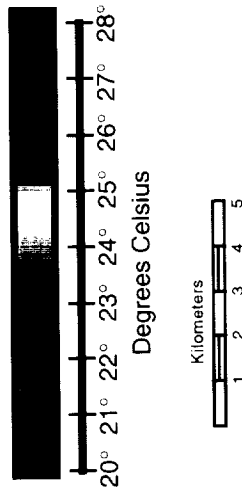
Figure 9



Figure 10: Thermistor string locations within Mt. Hope Bay.

Temperatures of Mt Hope Bay, RI/MA August 30, 1996

Acquired by Aircraft



11:12 am



9:44 am Slack High



2:11 pm



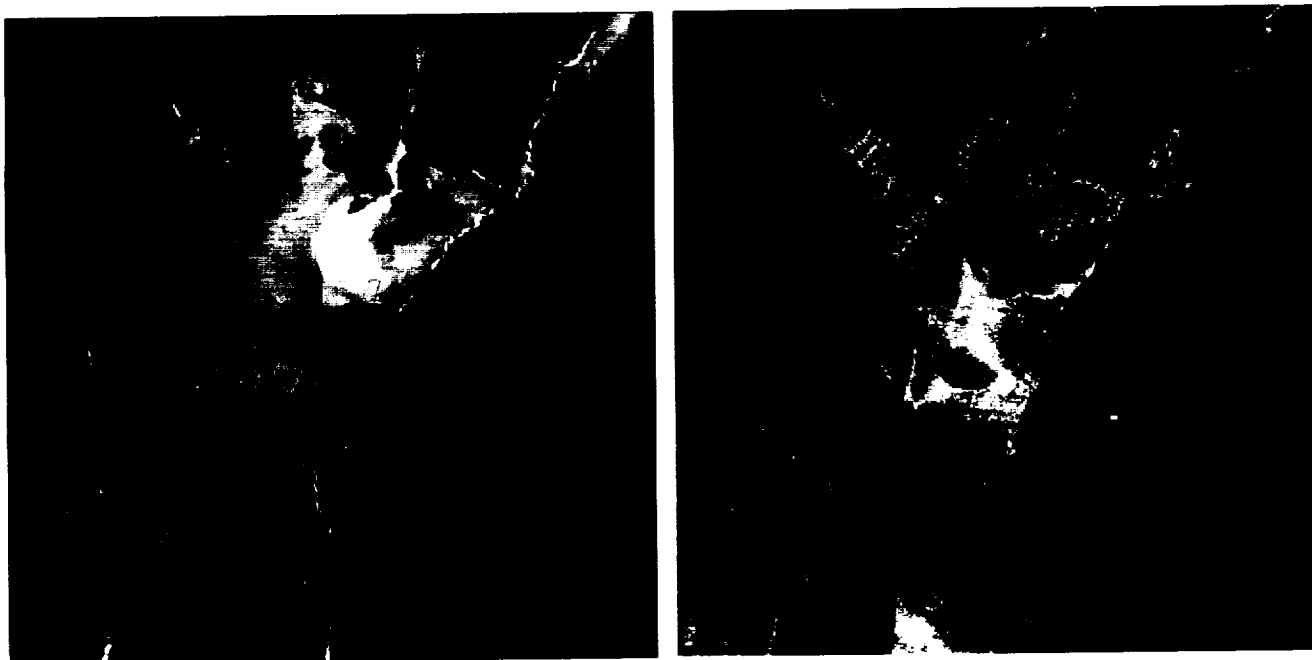
3:28 pm Slack Low

Figure 11. Temperature of Mt. Hope Bay derived from the GER sensor on August 30, 1996.

MODIS Thermal Infrared Temperatures, August 19, 1997



10:58 AM



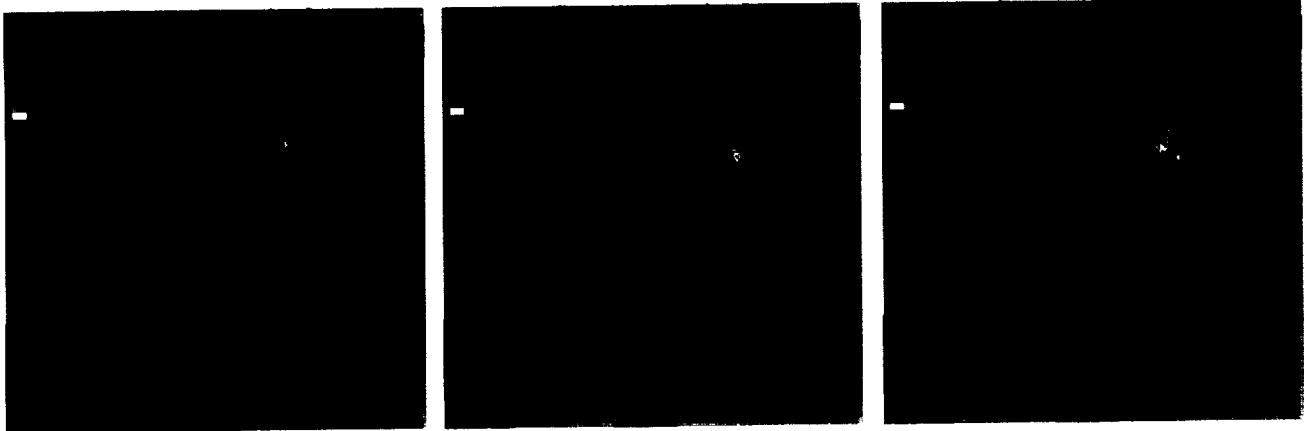
- Thermal Front 1
- Thermal Front 2
- Transport Vector

11:24 AM



Figure 12. Two MODIS Airborne Simulator thermal infrared data sets of Mt. Hope Bay acquired 26 minutes apart. Thermal fronts are outlined showing the movement of water bodies over this time period.

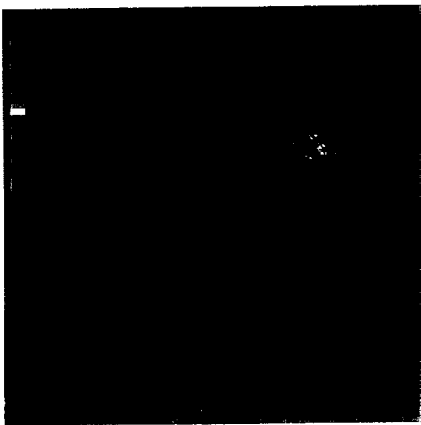
Temperatures of Mt Hope Bay, RI/MA
Acquired September 11, 1998 by the GER scanner



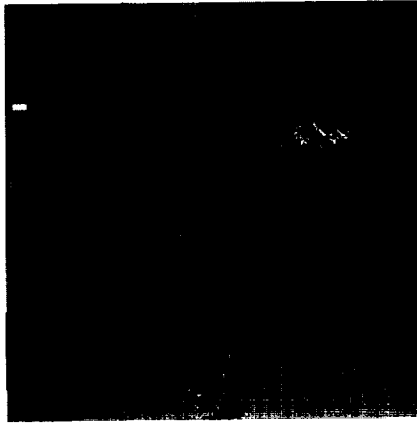
Time1 06:00 (Low Tide)

Time2 07:42

Time3 09:24



Time4 11:26



Time5 12:48 (High Tide)



Time6 14:11



Time7 15:34



Time8 16:57



Time9 18:20



20

21

22

23

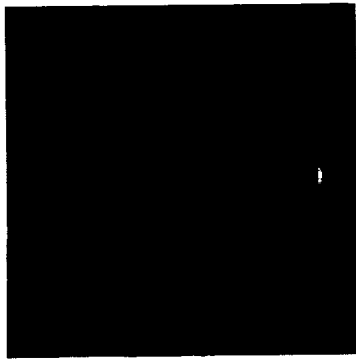
24

25

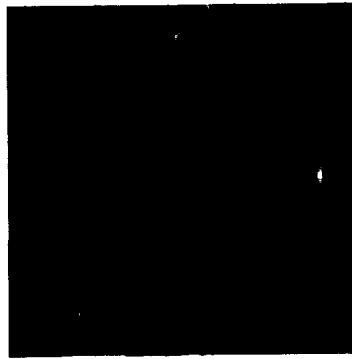
26

Temperature °C

Figure 13



6:47 AM



8:24 AM



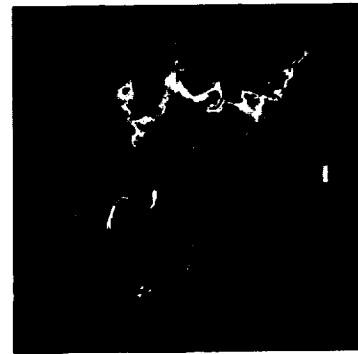
10:13 AM



12:06 AM



2:09 AM



3:20 PM



4:25 PM



5:46 PM



7:02 PM



12

Degrees Centigrade

21

Figure 14. Temperature of Mt. Hope Bay acquired by the ATLAS sensor on May 28, 1997

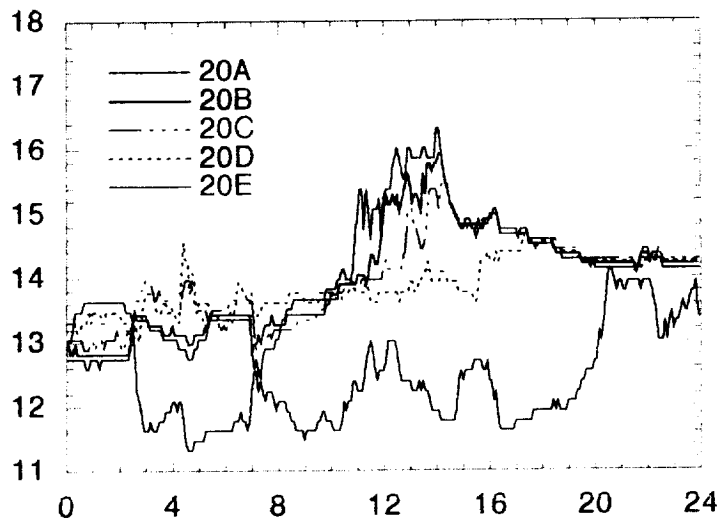
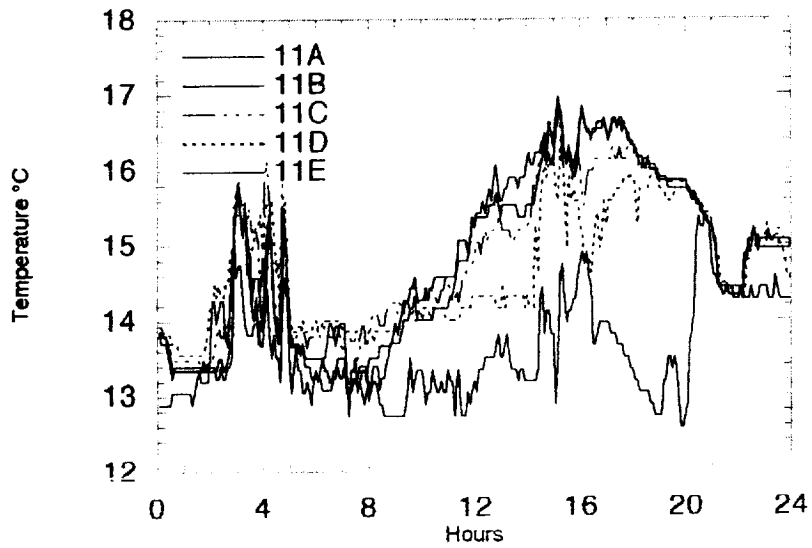
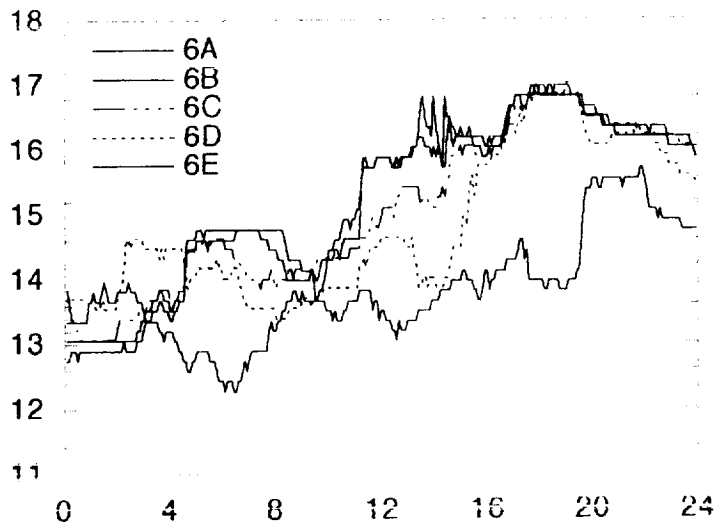


Figure 15

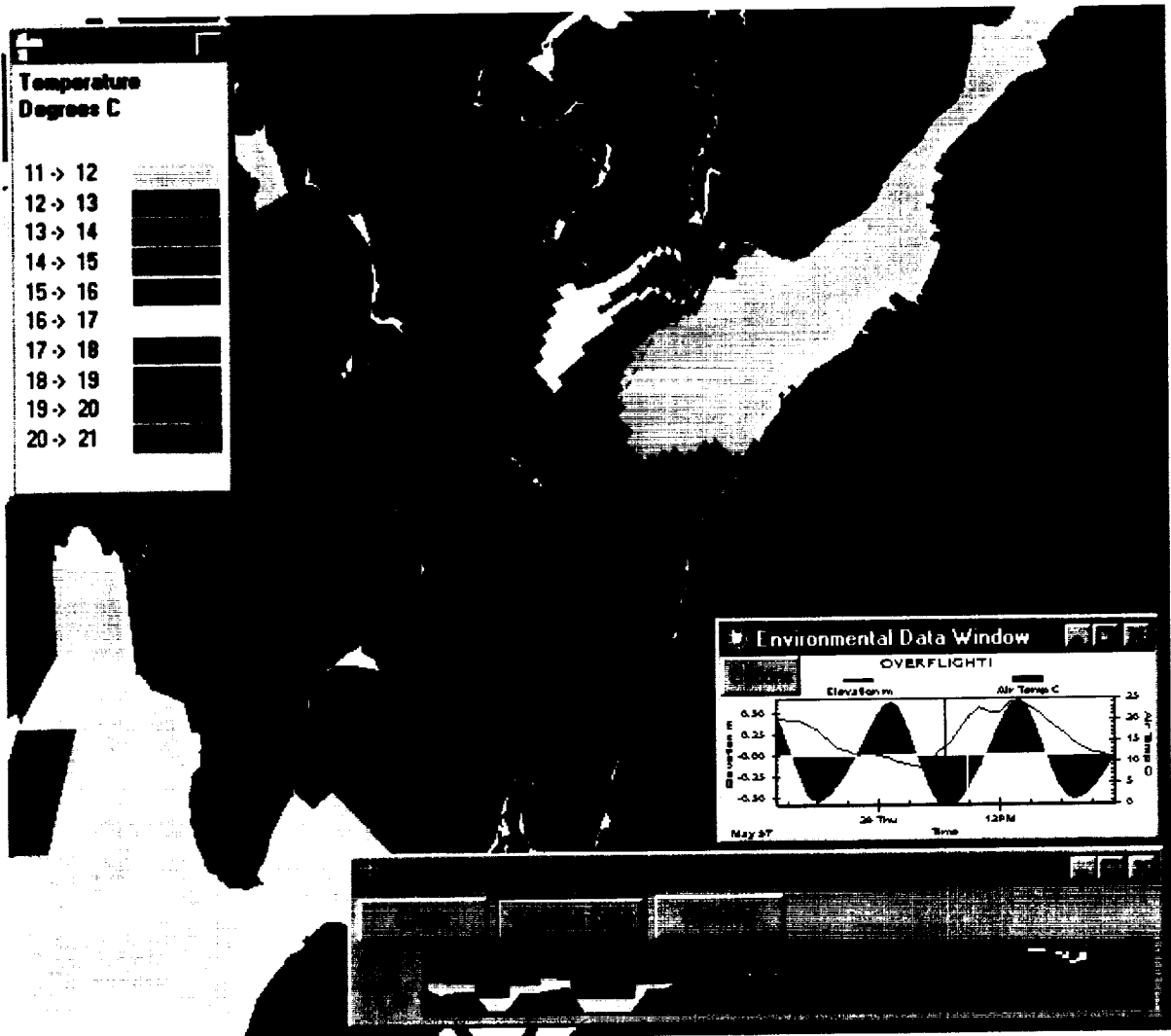


Figure 16: Example WQMAP output.

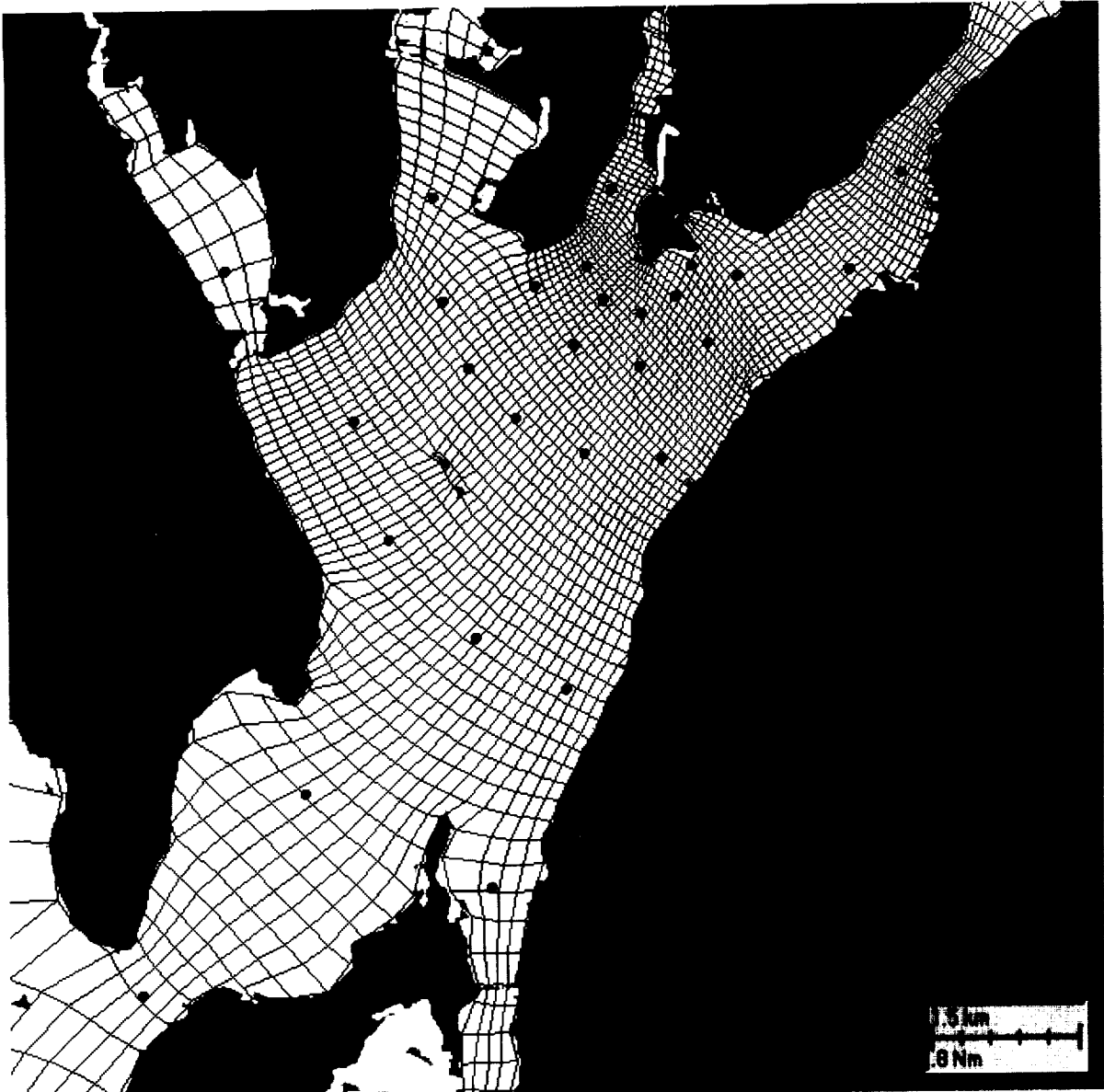


Figure 17: Computational grid for Mt. Hope Bay application.

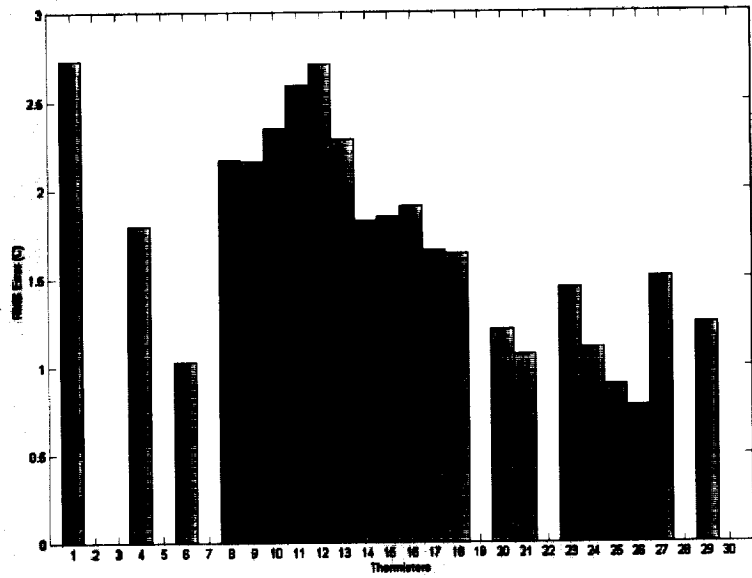


Figure 18: RMS error between baseline simulation and thermistor data at the surface.

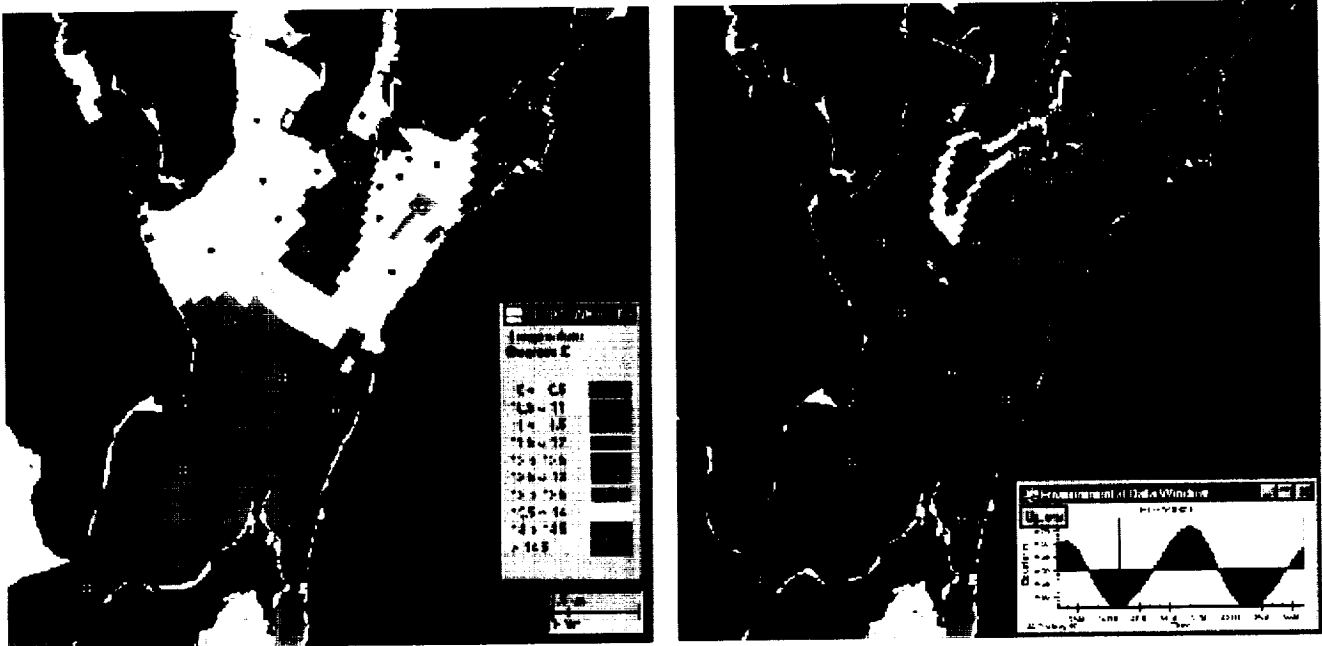


Figure 19: Plan view of surface temperature a) contoured thermistor data b) model predicted temperature

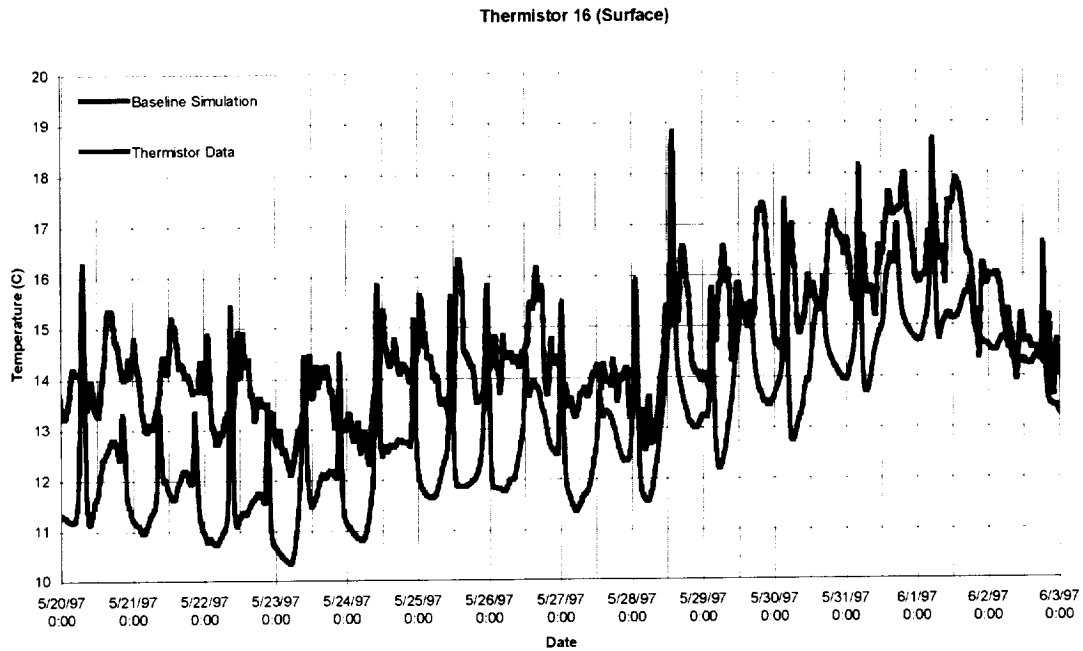


Figure 20: Model predicted temperature and thermistor data at the surface near the outfall.

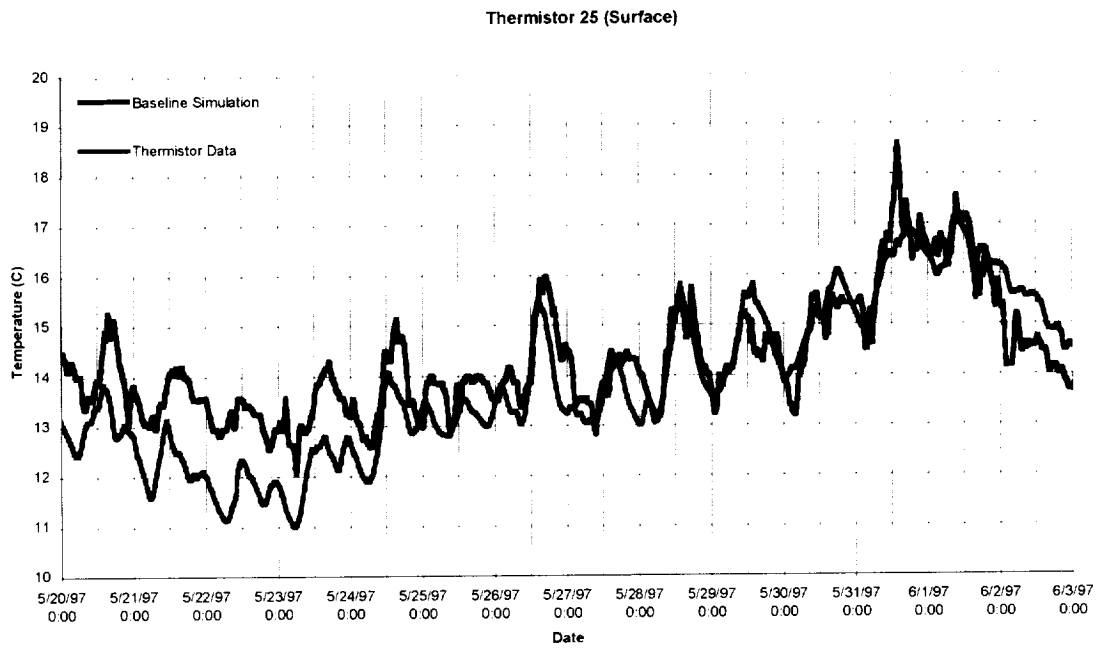


Figure 21: Model predicted temperature and thermistor data at the surface near the mouth of the bay.

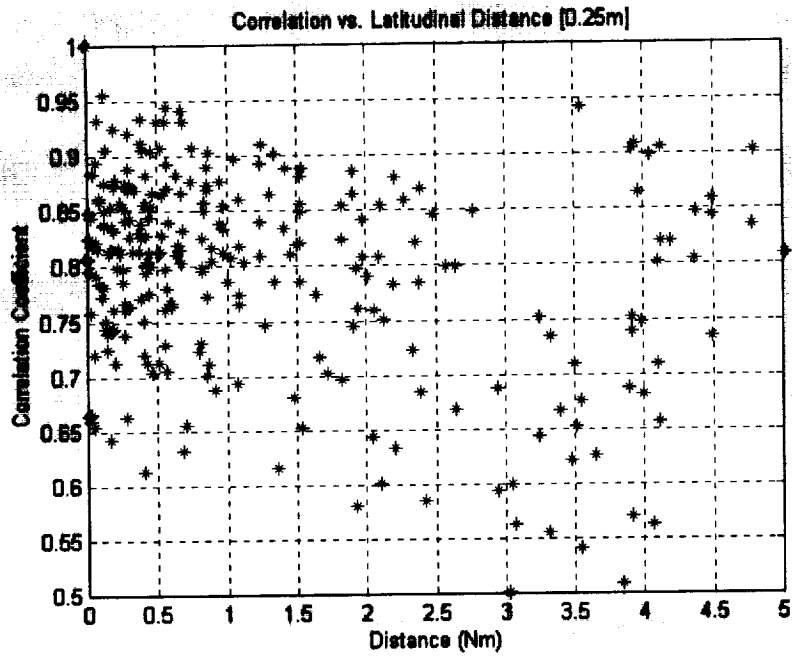


Figure 22: Correlation matrix clustering within a distance of 0.5NM (0.93km)

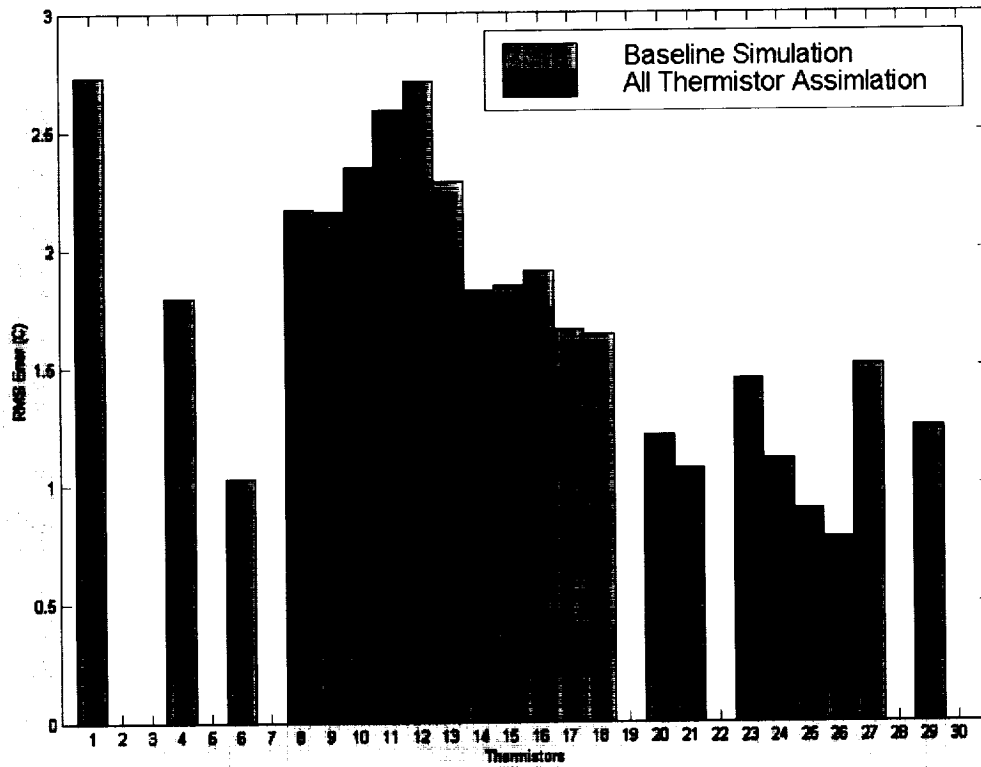


Figure 23: RMS error at the surface for continuous assimilation of all 30 thermistor strings.

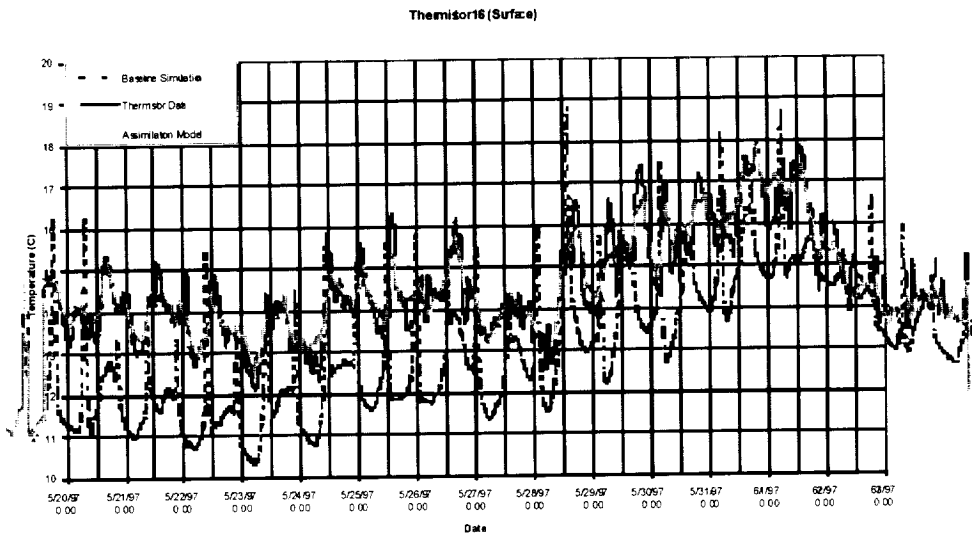


Figure 24: Time series of the temperature in the region of the outfall at the surface for continuous assimilation of all 30 thermistor strings.

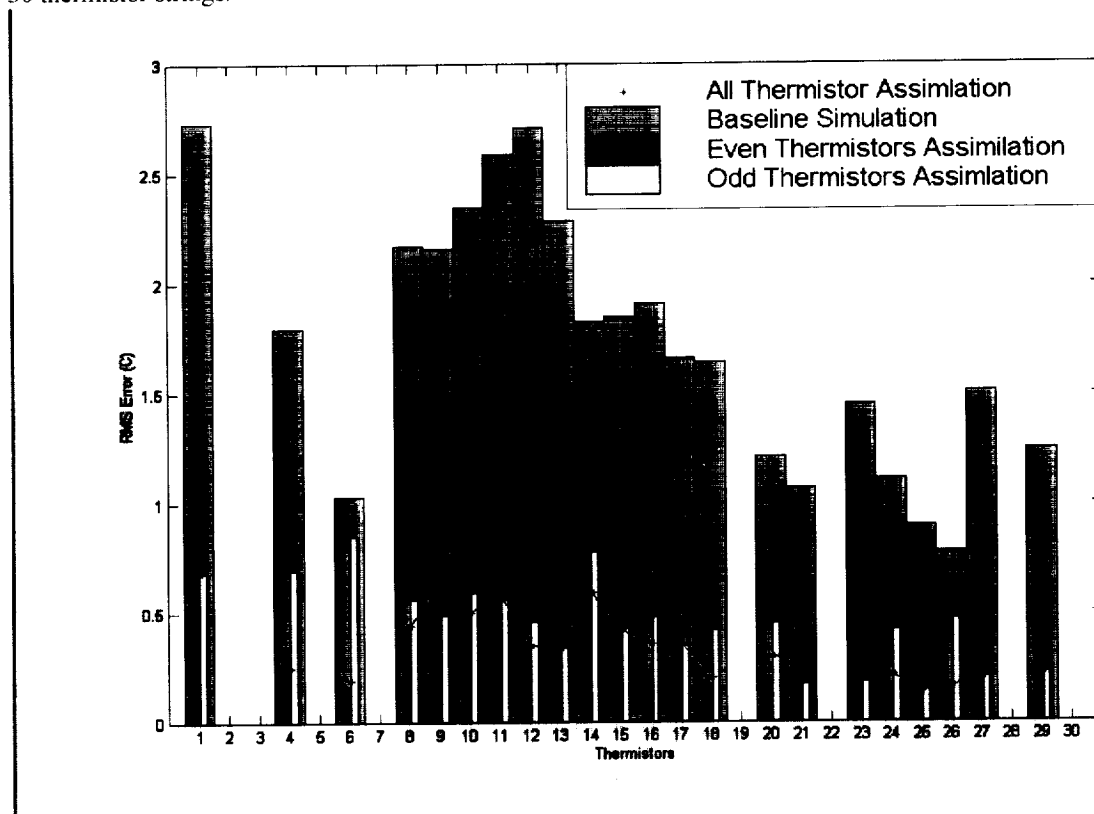


Figure 25: RMS error at the surface for the assimilation of only even and odd numbered thermistor strings.

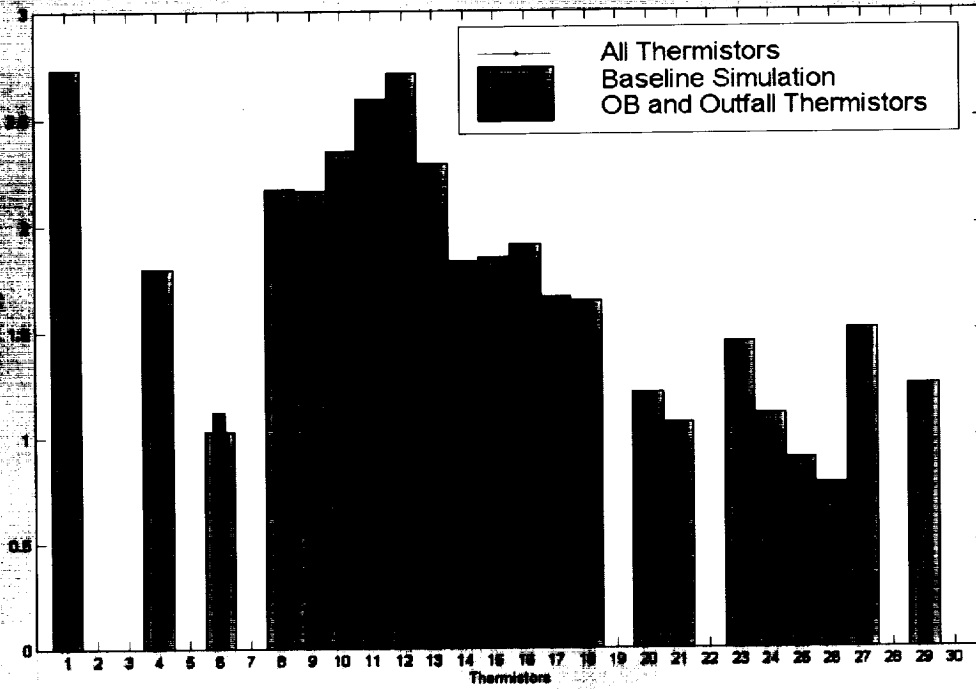


Figure 26: RMS error at the surface for continuous assimilation of thermistor strings in the vicinity of the open boundary and outfall.

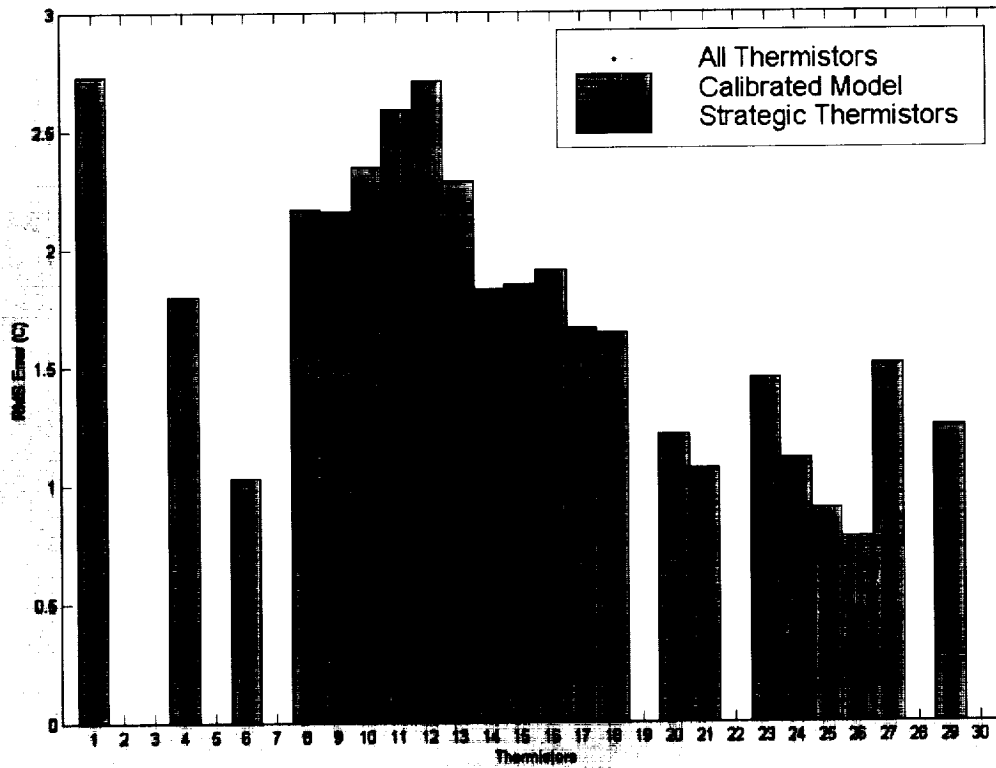


Figure 27: RMS error at the surface for the assimilation of 5 strategically located thermistor strings.

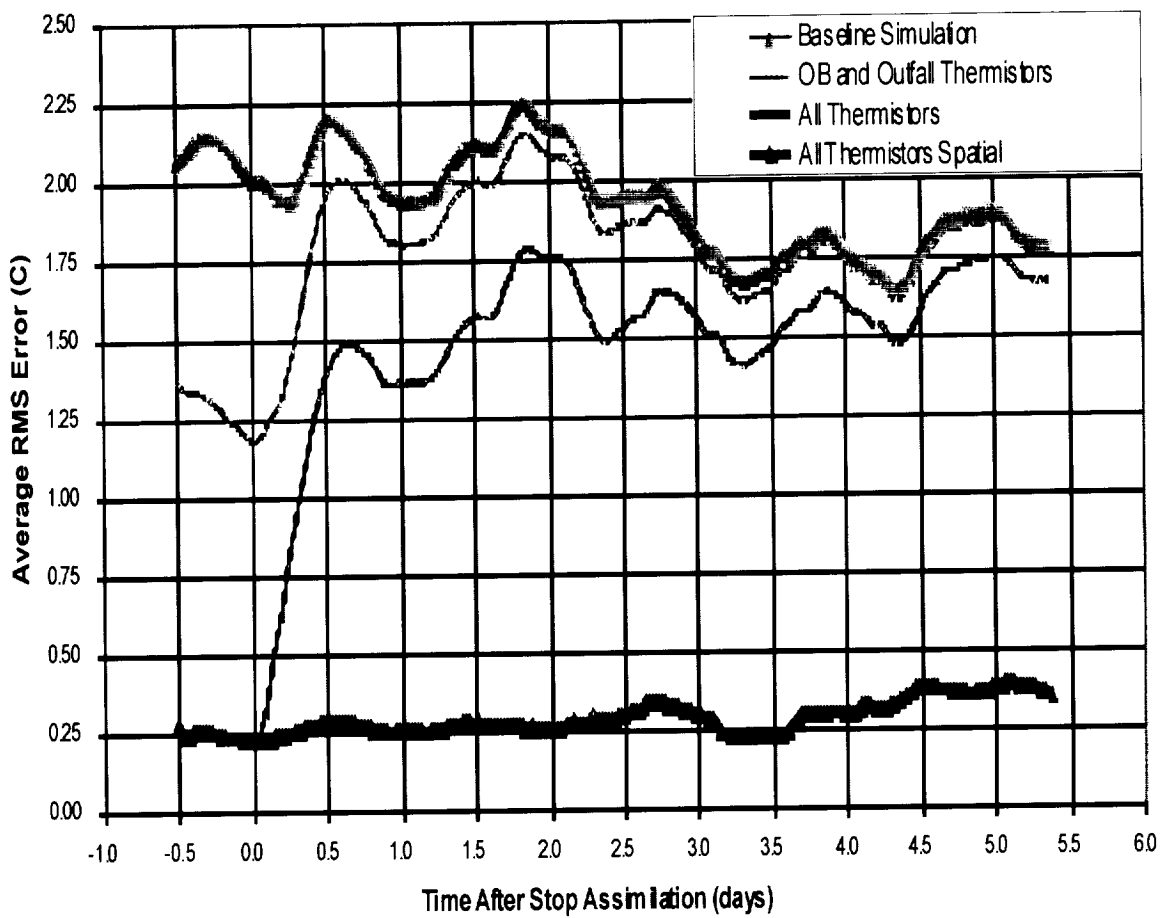


Figure 28: Mean RMS error at the surface as a function of time for predictive capability tests, baseline simulation and the continuous assimilation of all thermistor data.



Figure 29: Overlay of Computational Grid on an remotely sensed thermal data for 3:20 pm, May 28, 1997.

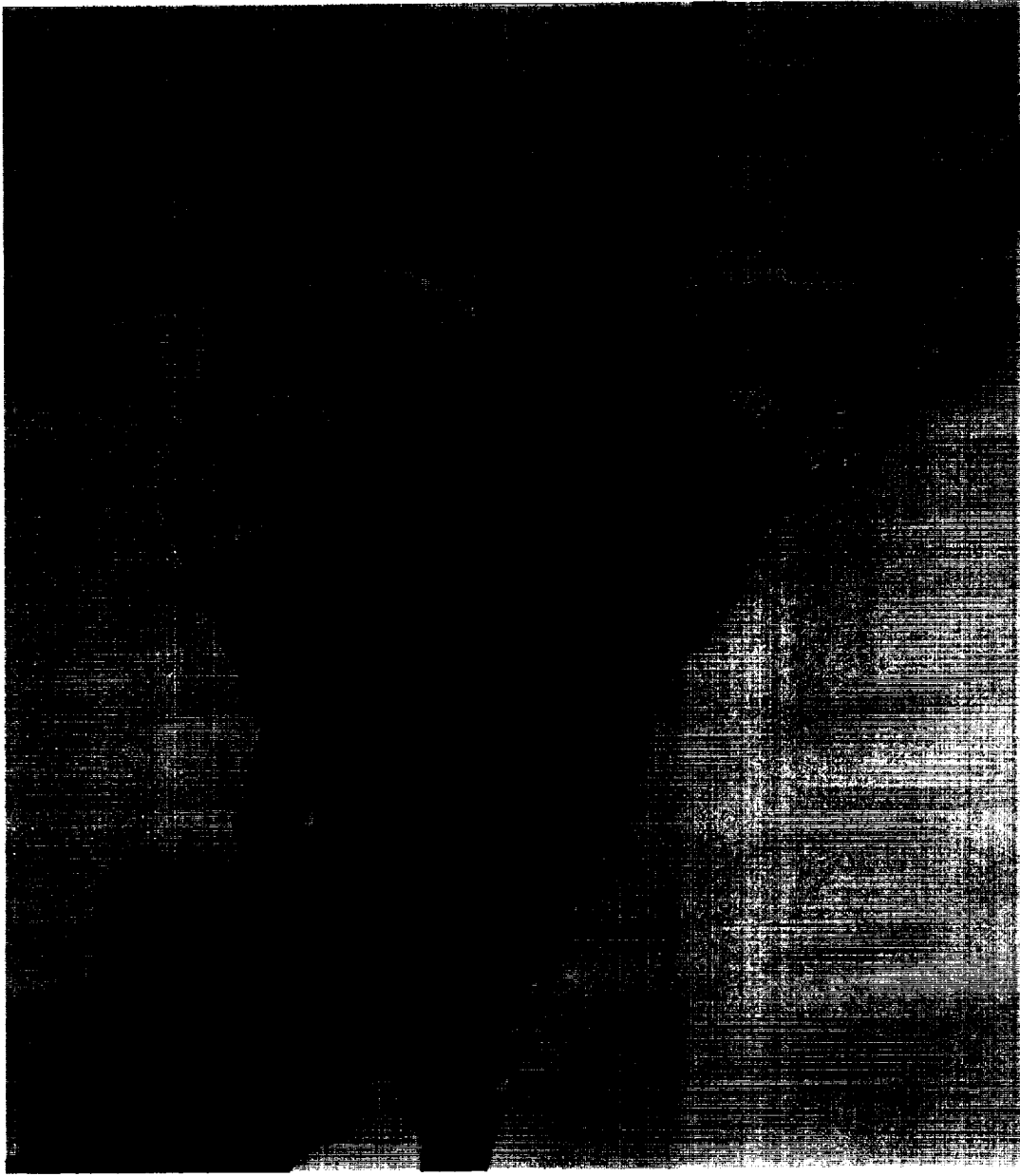


Figure 30: Sub-sampled remotely sensed thermal data shown in Figure 29.

May 28, 1997 Overflight Observations Relative to Tide

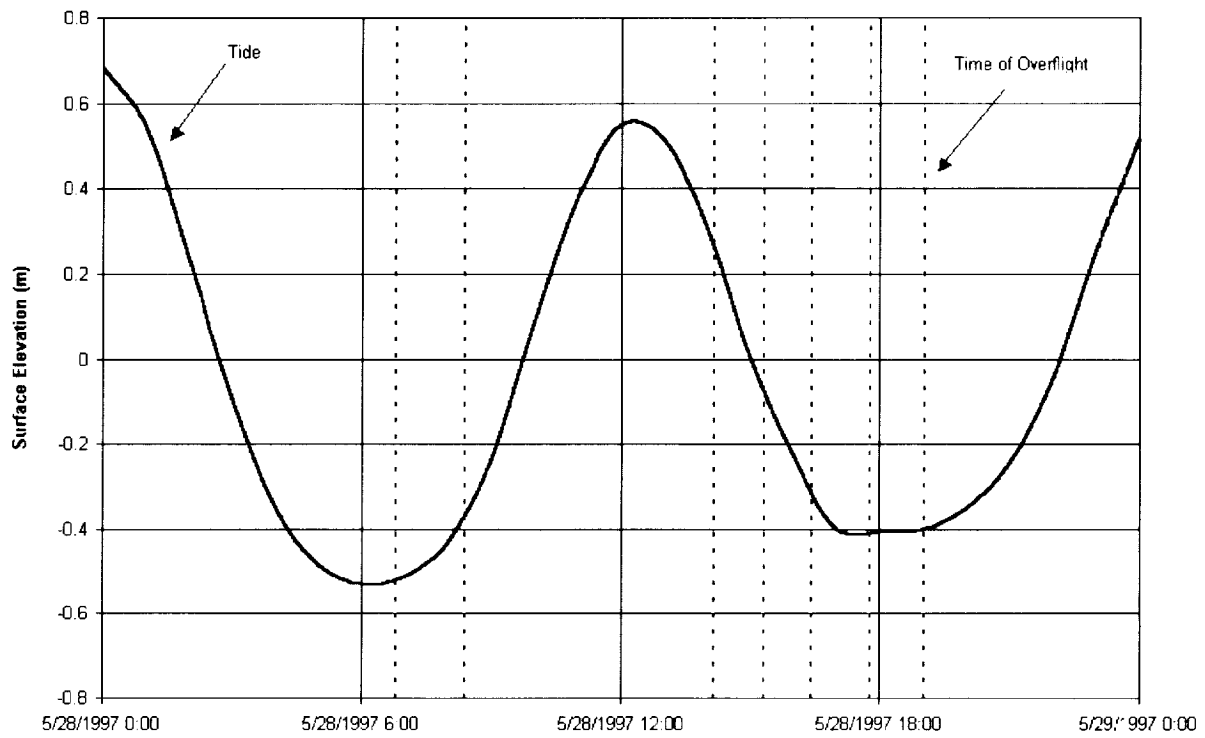


Figure 31: May 28, 1997 Overflight Observations Relative to Tide.

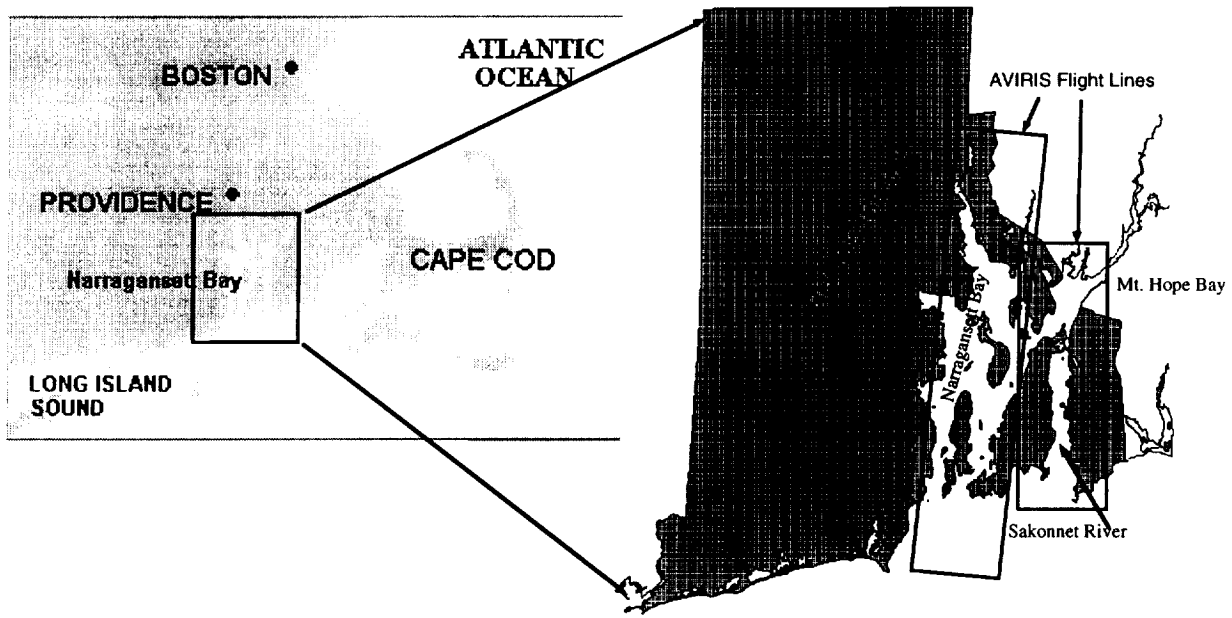


Figure 32. Location of Narragansett Bay and the AVIRIS Flight Line.

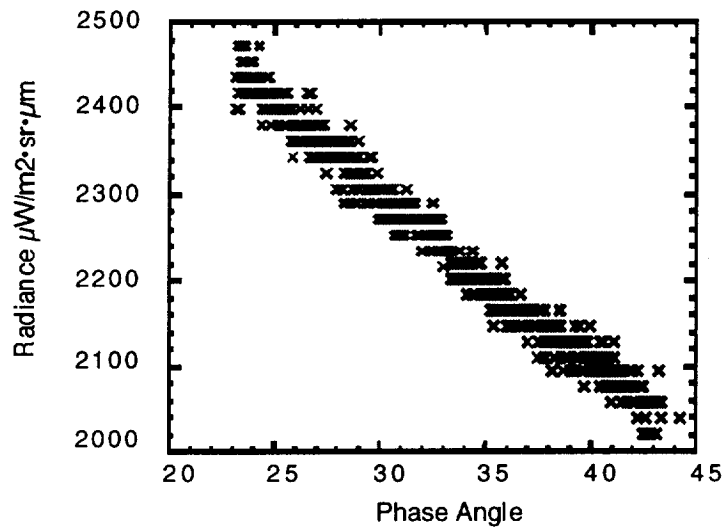


Figure 33. Phase Angle Dependence of Path Radiance.

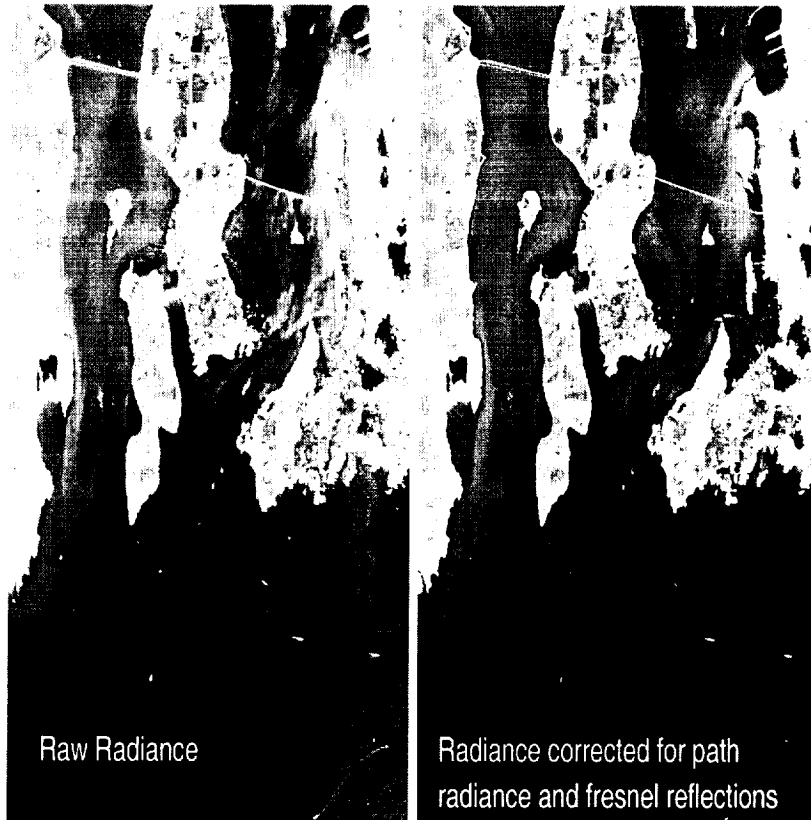


Figure 34. Example of Removal of Pixel Dependent Path Radiance and Fresnel Reflections for the 580 nm Band.

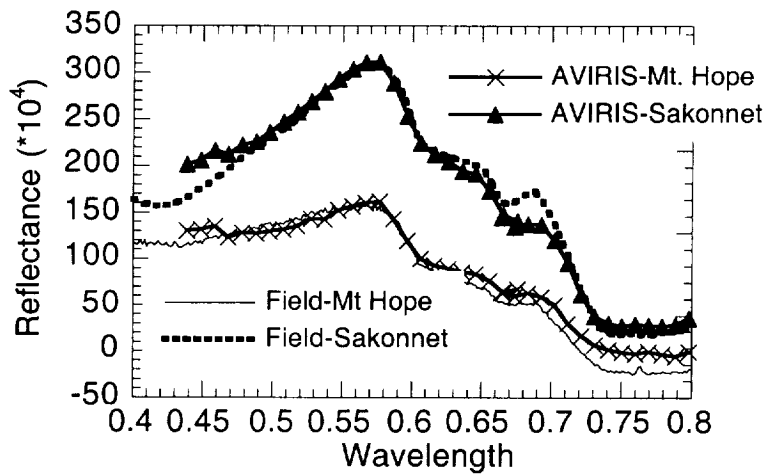


Figure 35. Comparison Between AVIRIS Apparent Reflectance Spectra and Field Spectra Acquired with an ASD FieldSpec FR.

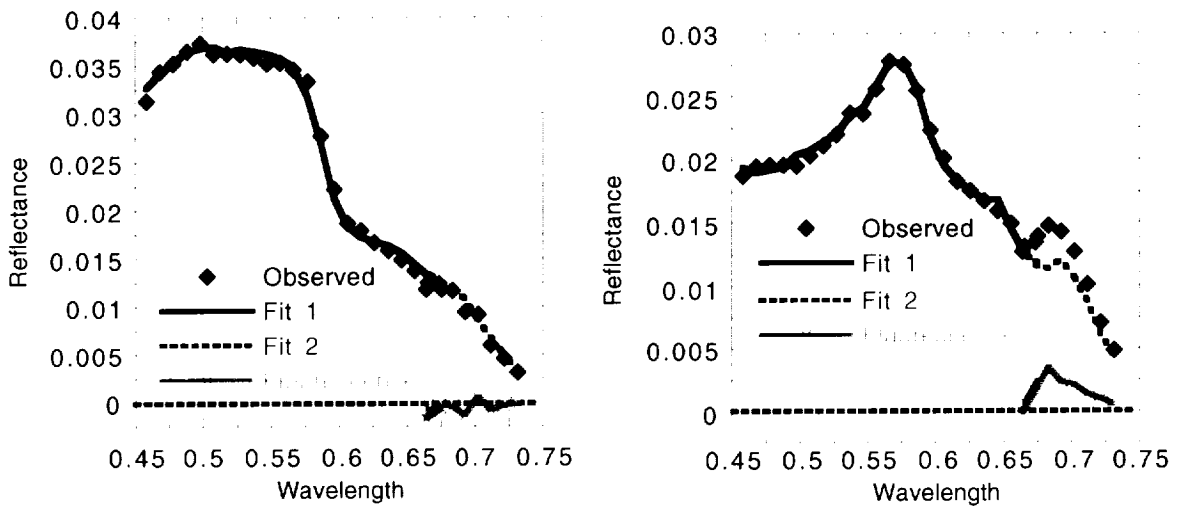


Figure 37. Example solutions of the fit of the model equation to two AVIRIS spectra. The plot on the left shows a low phytoplankton, low fluorescence solution, while the plot on the right shows a high phytoplankton, high fluorescence solution.

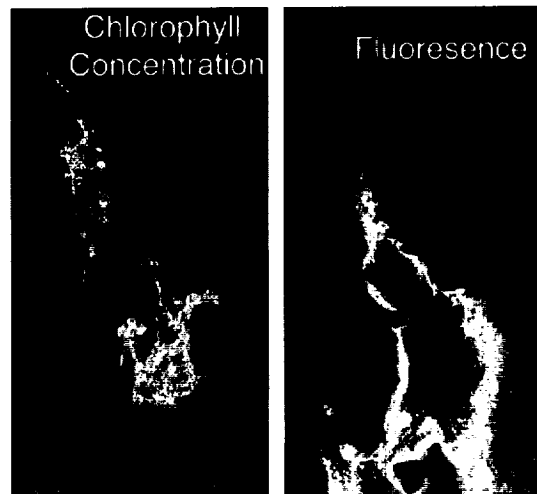


Figure 38. Concentration of phytoplankton represented as chlorophyll contrasted against the activity of the same represented as fluorescence.

